Doctoral Thesis

Thermal Aging Effects on Fusion Boundary of Dissimilar Metal Weldments in Primary Coolant System of Nuclear Power Plant

Kyoung Joon Choi

Department of Nuclear Engineering

Graduate School of UNIST

2017

Thermal Aging Effects on Fusion Boundary of Dissimilar Metal Weldments in Primary Coolant System of Nuclear Power Plant

Kyoung Joon Choi

Department of Nuclear Engineering

Graduate School of UNIST

Thermal Aging Effects on Fusion Boundary of Dissimilar Metal Weldments in Primary Coolant System of Nuclear Power Plant

A dissertation
submitted to the Graduate School of UNIST
in partial fulfillment of the
requirements for the degree of
Doctor of Philosophy

Kyoung Joon Choi

07. 16. 2017
Approved by

Advisor
Prof. Ji Hyun Kim

Thermal Aging Effects on Fusion Boundary of Dissimilar Metal Weldments in Primary Coolant System of Nuclear Power Plant

Kyoung Joon Choi

This certifies that the thesis of Kyoung Joon Choi is approved.

07. 16. 2017

[signature]
Advisor: Ji Hyun Kim

[signature]
Soon-Yong Kwon

[signature]
Chi Bum Bahn

[signature]
In Cheol Bang

[signature]
Sangjoon Ahn

Abstract

In the primary coolant system of the pressurized water reactor, austenitic Ni-base weld metals are deposited on low-alloy steel to form dissimilar metal weld joints. An example is the weld joint between head penetration nozzle (austenitic Ni-base alloy) and reactor pressure vessel (low-alloy steel). Leakage issues from Alloy 82/182 Ni-base weld metal have frequently been reported since 2000. In addition, the cumulative number of cracked welds increased with the operation time of the pressurized water reactors. Recently, the Ni-base weld metal was replaced from Alloy 82/182 (about 15 wt.% of Cr) into Alloy 52/152 (about 30 wt.% of Cr), and the incident of cracking in Alloy 52/152 has not been reported since the replacement. Recently, the cracks, which approach fusion boundary of Ni-base weld metal / low-alloy steel, were reported.

To investigate the effects of (1) weld metals and (2) long-period thermal aging in operating PWRs on the integrity of the fusion boundary, a program of microstructural characterization, mechanical evaluations, corrosion testing and crack growth rate measurements was performed. Two different weld metals were compared: (a) Alloy 182, Ni-base weld metal, and (b) Alloy 152, Ni-base weld metal with a higher chromium content than the Alloy 182. The effect of thermal aging on microstructure evolution, mechanical property and resistances on corrosion and cracking was studied by applying heat treatments to the as-welded mock-up samples. Corrosion testing and crack growth rate measurements, in a simulated primary coolant environment of pressurized water reactors, were performed to rank the resistances to corrosion and cracking.

Microstructural examination represents several $M_{23}C_6$ precipitates formed at the fusion boundary of Ni-base weld metal / low-alloy steel at the as-welded state because of the high solubility of C in the low-alloy steel. Nucleation and growth of the precipitates occurred with thermal aging heat treatments. Alloy 152, which has the higher Cr content compared to Alloy 182, had more Cr rich precipitates at the fusion boundary, compared to the one of Alloy 182. Based on the results of corrosion testing and crack growth rate measurements, the corrosion rates and crack growth rates were dependent on the number of the precipitates. The fusion boundary of the Alloy 152 / low-alloy steel is highly susceptible to cracking compared to the one of the Alloy 182 / low-alloy steel and can be weakened with thermal aging heat treatment. In addition, the fusion boundary showed lower resistance to cracking than Ni-base weld metals of Alloy 182 and Alloy 152.

Contents

LIST OF FIGURES

LIST OF TABLES

ACRONYMS

APT	Atom probe tomography
BCC	Body-centered cubic
DP	Diffraction pattern
EBSD	Electron backscattering diffraction
ED	Electro-discharge (machining)
EDS	Energy dispersive x-ray (spectroscopy)
FB	Fusion boundary
FCC	Face-centered cubic
FE-SEM	Field emission gun scanning electron microscope
FIB	Focused ion beam
GB	Grain boundary
HAZ	Heat affected zone
LAS	Low-alloy steel
NPP	Nuclear power plant
PM	Parent metal
PWHT	Post weld heat treatment
PWR	Pressurized water reactor
SEM	Scanning electron microscopy
SMAW	Shield Metal arc welding
TEM	Transmission electron microscopy

I. INTRODUCTION

1.1 Background:

Pressurized water reactors (PWRs) are mainly placed and operated in Republic of Korea. In a PWR, water of H_2O, which plays as roles as coolant and neutron moderator in the primary coolant system, flows under high temperature and high pressure of about 320 °C and 15 MPa to the reactor core including nuclear fuels. There, water is heated by thermal energy released through the nuclear fission, the heated water transfers the thermal energy into the secondary coolant system through a steam generator. In the secondary coolant system, water used as the secondary coolant has volume expansion with the phase transient (from liquid into gas) by the transferred thermal energy. The expansion of the steam operates turbines and generates electrical energy.

In this regard, a primary coolant system of pressurized water reactors is in high temperature and high pressure environment, which is acknowledged as corrosive environment. Although the large components are mainly made of low-alloy steel (LAS), the area exposed to the corrosive environment are usually covered with stainless steel or Ni-base alloy. And the pipes or nozzles consist of stainless steel or Ni-base alloy. These alloys are generally used as a filler metal to joining dissimilar metals due to the feature that is thermal expansion coefficient among those of Ni-base alloy and a LAS. In addition, Ni-base weld metal significantly retards C diffusion from LAS into the weld metal [1–3].

Stress corrosion cracking (SCC) issues have been reported to occur in Ni-base weld metal used in the primary coolant system of PWRs since 2000s. The initiation and growth of SCC in the Ni-base weld metal is acknowledged to be caused by the inferior corrosion resistance due to micro-segregation, formation of an unmixed zone, and precipitation [4].

Figure I-1 represent the SCC issues in Alloy 600 and Alloy 182. In 1970s many cases of SCC were detected in Steam Generator tubes especially those made of Alloy 600 Ni-based alloy (base metal) [5]. In addition to Alloy 600 base metal, failures were also observed in Alloy 600 weld metal, such as the outlet nozzle and the head penetration nozzles of the reactor vessel in VC Summer of US in 2000 (as shown in Figs. I-2). And, in 2003 one of the pressurizer nozzles in Tsuruga-2 of Japan had a small leak at the dissimilar weld joint.

The SCC susceptibility is acknowledged to be determined by three factors of (a) material factor, (b) stress factor, and (c) environmental factor. By controlling the material factor, the susceptibility of SCC in Ni-base weld metals is known to be depressed by the increase of Cr concentration, this led to the replacement of Alloy 182 (Low-Cr weld metal; about 15 wt.% of Cr) to Alloy 152 (High-Cr weld metal; about 30 wt.% of Cr) [6]. The effect on SCC susceptibility has been investigated in previous studies [7–11]. The previously conducted test results, including the crack growth rate measurement,

crack initiation test and corrosion test performed in the simulated pressurized water reactor environment, represent that SCC susceptibility decreased with the increase of Cr content from 1% up to 20% in Ni-base alloys. And the increased Cr content caused Cr content increase in protective oxide layer (Cr rich oxide), decreased the oxide thickness and finally suppressed the corrosion rate. Although this phenomenon is generally recognized, the effects of Cr are not fully understood. High-Cr weld metal (Alloy 152) is recently used as a replacement filer metal of Alloy 182, no leakage issue has occurred in High-Cr weld metal of the dissimilar metal weld joints used in the primary coolant system of PWRs.

In this regard, the weld metal consisting of High-Cr weld metal (Alloy 152) seems to be immune area. But, the unexpected phenomenon was observed in the DMW after replacing Alloy 182 as Alloy 152. It was observed that the crack was propagated into the interfaces of the weld metal and LAS [12]. If the SCC is propagated across the Ni-base alloy with 6 mm thickness as shown in Fig. I-3, the fusion boundary (FB) region of Ni-base weld metal and LAS can be exposed to primary coolant environment of NPPs. In this reason, this study is largely focused on the FB region.

And, the tensile residual stress is formed, as shown in Fig. I-4, due to different thermal cycle such as heating rates, peaks of temperature and cooling rates during multi-paths welding. It is also known as a factor to cause the SCC, and the head penetration nozzle is susceptible to cracking. In this reason, it is thought that there can be three simplified potential paths for leakage in the head penetration nozzle: (a) SCC initiation and growth in nozzle (inner wall to outer wall), (b) SCC initiation and growth in weld and (c) SCC initiation and growth in Weld (into FB region of Ni-base weld metal and LAS) and crack propagation along the FB region.

Among these paths, this study is mainly focused on (c) SCC initiation and growth in Weld (into FB region of Ni-base weld metal and LAS) and crack propagation along the FB. There are several reasons to support this. Firstly, although many study on Ni-base metal weld were performed, there is not sufficient study on interface of LAS and weld.

Next, the non-destruction inspection is not available to the FB. And it is still difficult to find stress corrosion cracking in weld. The lack of the non-destruction inspection was partially attributed to surface contour, surface roughness, and so on.

And, the FB can be degraded by thermal aging affecting the local microstructure and the material strength by accelerating Cr diffusion and changing the morphology of Cr-rich precipitates. Near the FB region of LAS and Ni-base weld metal, the element can be diffused at the operation temperature of nuclear power plants, which causes the changes of Cr-rich precipitate morphology and other properties. Because LAS and Ni-base weld metal have enough C and Cr contents, the thermal aging can sufficiently induce additional precipitation and coarsening of Cr-rich precipitates. It may worsen the corrosion resistance and SCC susceptibility in the FB region of the DMWs [13–15].

Finally, when the FB was exposed to the primary water environment, galvanic corrosion can occur because the more noble metal of Ni-base alloy is contacted with the more active metal of LAS as shown

in Figs. I-7 and I-8. If two dissimilar materials are immersed in a corrosive solution, each material will a develop an electrochemical potential. When the electrochemical potentials of the two materials are significantly different, the more active material will act as the anode and the more noble material will act as the cathode. In case of the weld joint used in this study, LAS is more active metal and plays a role of the anode and Ni-base alloy steel is more noble metal and plays a role of the cathode. In this regard, the replacement of Ni-base weld metal can degenerate the resistance on the crack proportion along the FB because Alloy 152 is more noble than Alloy 182.

Therefore, this study investigated the effects of long-period thermal aging and type of Ni-base weld metal on microstructures, material properties, corrosion rates and crack propagations in the FB region located between LAS and Ni-base weld metal. Ultimately, such data will do the important role to assess the effects of long-period thermal aging and Cr content of Ni-base weld metal on the integrity of the dissimilar weld joints and for managing the long-term operated PWRs.

1.2 Objectives and Scope

This present study aims to evaluate the integrity of dissimilar metal weld joints, used in the primary coolant system of PWRs, through the comparison evaluation with the quantifiable data on the susceptibility to cracking of the FB region (of Ni-base weld metal / LAS), Ni-base weld metal, and LAS. The data of Ni-base weld metal and LAS were get the experimental results of the previous studies, and the data of the FB region were obtained through the experiment (crack growth rate measurements) performed in the present study since there is no data of the FB region in the primary coolant system of PWRs.

In addition, it was conducted to study effects of (a) long-period thermal aging and (b) Cr content of Ni-base weld metal on the integrity of the weld joints microstructures, material properties, corrosion rates and crack propagations in the FB region located among LAS and Ni-base weld metal. For investigating the effect of long-period thermal aging on the FB region, the method to simulate thermal aging degradation in the primary coolant system was developed with Arrhenius's equation, JMatPro (calculator to estimate the phase diagram) and so on. And, it was conducted to investigate the effect of Cr content of Ni-base weld metal by varying the weld metals (Alloy 182 and Alloy 152)

The present work can be divided into the 5 parts.

1) Accelerated heat treatment for simulating long-period thermal aging effects.

2) Evaluation of the microstructural changes in the FB region varying thermally aging heat treatment time (0, 15 and 30 y of the full-power operation times) and Cr contents in Ni-based weld metal.
3) Evaluation of changes of mechanical properties in the FB region varying thermally aging heat treatment time and Cr contents of Ni-based weld metal.
4) Evaluation of corrosion behavior in the FB region varying thermally aging heat treatment time and Cr contents of Ni-based weld metal
5) Evaluation of crack propagation rate in the FB region varying thermally aging heat treatment time and Cr contents of Ni-based weld metal.

In chapter I, research background and motivation, and general literature reviews related dissimilar metal weldments, thermal aging and Cr content were introduced with the objective of the present research. Chapter II covers the preparation procedures of two different DMW buttered with Alloy 152 and Alloy 152 and the method to simulate the long-period thermal aging in the primary coolant system of PWRs.

In chapter III, the changes of the FB region, related to long-period thermal aging and Cr content of Ni-base weld metal, was investigated in terms of microstructures to provide the reference data for explaining the degradation or enhancement of the integrity by these effects, where several instruments, such as scanning electron microscopy, transmission electron microscopy and 3-dimenssional atom probe tomography, were required.

In chapter IV, the nanoindentation testing was selected to evaluate the material properties of the FB region due to the space limitation. (mechanical properties) and the microstructural changes by the thermal aging and the Cr content of the weld metal were discussed to explain the material hardening and re-softening with the thermal aging and the difference of the hardness values between the FB regions buttered with Alloy 182 and Alloy 152.

In chapter V, corrosion rates of the FB region, which acts as the important role in determining the susceptibility to cracking in the primary coolant system of PWRs, were covered to explain the effects of the thermal aging and the Cr content of the weld metal on the integrity of the FB region. Corrosion rate were evaluated with COMSOL simulation, polarization testing in room temperature water and the primary coolant environment, and weight loss measurements during the exposure to the primary coolant environment.

In chapter VI, the quantifiable data, measured through the crack growth rate measurements under constant loading for the evaluation of the susceptibility to cracking at steady-state of the operation PWRs, were discussed to explain the effect effects of the thermal aging and the Cr content of the weld metal on the integrity of the FB region. And, the comparison evaluation was conducted with the data of

Ni-base weld metal and LAS to evaluate whether the FB is highly susceptible to cracking compared to the other materials.

The summary and recommendations were described in chapter VII,

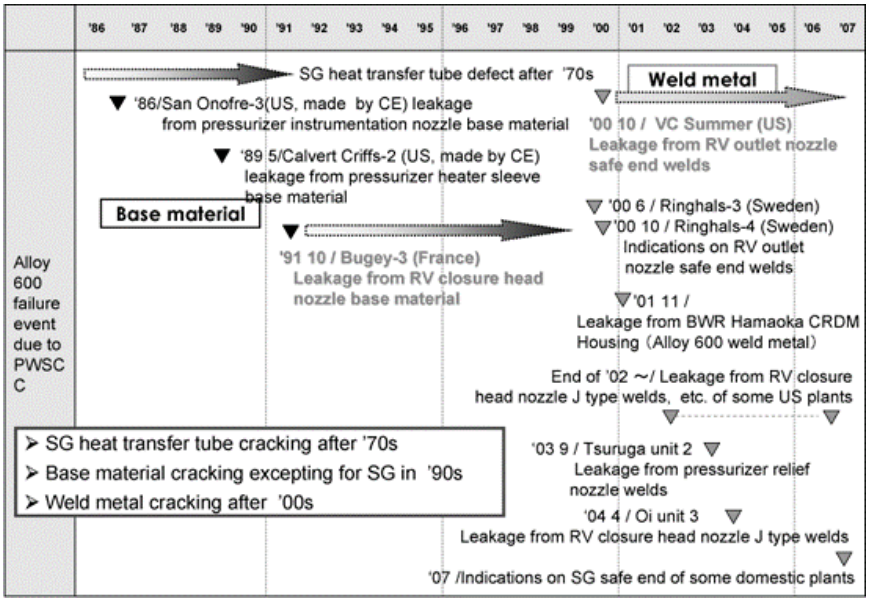

Figure I-1 The major issues of Ni-base alloy used in the primary coolant system of pressurized water reactors in the past [5]

(a) Large volume of waste on reactor vessel head

(b) Small volume of waste on reactor vessel head

Figure I-2 Leakage from head penetration nozzle of reactor vessel [16]

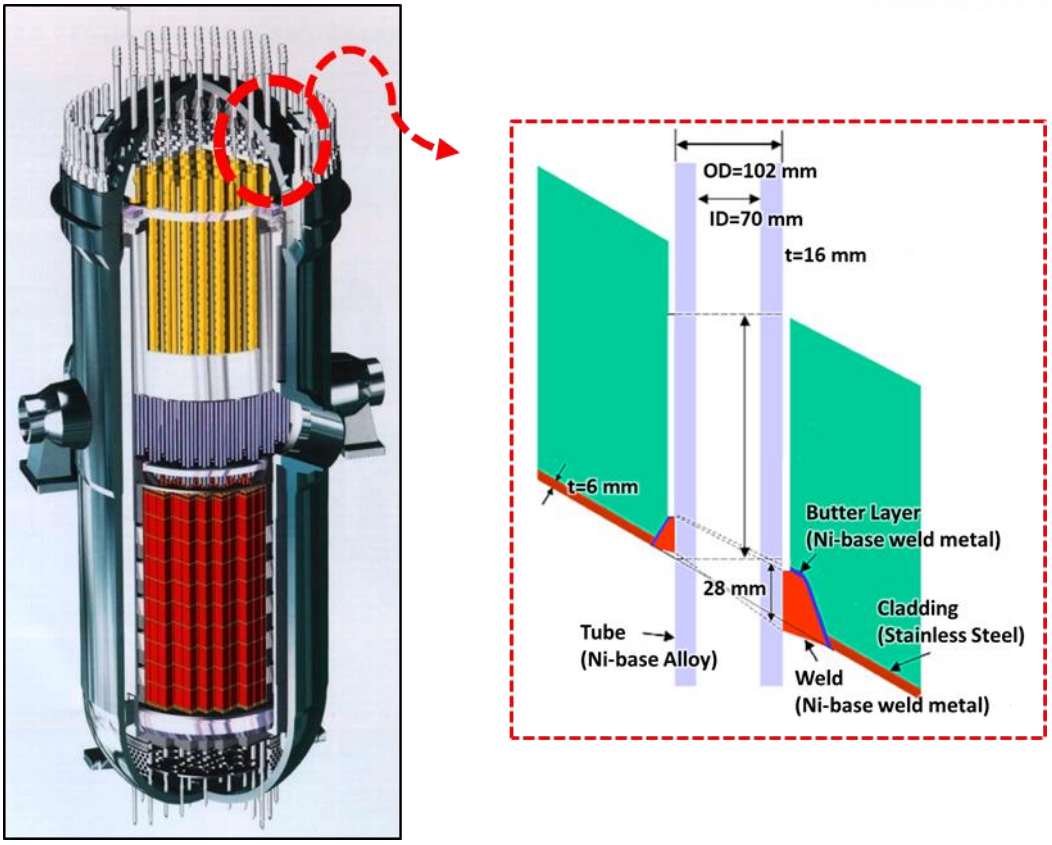

Figure I-3 Schematics of head penetration nozzle of pressure vessel [17]

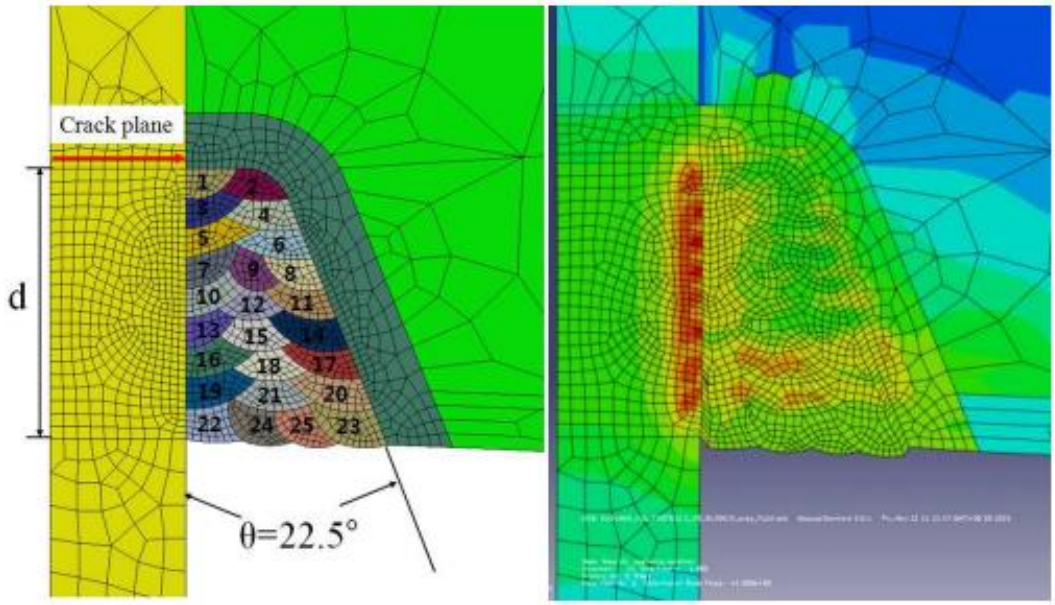

Figure I-4 Distribution of residual stress formed in a head penetration nozzle during a multi-path welding process [17]

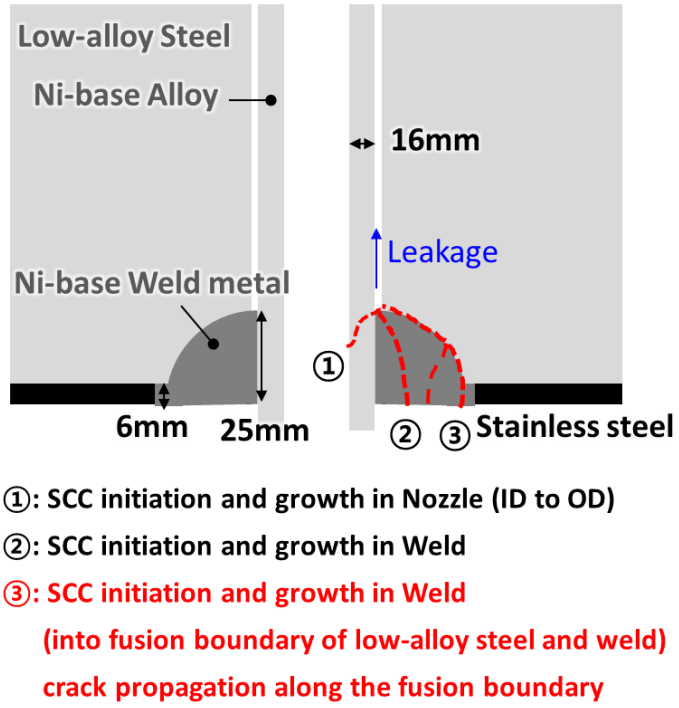

Figure I-5 Simplified potential paths for cracking in a head penetration nozzle.

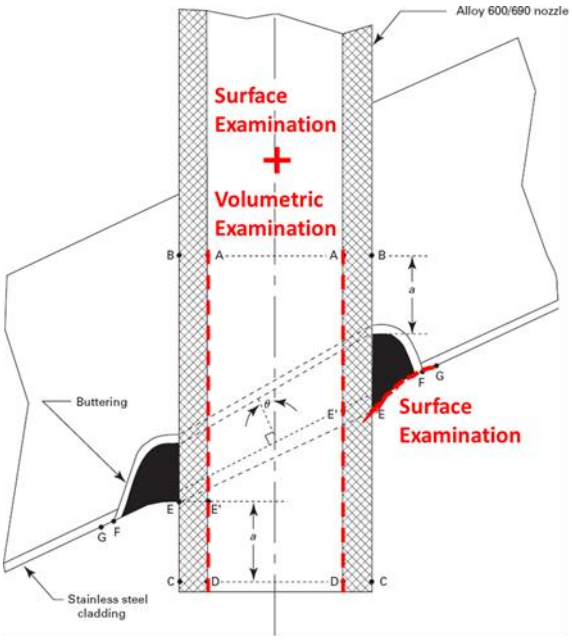

- **Visual inspection (Nozzle, J-groove weld)**
- **Ultrasonic testing inspection (Nozzle)**
- **Penetration inspection (Nozzle, J-groove weld)**

Figure I-6 Several inspections of flaw in a head penetration nozzle.

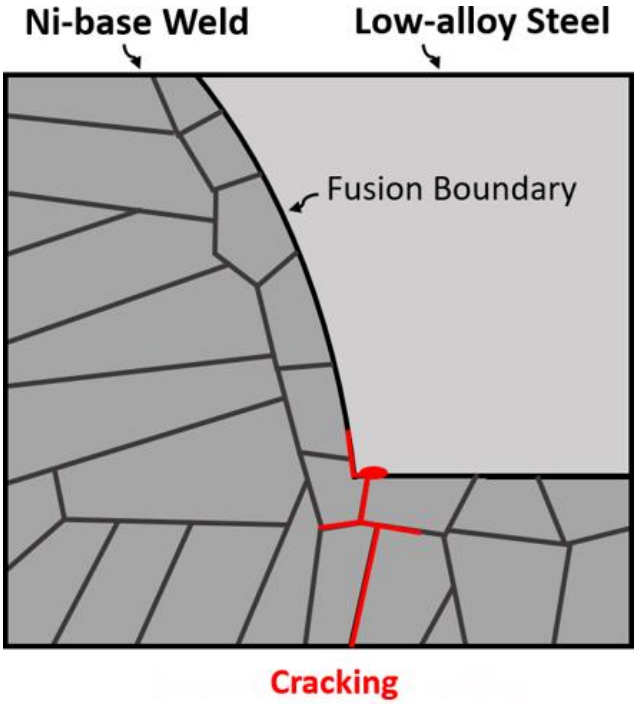

(a) Cracking in Ni-base weld metal, which approach FB located among Ni-base weld metal and LAS

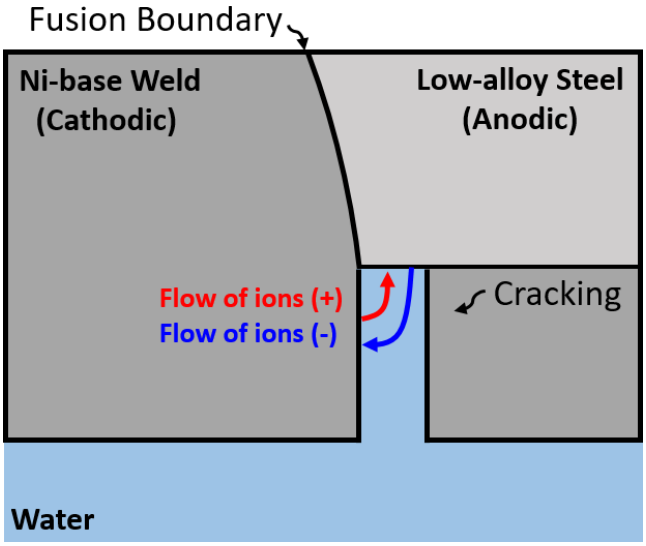

(b) a galvanic cell in a dissimilar weld joints

Figure I-7 Schematics indicating a galvanic cell formed in a dissimilar weld joints when crack from Ni-base weld metal approaches the FB located among Ni-base weld metal and LAS.

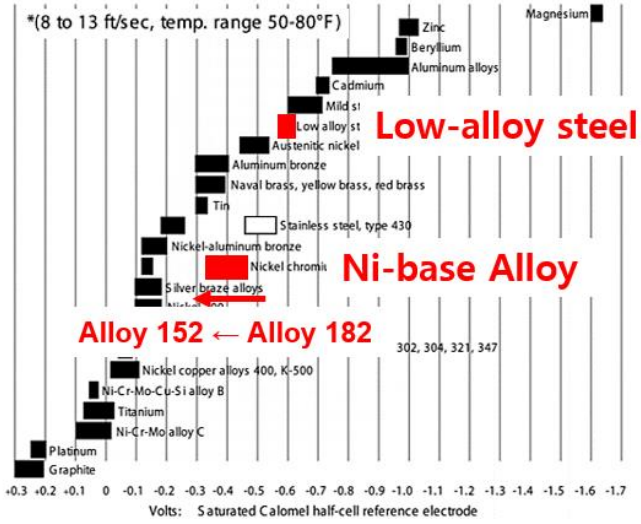

Figure I-8 Galvanic series chart in seawater [18]

II. WELDING AND THERMAL AGING HEAT TREATMENT

2.1 Materials

Dissimilar metal weldment (DMW) joints were prepared by joining low-alloy steel (LAS) and Ni-based Alloy with a filler metal of Ni-based weld metals (Alloy 182 / 152) due to the features of the weld metals, which are (a) thermal expansion coefficient among those of LAS, austenitic stainless steel, and Ni-based alloy, and (b) ability to retard the diffusion of C from LAS to the weld metal. Two different DMW joints were prepared: (1) A508 Gr. 3 / Alloy 182 / Alloy 600 and (2) A533 Gr. B/Alloy 152/ Alloy 690 as shown in Figure II-1 (a). Figure II-1 (b) shows several regions between Ni-base weld metal and LAS of the DMW, representing Type-II boundary, fusion boundary (FB), and heat-affected zone. Type-II boundary is parallel to the FB and located within 100 μm from the FB [2,14,19]. The FB is a line between Ni-based weld metal and LAS. And heat-affect zone is the region that experiences the microstructural changes by the thermal energy generated during the multi-paths welding. The welding procedures are described below.

A representative mockup sample, consisting of (1) A508 Gr. 3 / Alloy 182 / Alloy 600, was fabricated following welding processes and criteria described on ASME Section IX. Firstly, LAS (A508 Gr. 3) plate was buttered with Alloy 182 Ni-base weld metal, making 3 of buttering layers on LAS plate. The buttered plate had a post-weld heat treatment at 595–620 ºC for 3 h. Next, the buttered plate and Alloy 600 plate were attached and welded with Alloy 182, as shown in Figure II-1. The chemical compositions of the materials were arranged in Table II-11.

The other representative mockup sample, consisting of (2) A533 Gr. 3 / Alloy 152 / Alloy 690, was also fabricated following welding processes and criteria described on ASME Section IX. Once, A533 Gr. 3 was buttered with Ni-based weld metal Alloy 152, Ni-base weld metal, making 3 of buttering layers on LAS plate. The buttered plate had a post-weld heat treatment at 607–635 ºC for 3 h. Next, the buttered plate and Alloy 690 plate were attached and welded with Alloy 152. The chemical compositions of the materials were arranged in Table II-1.

The bulk mock-up sample of the weld joint were cut through an electrical discharge machining to prepare 3 samples for the different heat treatments simulating the thermal aging degradations for 0 y, 15 y and 30 y. The thermally aging heat treatments were done to prepared thermally aged DMWs during the full power operating times of 0 y, 15 y and 30 y in the primary coolant system of PWRs (where the normal operation temperature is approximately 320 ºC).

2.2 Thermally Aging Heat Treatments

Thermally aging heat treatments were done with the partial mock-up samples to prepare thermally aged DMWs during the full power operating times of 0 y, 15 y and 30 y in the primary coolant system of PWRs (where the normal operation temperature is approximately 320 ºC), respectively. Although it is the best way to perform the heat treatment at 320 ºC which is same with the operation temperature, but, it takes too long time to prepare the thermally aged DMWs during the full power operating times of 0 y, 15 y and 30 y in the primary coolant system. So, in this study, the accelerated heat treatment with higher temperature than the operation temperature was selected to for preparing the aged DMWs. When the condition of the heat treatment was determined, the selection criteria are (1) whether it can be possible to simulate the Cr diffusion length at 320 ºC for 15 y and 30 y with the heat treatment at other temperatures and (2) whether unexpected microstructure phases (e.g. the sigma phase) will be formed.

Firstly, the Cr diffusion length is an important factor to consider when the accelerated heat treatment is performed to prepare thermally aged DMWs during the full power operating times of 0 y, 15 y and 30 y in the primary coolant system since the influence of Cr content is a key source of Cr rich oxide (protective oxide layer) and Cr rich precipitate, affecting microstructures, mechanical properties, corrosion behavior and crack initiation & propagation in Ni-base alloy, stainless steel and low alloy steel. For example, T. Moss et al. [20,21] observed that Cr oxide of Alloy 690, which includes higher Cr concentration than Alloy 600, is thick and has relatively many Cr concentration due to relatively fast diffusion of Cr. It can reduce the Cr depleted zone and intergranular oxidation along grain boundaries, resulting in the improved resistances on corrosion and cracking. In addition, the previously conducted test results, including the crack growth rate measurement, crack initiation test and corrosion test performed in the simulated pressurized water reactor environment, represent that SCC susceptibility decreased with the increase of Cr content from 1 up to 20 wt.% in nickel-based alloys [7–11]. And the increased Cr content caused Cr content increase in protective oxide layer (Cr rich oxide), decreased the oxide thickness and finally suppressed the corrosion rate. In case of LAS, The Cr's addition in LAS changes the oxide structures from Fe oxide (one layer) into two layers of Fe oxide and Cr oxide, resulting in the improvement of corrosion resistance. In this regard, Cr is act as a key parameter determining affecting microstructures, mechanical properties, corrosion behavior and crack initiation & propagation. Therefore, the Cr diffusion length was selected as a criterion for the aged DMWs.

Next, it is necessary to prevent the formation of unwanted microstructures, which is not observed in the aged DMW at 320 ºC. Therefore, the temperature condition of the thermally aging heat treatment was set below the maximum of 500 ºC, which was confirmed through thermodynamic program JMatPro [19,22]. Thus, to prepare the thermally aged DMWs during the full power operating times of 0 y, 15 y and 30 y in the primary coolant system of PWRs, the heat treatment temperature is 400 ºC.

The thermally aging times (for preparing thermal aging during the full power operating times of 0 y, 15 y and 30 y in the primary coolant system) were determined following the Arrhenius equation of

thermal diffusion [23,24]. Activation energy, which is used in the upper equation, is considered for the diffusion of Cr since Cr plays a key role in precipitation, material hardening, and resistances to corrosion and crack propagation, as described above [2]. The activation energy values for Cr diffusion are 180 kJ/mol for Alloy 182 or 125 kJ/mol for Alloy 152, suggested in the previous studies [2,19,25–28] investigating austenitic (FCC, face-centered cubic) Ni-base alloys. So, the thermally aging conditions for two different weld joints are unlike since theses have the different activation energy values.

With the dissimilar weld joints of A508 Gr. 3 and Alloy 182, the thermally aging heat treatments were performed at 400 °C of the accelerated heat treatment temperatures during the full power operating times of 0 y, 15 y and 30 y in the primary coolant system of PWRs. So, the thermally aging heat treatment were done at 400 °C for 0 h, 1,713 h and 3,427 h, corresponding to 0 y, 15 y and 30 y of the full power operating times of in the primary coolant system of PWRs

In the similar way described above, with the weld joints of A533 Gr. 3 and Alloy 152, the thermally aging heat treatments were performed at 400 °C of the accelerated heat treatment temperatures during the full power operating times of 0 y, 15 y and 30 y in the primary coolant system of PWRs. So, the thermally aging heat treatment were done at 400 °C for 0 h, 1,375 and 2,750 h, corresponding to 0 y, 15 y and 30 y of the full power operating times of in the primary coolant system of PWRs, respectively.

To avoid confusion due to many specimens, the specimen will be called as their sample I.D. (HT + ‘heat treatment temperature [°C]’ + Y + ‘operation time at 320 °C [year]’).

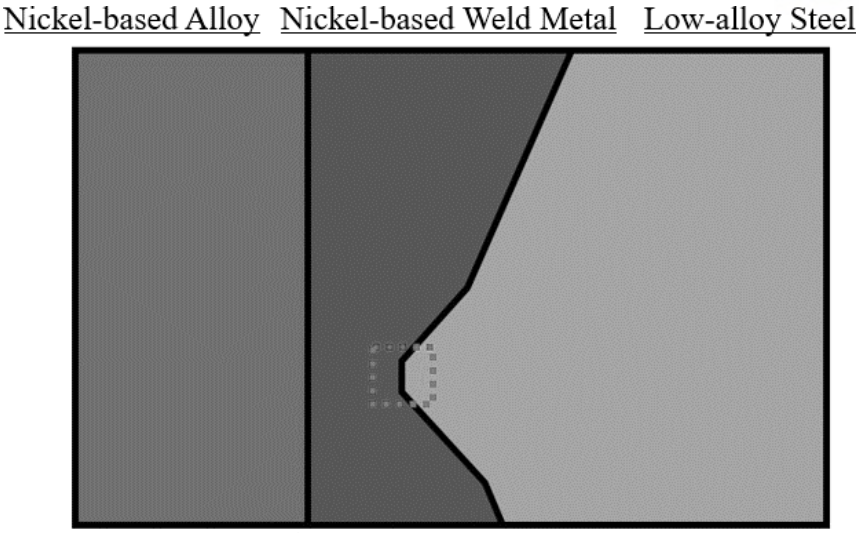

(a) Cross section of a dissimilar metal weld

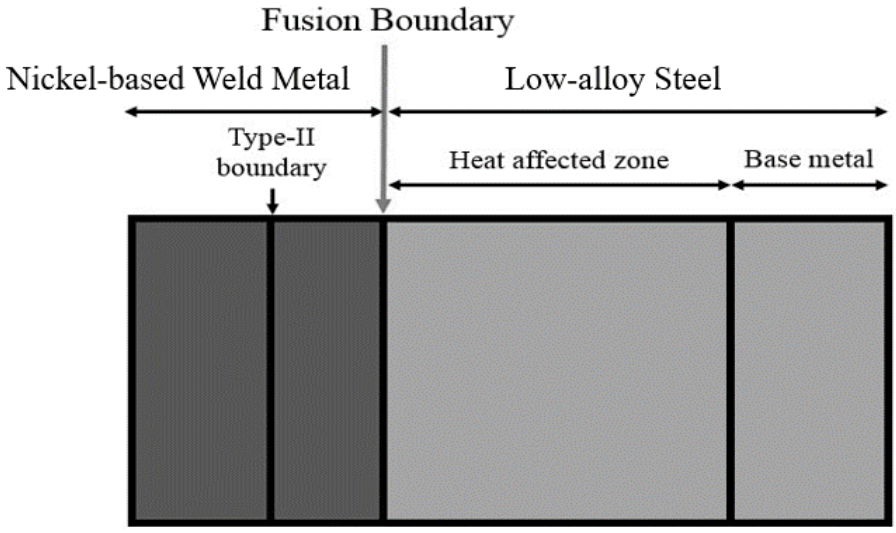

(b) Analysis area (magnification of the red dotted region in (a))

Figure II-1 Schematic representing a DMW made up of Ni-based alloy, Ni-based weld metal, and LAS used in this study.

Table II-1 Chemical Compositions of A508 Gr. 3 (LAS), Alloy 182 (Ni-base weld metal), and Alloy 600 making up the DMW (where the unit is wt. %)

Material	Composition												
	C	Si	Mn	P	S	Fe	Cu	Ni	Cr	Al	Nb+Ta	Mo	Ti
Alloy 600	0.06	0.3	0.07	-	0.001	8.13	0.01	74.9	15.6	-	-	-	-
Alloy 182	0.05	0.37	7.42	0.01	0.010	4.48	0.01	70.9	14.9			0.03	1.77
A508 Gr.3	0.19	0.22	1.33	0.008	0.002	Bal.	0.02	0.91	0.19	0.02	0.47		

Table II-2 Chemical Compositions of A533 Gr. B (LAS) / Alloy 152 (Ni-base weld metal) / Alloy 690 making up the DMW (where the unit is wt. %) [19]

Material	Composition												
	C	Si	Mn	P	S	Fe	Cu	Ni	Cr	Al	Nb+Ta	Mo	Ti
Alloy 690	0.03	0.07	0.20		0.001	9.90	0.01	59.50	29.50				
Alloy 152	0.04	0.46	3.56	0.003	0.001	9.36	0.01	55.25	29.04	0.24	1.84	0.01	0.15
A533 Gr. B	0.22	0.19	1.28	0.01	0.012	Bal.		0.51	0.18			0.48	

III. MICROSTRUCTURAL EVALUATION

3.1 Introduction

There is a concern that the fusion boundary (FB) region (consisting of low-alloy steel (LAS) and Cr-rich precipitates near FB) might be more susceptible to cracking than Ni-base weld metal which experienced frequently cracking issues in the primary coolant system of PWRs. However, the sufficient research was not conducted to evaluated the integrity of the FB region due to some reasons: (i) LAS has good resistance on the cracking compared to Ni-base weld metal and it can seem that the FB region is also resistive to the cracking, and (ii) it is difficult to investigate the resistance on the cracking in the FB region due to the narrow and un-uniform region. In addition, the FB region can additionally be degenerated by the effect of the long-period thermal aging and the replacement of Ni-base weld metal (Alloy 182 into Alloy 152) as described in Section of 'I. INTRODUCTION'. For these reasons, crack growth rate measurements were conducted varying two options: (a) the thermal aging heat treatment condition and (b) Ni-base weld metal (Alloy 182 and Alloy 152). Therefore, this study investigated the effects of long-period thermal aging and type of Ni-base weld metal on microstructures, material properties, corrosion rates and crack propagations in the FB region located between LAS and Ni-base weld metal in dissimilar metal weldments at as-welded and aged states. The weld metals were varied with Alloy 182 and Alloy 152, respectively. In this chapter, the microstructural investigation was conducted and covered to improve the understanding of these effects on resistance on crack propagation in the FB region.

In case of Ni-base weld metals of Alloy 182 and Alloy 152 (which has 2 times compared to Alloy 182). As the previous study, T. Moss et al. [20,21] observed that Cr oxide of Alloy 690/Alloy 152, which includes higher Cr concentration than Alloy 600 / Alloy 182, is thick and has relatively high Cr concentration due to relatively fast diffusion of Cr. It can reduce the Cr depleted zone and intergranular oxidation along grain boundaries, resulting in the improved resistances on corrosion and cracking. Although Alloy 152 was verified through many previous study for the integrity evaluation of the weld metal, resistances on corrosion and crack propagation in the FB region can be more degenerated than before the replacement of Ni-base weld metal (Alloy 182 into Alloy 152).

Additionally, thermal aging in the primary coolant system of PWRs can cause Cr diffusion along grain boundary of Ni-base weld metal, resulting in the enrichment of Cr in LAS side region near the FB between Ni-base weld metal and LAS. Cr enriched region in the LAS side near FB is very narrow (about 0.4 μm) due to low diffusivity of Cr in α-Fe. Therefore, in the Cr enriched region (is called as FB region in this paper), thermal aging can affect the morphology of Cr-rich precipitates, which play a key role in determining material hardness, corrosion resistance, and crack propagation. In that, thermal aging can

degenerate or enhance the resistance of the welds against crack propagation. Since the influence of the thermal aging is a key parameter affecting the crack propagation, the mechanical and microstructural investigations on the influence may improve the understanding of resistance on corrosion and crack propagation at the FB region. Hou et al. [3,14] found that the FB region, which is located among Alloy 182 and LAS in an as-welded DMW, has only a few precipitates of $Cr_{23}C_6$ due to the high solubility of C in the LAS. Nelson et al. [29–31] observed that the FB might be a potential path for crack growth due to the feature: random misorientations were measured between AISI 1080 alloy and 409 stainless steel in a dissimilar metal weld joint through electron backscatter diffraction analysis of scanning electron microscopy (SEM).

In these regards, the thermal aging and Cr content of Ni-base weld metal are key parameters affecting the crack propagation, the microstructural investigations on the influence may improve the understanding of resistance on corrosion and crack propagation at the FB region. For these reasons, this study aims to investigate the effects of long-period thermal aging heat treatment on the microstructures of (a) the FB region of Alloy 182 / LAS and (b) the FB region of Alloy 152 / LAS through several instrumental analyses through optical microscopy (OM), SEM, transmission electron microscopy (TEM) and 3-dimensional atom probe tomography (3-D APT). This study determines the common features of and disparity in the effects of thermal aging by comparing the results of the DMW welded with Alloy 182 and the DMW welded with Alloy 152. Ultimately, such data will do the important role to assess long-period thermal aging and the effects of Cr content in Ni-base weld metal on the integrity of the dissimilar weld joints and for managing the long-term operated PWRs.

3.2 Experimental

In this study, two different DMW joints were prepared: (1) A508 Gr. 3 / Alloy 182 / Alloy 600 and (2) A533 Gr. B/Alloy 152/ Alloy 690. The bulk mock-up samples of the weld joints were cut with wire-cutting machines and electro-discharging machines to prepare 3 samples for the different heat treatments simulating the thermal aging degradations for 0 y, 15 y and 30 y. The chemical compositions of the used materials are described in Section III. 1. DMW joint of A533 Gr. B/Alloy 152/ Alloy 690 was heat-treated at 400 ^{o}C during the equivalent times to the full power operating times of 0 y, 15 y and 30 y in the primary coolant system of PWRs, preparing the sample treated at 3 conditions. And DMW joint of A508 Gr. 3/ Alloy 182/ Alloy 600 was heat-treated at 400 during the equivalent times to the full power operating times of 0 y, 15 y and 30 y in the primary coolant system of PWRs preparing the sample treated at 3 conditions.

Microstructural characterizations were conducted through (1) an SEM with field emission gun systems (Nanonova 230, FEI) (2) a TEM with thermal field emission gun (JEM-2100F, JEOL), and (3) a 3-D APT (LaWaTAP, CAMECA).

For these microstructural characterizations, the plate specimens with 15(length, mm) × 15 (width, mm) × 2 (thickness, mm) were prepared through an electrical discharge machining, and then were polished with emery paper up to 9 μm (particle size), diamond paste up to 1 μm, and finally alumina powder of 0.05 μm for creating a flat section with negligible mechanical deformation.

These specimens were used for investigating the general microstructures of LAS, and FB region and precipitate's morphology in the FB region with SEM after etching with 3% Nital etching solution.

For advanced instrumental analyses through TEM and 3-D APT, the certain shape specimens should be created from the polished section of plate samples by using a dual beam focused ion beam (Helios Nanolab 600), which allows to fabricate thin and small specimen (within several nanometers) with gallium ion milling and Pt deposition [19,32–40]. In TEM analysis, the thin specimen with 100 nm thickness was used for the electron to transmit the specimen easily. The 3-D APT analyses were performed with a needle shape specimen with less than 100 nm diameter at the certain condition: 30 K～40 K (temperature), 2～14 kV (probing voltage), and 100 kHz (pulse frequency). It is conducted to reconstruct and mine the raw data through the 3-D APT data program (CAMECA)

3.3 Results

Dissimilar metal welding has significantly complex microstructures near the FB between Ni-base weld metal and LAS: austenitic dendrite structure in Ni-base weld metal, martensitic structure in heat-affected zone of LAS, and bainitic structure in parent metal of LAS (as shown in Figure IV-1). The Ni-base weld metal consists of austenitic dendrite structures formed through epitaxial growth, where the nucleation occurs at the FB as the liquid weld pool is in contact with the parent metal of LAS during the welding. In heat affected zone of LAS, the microstructural changes, such as the morphology and the size, were dependent on the thermal cycle in shielded metal arc welding consisting of rapid heating and fast cooling. Near the FB, coarse grained heat-affect zone is present due to the elevated temperature above the austenitic transformation temperature. As shown in Fig. IV-2, the FB region is located between Ni-base weld metal and LAS, representing the FB region of Alloy 182 / LAS (indicated in Fig. IV-2(a)) and Alloy 152/LAS (indicated in Fig. IV-2(b)).

Commonly, microstructures of LAS side consist of coarse grained heat affect zone and were not dependent on the type of Ni-base weld metals. It seems to be because the heat input histories during welding processes are similar as described in section III. The LAS side near the FB region, which consists of Cr-rich precipitates and LAS, is called as 'FB region' in this study, respectively. The region is within about 0.4 μm due to the low diffusivity of Cr in LAS [41].

Also, the EDS line profiles, which measured across the FB, were performed to evaluate the chemical changes by thermal aging. Figure IV-3 indicate the semi-quantitative profiles measured across

the FB between Alloy 182 Ni-base weld metal and LAS. And, figure IV-4 indicate the EDS line profiles measured across the FB between Alloy 152 Ni-base weld metal and LAS.

Usually, the dominant changes were not observed due to low temperatures heat treatment temperature (400 °C) and operation temperature (320 °C) in the primary coolant system of PWRs, which cannot cause volume diffusion [26,41]. During the thermal aging heat treatment, Cr diffusion can diffuse along interfaces such as grain boundaries or FB. Through the SEM-EDS analyses, it was too difficult to detect the slight chemical changes in the FB region due to the resolution limit of SEM-EDS.

In this reason, the 3-D APT analysis was conducted to investigate the enrichment of Cr in the FB region. Figure IV-5 are 3D atomic maps reconstructed trough 3-D APT data program (CAMECA), representing the distribution of Cr ('violet' point), C ('green' point), and Ni ('blue' point) in the FB region of Alloy 152 / LAS at as-welded and 15 y & 30 y aged weld states. In these maps, there are two different regions: (1) LAS and (2) Cr-rich precipitates consisting of the relatively many Cr and C content compared to the nearest region. To investigate the Cr enrichment in the FB region by thermal aging heat treatment, the Cr content was estimated by dividing these regions through the APT data program. The Cr concentrations were measured in the FB regions (except for the precipitates) were arranged in Fig. IV-6, representing that the Cr concentration was increased with thermal aging heat treatment. In details, the FB region at as-welded state contains about 0.5 at. % of Cr, and the Cr concentration was enriched up to 2 at. % in the FB region of HT400Y30. In that, thermal aging at 400 °C leaded to the enrichment of Cr in the FB region.

Based on the chemical compositions estimated based on 3-D APT results, JMatPro simulation was performed to expect the weight percent of the phases which are stable in the FB region, and are shown in Fig. IV-7. Based on the simulations, the FB regions consist of ferrite phase and $M_{23}C_6$ precipitate. With the enrichment of Cr in the FB region, the weight percent of the precipitates increased. In summary, it was observed that the Cr enrichment by the thermal aging heat treatment can cause the increment of the weight percent of the precipitates in the FB region.

And then, to investigate the effects of the thermal aging and Cr content in Ni-base weld metal on the precipitate's morphology in the FB region, SEM and TEM analyses were conducted and arranged in Figs. IV-8, IV-9, IV-10, and IV-11.

Figure IV-8 represents Cr-rich precipitates in the FB region of Alloy 182 / LAS aged at 400 °C during the equivalent times to the full power operating times of 0 y, 15 y and 30 y in the primary coolant system of PWRs. In the figure, the relatively bright circles (pointed with white arrows), shown as the Cr-rich precipitates. The number of Cr-rich precipitates per unit length of FB and the average size of Cr-rich precipitates were statistically by measuring the number and size of Cr-rich precipitates in the FB represented in the SEM images. Based on the results, the number of the precipitates in the FB region initially has the increment by the nucleation of the precipitates, showing 2.937 #/μm (HT400Y15, Alloy 182 / LAS) higher than 1.678 #/μm (as-welded, Alloy 182 / LAS). And then, the number was re-

decreased up to 1.469 #/μm (HT400Y30, Alloy 182 / LAS) by the coarsening of the precipitates but, the size became larger: 0.156 ± 0.023 μm (as-welded, Alloy 182 / LAS), 0.191 ± 0.068 μm (HT400Y15, Alloy 182 / LAS), and 0.370 ± 0.175 μm (HT400Y30, Alloy 182 / LAS).

Moreover, figure IV-9 represents Cr-rich precipitates in the FB region of Alloy 152 / LAS in aged weld joints at 400 ^{o}C during the equivalent times to the full power operating times of 0 y, 15 y and 30 y in the primary coolant system of PWRs. In the figure, the relatively bright circles (pointed with white arrows), shown as the Cr-rich precipitates. The number of Cr-rich precipitates per unit length of FB and the average size of Cr-rich precipitates were statistically by measuring the number and size of Cr-rich precipitates in the FB represented in the SEM images. Based on the results, the number of the precipitates in the FB region initially has the increment by the nucleation of the precipitates, showing 3.563 #/μm (HT400Y15, Alloy 152 / LAS) higher than 1.782 #/μm (as-welded, Alloy 152 / LAS). And then, the number was re-decreased up to 1.425 #/μm (HT400Y30, Alloy 152 / LAS) by the coarsening of the precipitates but, the size became larger: 0.206 ± 0.016 μm (as-welded, Alloy 152 / LAS), 0.189 ± 0.022 μm (HT400Y15, Alloy 152 / LAS), and 0.469 ± 0.080 μm (HT400Y30, Alloy 152 / LAS).

Commonly, in both the FB regions of (a) Alloy 182/LAS and (b) Alloy 152/LAS, thermal aging caused the changes of the Cr-rich precipitate morphology by Cr diffusion, indicating the peak number of the precipitates in HT400Y15 and the peak size of the precipitates in HT400Y30 among results at three heat treatment conditions. In the other words, between as-welded state and HT400Y30, the precipitation was saturated and the coarsening of the precipitates occurred.

In comparison with the FB regions of (a) Alloy 182/LAS and (b) Alloy 152/LAS, totally, the FB region of Alloy 152 / LAS has relatively large and many precipitates compared to the FB region of Alloy 182 / LAS. Alloy 152 contains 29.0 wt. % of Cr and the concentration of Cr is higher than one of Alloy 182 (14.9 wt. % of Cr). It seems that the gap of Cr content caused the slight different effects of thermal aging, respectively. The Cr-rich precipitates formed in the FB region was confirmed as $Cr_{23}C_6$ through TEM analysis, as shown in Figs. IV-10 and IV-11. It seems to be because LAS plays as a role of C source and Ni-base alloy provide Cr through grain boundary diffusion.

3.4. Discussion

To investigate the effects of long-period thermal aging and Cr content of Ni-base weld metal on the integrity of the weld joints, once microstructural characterization was conducted with the weld joints of Alloy 182 / LAS and Alloy 152 / LAS by using several techniques, including SEM, TEM, and 3-D APT. In this section, the effects of thermal aging (Section 3.4.1) on the microstructures of the FB region

will be discussed. The common features and disparities, between Alloy 182/LAS and Alloy 152/LAS, will be covered in Section 3.4.2.

3.4.1. Effects of thermal aging on the FB region

Chemical composition gradient between Ni-base weld metal and LAS is observed as shown in Figs. IV-2 and IV-3. The gradient seems not to be affected by thermal aging at 400 ºC and it is because volume or lattice diffusion cannot happen at the temperature. But, the grain boundary diffusion can occur at the temperature, resulting in that the Cr enrichment was observed in the FB region as shown in Fig. IV-4. The Cr diffusion in FB region plays an important role to cause the precipitations of the Cr-rich precipitates. Additionally, in the materials exposed to high temperature environment during the operation of nuclear power plants, Cr-rich precipitates can be formed and grown because the high temperature acted as a thermodynamic driving force, too.

In these reasons, the distribution and the size of the precipitates in the FB region were affected and dependent on the equivalent times to the full power operating times of 0 y, 15 y and 30 y in the primary coolant system of PWRs. In the SEM images and TEM images, the relatively bright and round regions were confirmed as the Cr-rich precipitates ($Cr_{23}C_6$). The number of the Cr-rich precipitates per unit length of FB and the average size of Cr-rich precipitates were statistically by measuring the number and size of Cr-rich precipitates in the FB represented in the SEM images. In both the FB regions of (a) Alloy 182/LAS and (b) Alloy 152/LAS, thermal aging caused the changes of the Cr-rich precipitate morphology by Cr diffusion, indicating the peak number of the precipitates in HT400Y15 and the peak size of the precipitates in HT400Y30 among results at three heat treatment conditions.

In that, thermal aging triggered the enrichment of Cr in the FB region and it caused additional precipitation and coarsening of the Cr-rich precipitates, affecting the morphology of the Cr-rich precipitates. The feature, described above, were observed in other materials of austenitic stainless steel and austenitic Ni-base alloy. Heat treatment can cause the addition precipitations and coarsening of Cr-rich precipitates, too. It seems thermal energy by the thermally aging and Cr diffusion can form the Cr-rich precipitates.

During thermally aging heat treatment during the equivalent time to the full power operating time of 15 y, the precipitates in the FB region were nucleated, and had the increased number of the precipitates compared to those in the as-welded weld joint due to the Cr enrichment. And, after thermally aging heat treatment during the equivalent time to the full power operating time of 30 y, the precipitate's coarsening reduced the decreased number of the precipitates and enlarged the size of the

precipitates. As the results, the number of the precipitates in HT400Y30 is small compared to the one in the as-welded weld joint.

The changes of the precipitate's morphology by the thermal aging can affect the corrosion resistance and mechanical properties of the FB region. First, on the corrosion resistance, since the Cr-rich precipitate is acknowledged to be nobble compared to LAS and can play a role as anode of galvanic cell when the precipitates located in LAS, can cause or accelerate the galvanic corrosion, resulting in the degenerated resistance of corrosion. In this way, HT400Y15, which has many precipitates or anode in the FB region compared to other weld joints, may show the low corrosion resistance compared to as-welded weld joint because the number and area of the anode accelerates the galvanic corrosion [42,43]. Then, it might be though that HT400Y30, where the precipitates show the less number but bigger size, has corrosion resistance with HT400Y15 because the area of anode or the precipitates of HT400Y30 is similar with the one of HT400Y15. The effects on the mechanical properties will be described in the next section "V. Mechanical Evaluation"

3.4.2. Effects of Ni-base weldment on the FB region

To investigate about the effects on the FB region, two types of the weld joints of Alloy182/LAS and Alloy152/LAS were prepared and heat-treated at 400 °C during the equivalent times to the full power operating times of 0 y, 15 y and 30 y in the primary coolant system of PWRs. In comparison with the FB regions of Alloy 182/LAS and Alloy 152/LAS, the common features were observed that there is the peak of the precipitate's number and the minimum size of the precipitates between two heat treatment conditions of the equivalent times to 0 y(as-welded) and 30 y of the full power operating times. In that, the saturation region of the precipitates seems to exist between the 2 conditions.

However, it is difficult to determine when dose the peak or the valley occur due to the limited result data. As the disparities of two weld joints, it seems that the precipitates in the FB region of Alloy 182 / LAS are few and smaller compared to the one of Alloy 152/LAS, totally. It seems to be because Alloy 182 has low Cr concentration compared to Alloy 152, resulting in the gap of Cr enrichment in the FB region. Thermodynamically, more Cr contents can make the Cr precipitates more stable. The Cr's enrichment in the FB region seems to be lower in Alloy 182 / LAS than in Alloy 182 / LAS.

Based on the results, the FB region of Alloy 182 / LAS might have good corrosion resistance compared to the FB region of Alloy 152 / LAS since the precipitates play roles as a galvanic corrosion source as described above. The details will be described in the next section "VI. Evaluation of Corrosion Resistance"

3.5 Conclusion

Several instrumental analyses, such as SEM, TEM, and 3-D APT, were conducted with the weld joints of Alloy 182 / LAS and Alloy 152 / LAS to investigate and Cr content of Ni-base weld metal on the integrity of the weld joints. The following conclusions can be drawn from the study.

- The area, where the Cr-rich precipitates was additionally formed and grown in LAS side near the FB, is called as “FB region”. Thermal aging causes the Cr diffusion in interface such as grain boundary and FB, resulting in formation and growth of Cr-rich precipitates in the FB region.
- In FB region, with thermal aging, the Cr-rich precipitates were additionally formed at the initial step (heat treatment during the equivalent time to the full power operating time of 15 y in the primary coolant system of PWRs) and the number density was increased. At the later step (heat treatment during the equivalent time to the full power operating time of 30 y in the primary coolant system of PWRs), the Cr-rich precipitates were coarsened and the number density was decreased.
- As the disparity between the FB regions of Alloy 182 / LAS and Alloy 152/LAS, the FB regions of Alloy 152/LAS have totally large and many Cr-rich precipitates compared to the FB regions of Alloy 182 / LAS. It might be because Alloy 152 have more Cr concentration than Alloy 182.

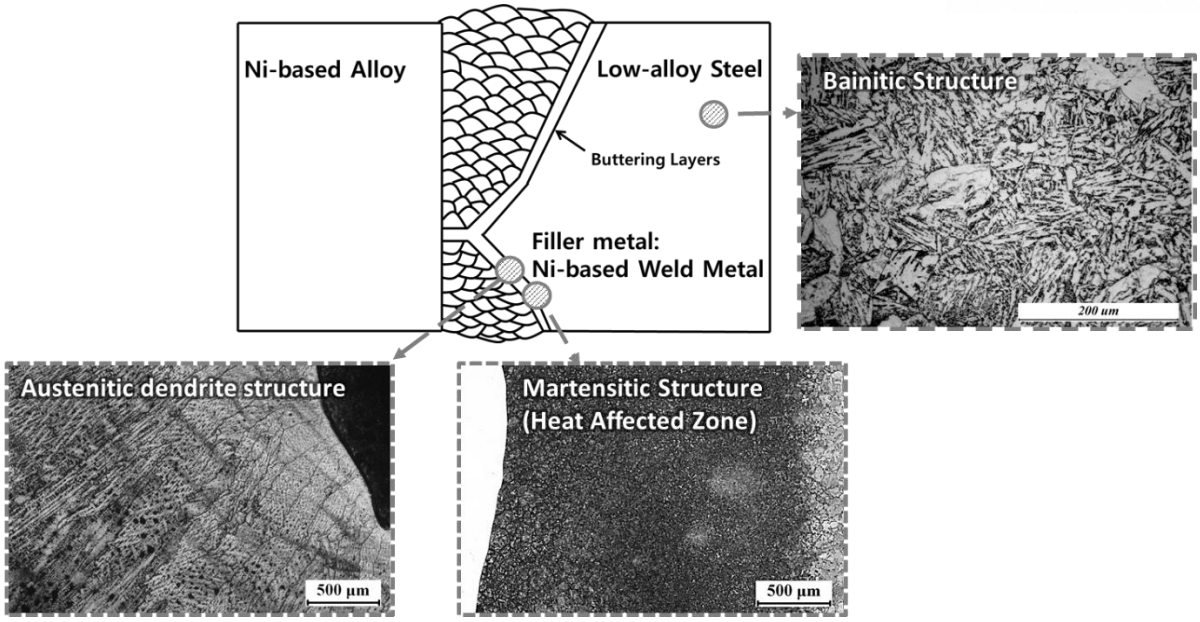

Figure III-1 Microstructures of different zones of dissimilar metal weld joint.

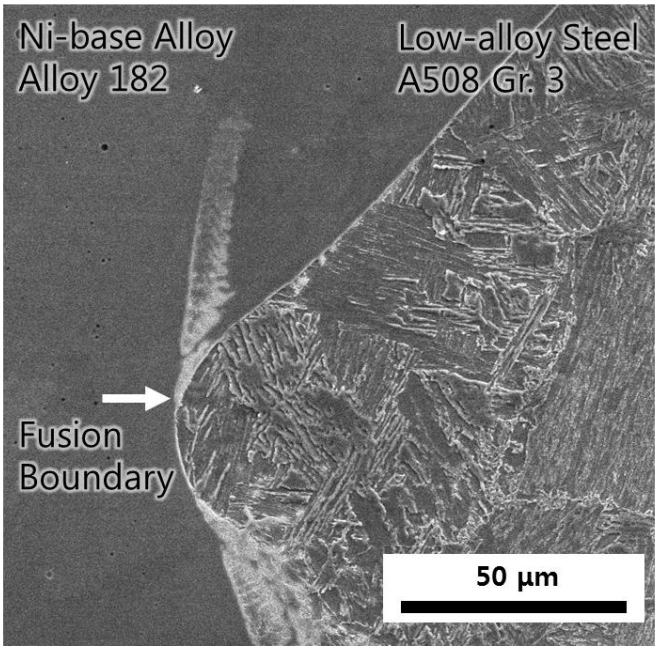

(a) FB of Alloy 182 / LAS

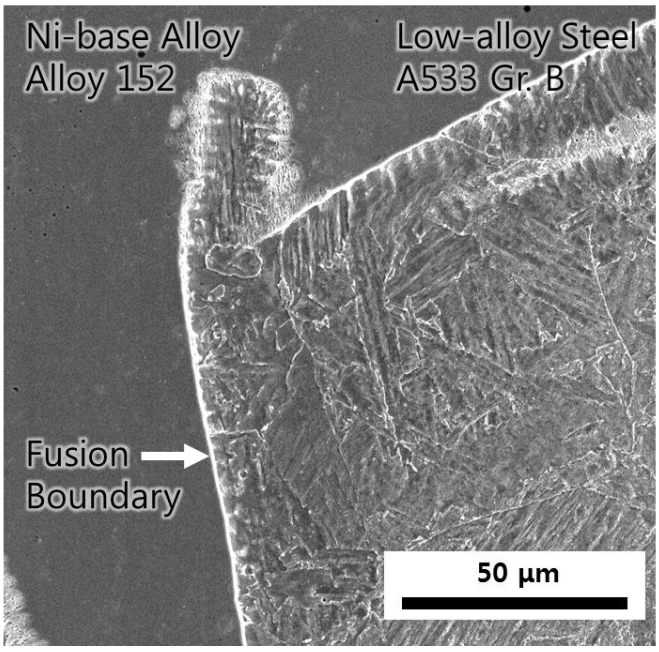

(b) FB of Alloy 152 / LAS

Figure III-2 SEM images indicating the microstructure of the as-welded joints, including austenitic Ni-base weld metal and LAS. The FB is located among the two different materials, as pointed with the white arrow.

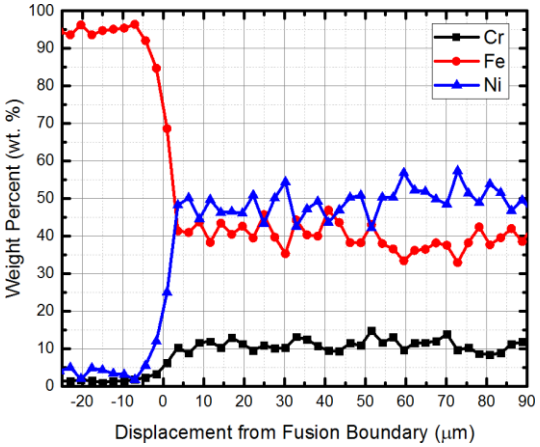

(a) As-welded DMW

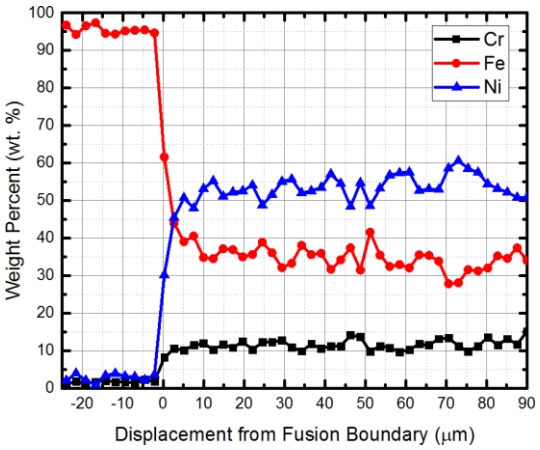

(b) HT400-Y15

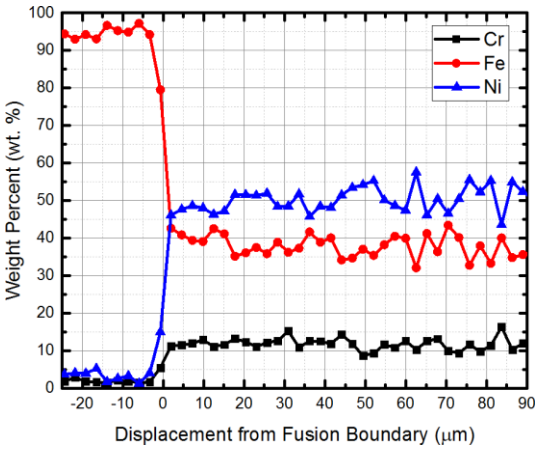

(c) HT400-Y30

Figure III-3 SEM-EDS profiles which were measured across the FB of Alloy 182 Ni-base weld metal and LAS in the as-welded and aged weld joints. The weld joints were heat treated during the equivalent times to the full power operating times of 0 y, 15 y and 30 y in the primary coolant system of PWRs

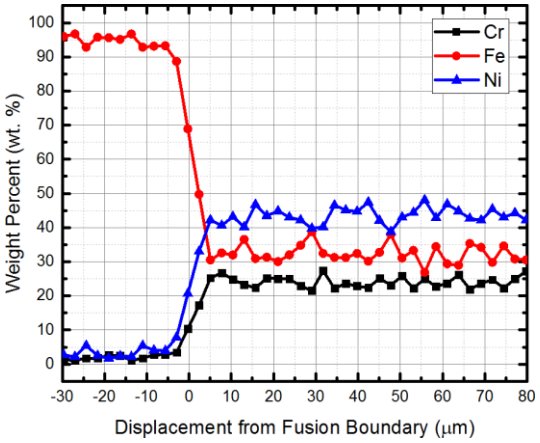

(a) As-welded DMW

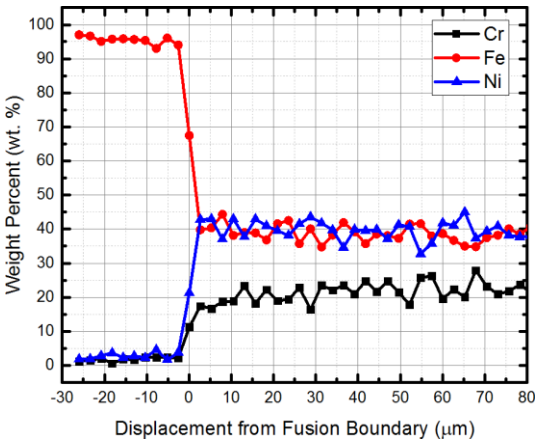

(b) HT400-Y15

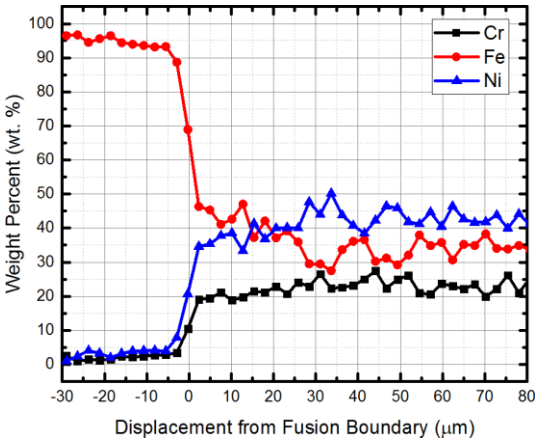

(c) HT400-Y30

Figure III-4 SEM-EDS profiles which were measured across the FB of Alloy 152 Ni-base weld metal and LAS in the as-welded and aged weld joints. The weld joints were heat treated during the equivalent times to the full power operating times of 0 y, 15 y and 30 y in the primary coolant system of PWRs.

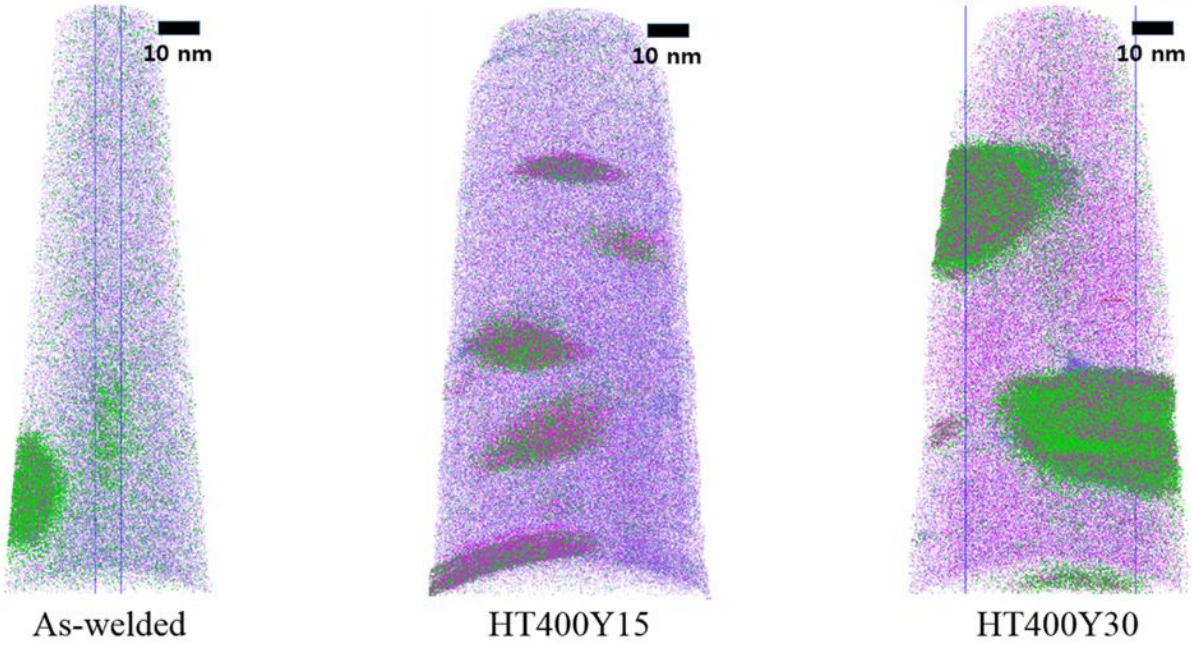

Figure III-5 Reconstructed 3-D atomic maps representing the distribution of Cr (‘violet’ point), C (‘green’ point), and Ni (‘blue’ point) in the FB region of Alloy 152 / LAS. The weld joints were heat treated during the equivalent times to the full power operating times of 0 y, 15 y and 30 y in the primary coolant system of PWRs [19].

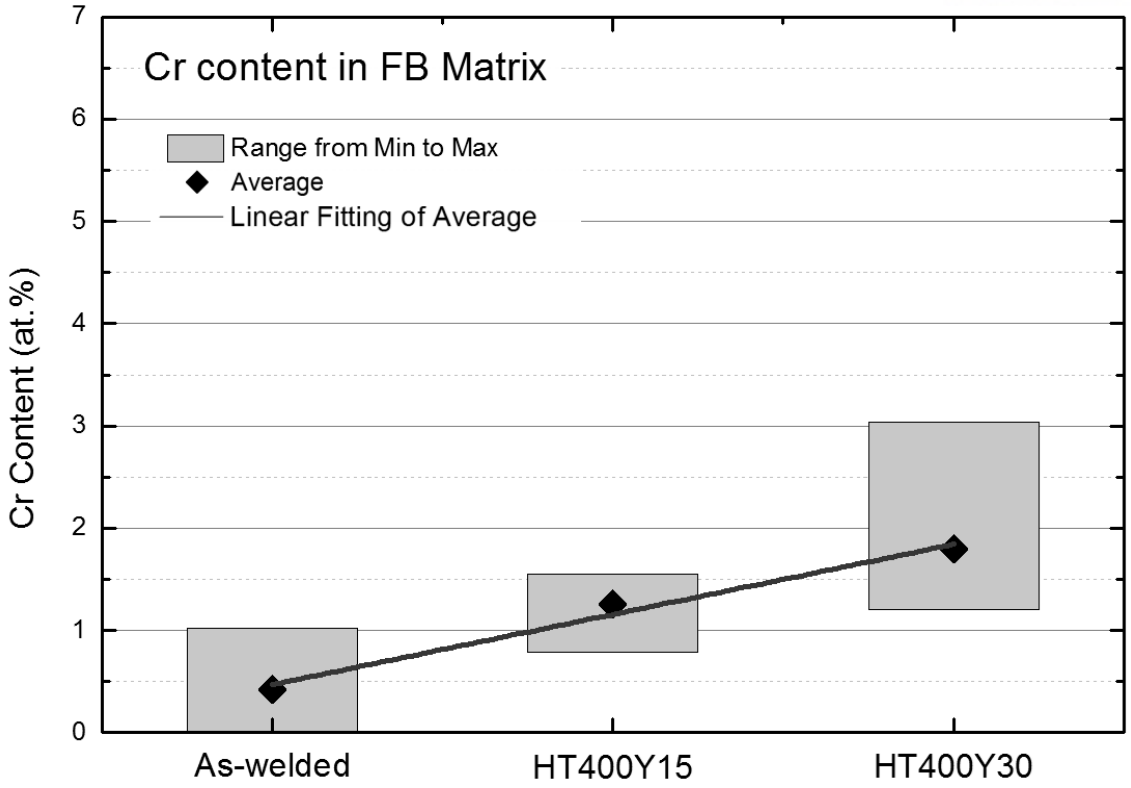

Figure III-6 Cr concentrations of the only FB region (except for Cr-rich precipitates) of Alloy 152 / LAS in as-welded and aged weld joints. The concentrations were estimated based on 3-D atomic maps (shown in Fig. III-5). The weld joints were heat treated during the equivalent times to the full power operating times of 0 y, 15 y and 30 y in the primary coolant system of PWRs [19].

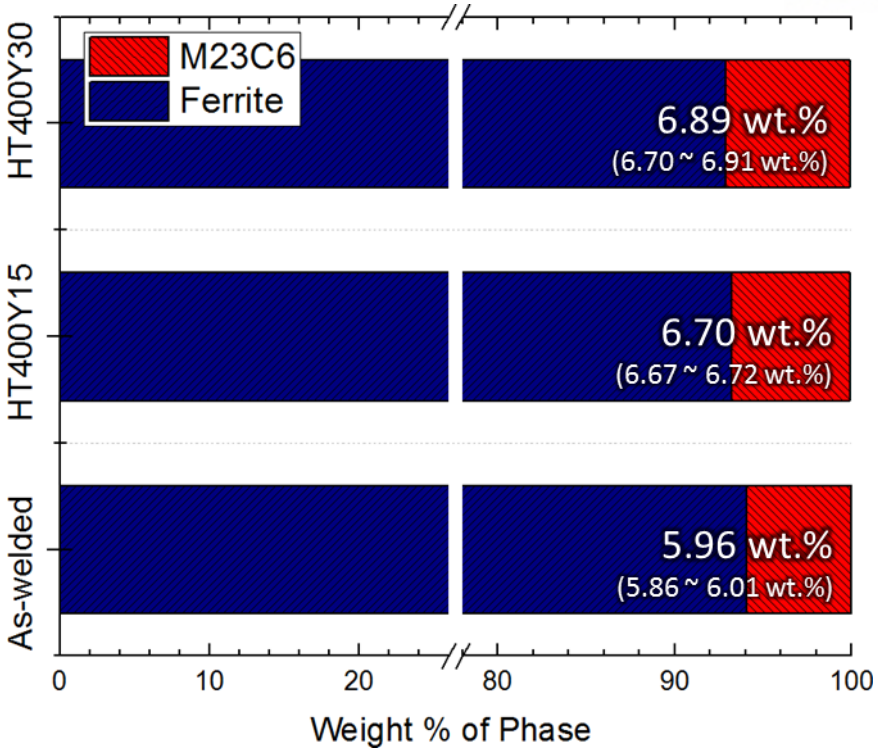

Figure III-7 Weight percent of phases in the FB regions of as-welded and aged weld joints including Alloy 152 and LAS. The JMatPro simulation was conducted with the input values: 400 ºC (temperature) and the chemical compositions of FB regions (measured through 3-D APT analysis described in Figs III-5 and III-6)

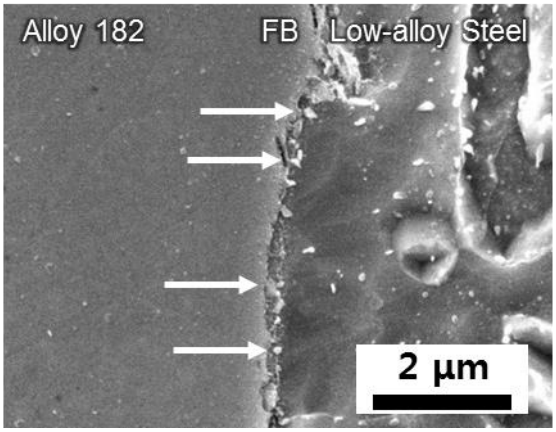

(a) As-welded DMW

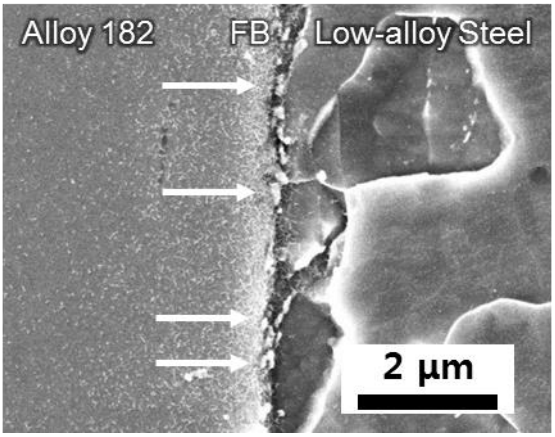

(b) HT400-Y15

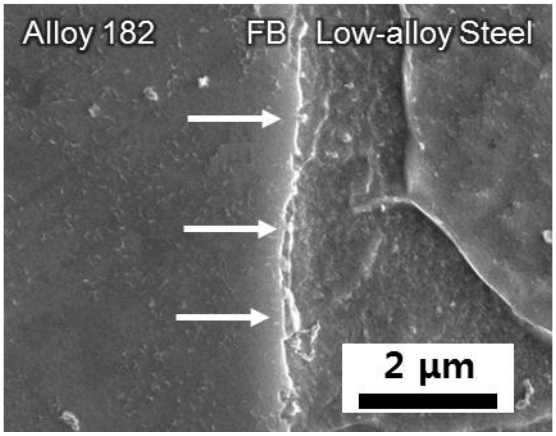

(c) HT400-Y30

Figure III-8 SEM images representing the distribution of Cr-rich precipitates in the FB region of Alloy 182 / LAS in aged weld joints at 400 ºC during the equivalent times to the full power operating times of 0 y, 15 y and 30 y in the primary coolant system of PWRs

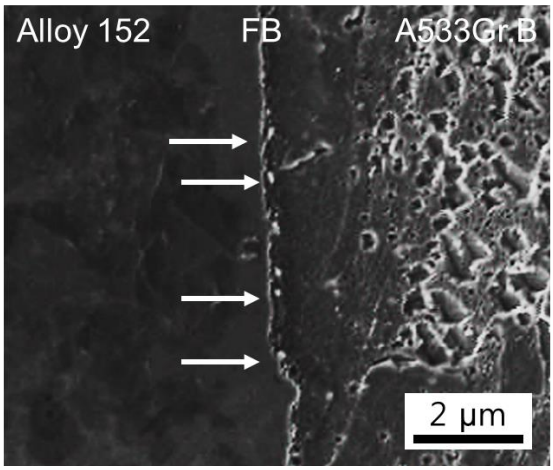

(a) As-welded DMW

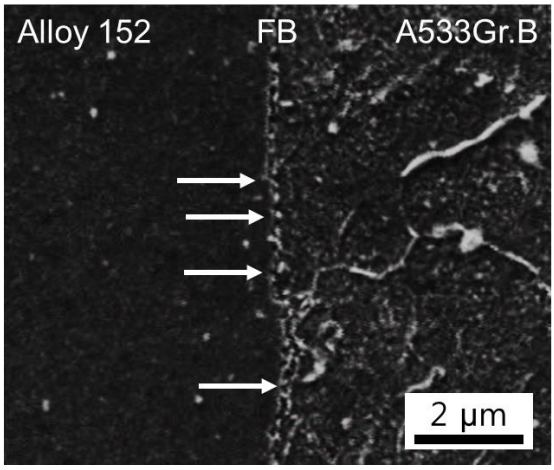

(b) HT400-Y15

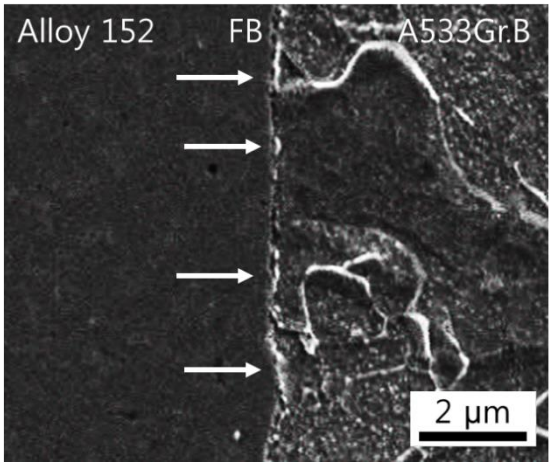

(c) HT400-Y30

Figure III-9 SEM images representing the distribution of Cr-rich precipitates in the FB region of Alloy 152 / LAS in aged weld joints at 400 ºC during the equivalent times to the full power operating times of 0 y, 15 y and 30 y in the primary coolant system of PWRs

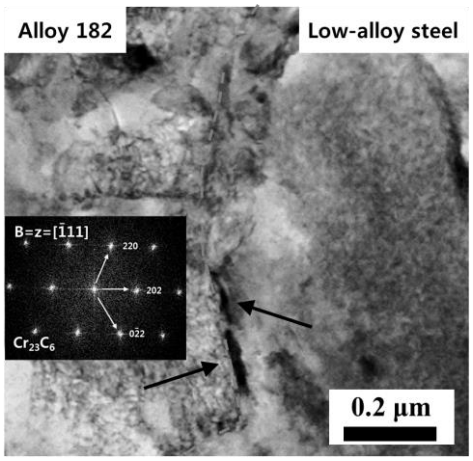

(a) As-welded DMW

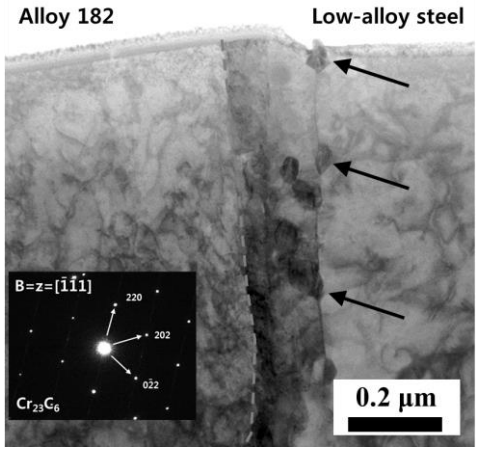

(b) HT400-Y15

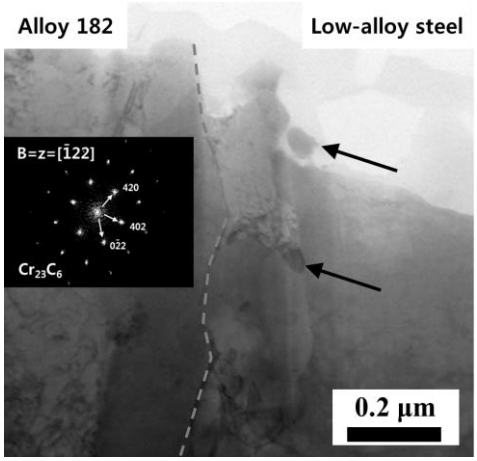

(c) HT400-Y30

Figure III-10 TEM BF images and diffraction pattern analyses indicating Cr-rich precipitates in the FB region of Alloy 182 / LAS in aged weld joints at 400 ºC during the equivalent times to the full power operating times of 0 y, 15 y and 30 y in the primary coolant system of PWRs

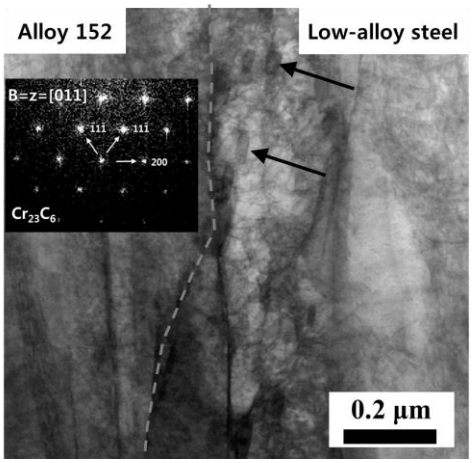

(a) As-welded DMW

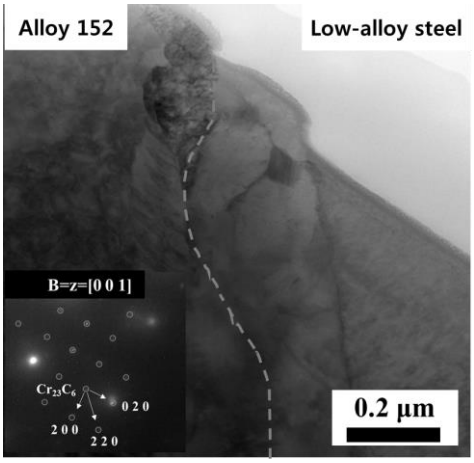

(b) HT400-Y15

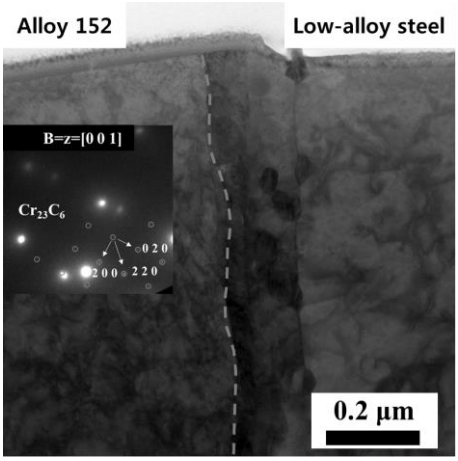

(c) HT400-Y30

Figure III-11 TEM BF images and diffraction pattern analyses indicating Cr-rich precipitates in the FB region of Alloy 152 / LAS in aged weld joints at 400 ºC during the equivalent times to the full power operating times of 0 y, 15 y and 30 y in the primary coolant system of PWRs

IV. MECHANICAL EVALUATION

4.1 Introduction

There is a concern that the fusion boundary (FB) region (consisting of low-alloy steel (LAS) and Cr-rich precipitates near FB) might be more susceptible to cracking than Ni-base weld metal which experienced frequently cracking issues in the primary coolant system of PWRs. However, the sufficient research was not conducted to evaluated the integrity of the FB region due to some reasons: (i) LAS has good resistance on the cracking compared to Ni-base weld metal and it can seem that the FB region is also resistive to the cracking, and (ii) it is difficult to investigate the resistance on the cracking in the FB region due to the narrow and un-uniform region. In addition, the FB region can additionally be degenerated by the effect of the long-period thermal aging and the replacement of Ni-base weld metal (Alloy 182 into Alloy 152) as described in Section of 'I. INTRODUCTION'. For these reasons, crack growth rate measurements were conducted varying two options: (a) the thermal aging heat treatment condition and (b) Ni-base weld metal (Alloy 182 and Alloy 152). Therefore, this study investigated the effects of long-period thermal aging and type of Ni-base weld metal on microstructures, material properties, corrosion rates and crack propagations in the FB region located between LAS and Ni-base weld metal in dissimilar metal weldments at as-welded and aged states. The weld metals were varied with Alloy 182 and Alloy 152, respectively. In this chapter, the investigation of mechanical properties was conducted and covered to improve the understanding of these effects on resistance on crack propagation in the FB region.

In case of Ni-base weld metals of Alloy 182 and Alloy 152 (which has 2 times compared to Alloy 182). As the previous study, T. Moss et al. [20,21] observed that Cr oxide of Alloy 690/Alloy 152, which includes higher Cr concentration than Alloy 600/Alloy 182, is thick and has relatively high Cr concentration due to relatively fast diffusion of Cr. It can reduce the Cr depleted zone and intergranular oxidation along grain boundaries, resulting in the improved resistances on corrosion and cracking. Although Alloy 152 was verified through many previous study for the integrity evaluation of the weld metal, resistances on corrosion and crack propagation in the FB region can be more degenerated than before the replacement of Ni-base weld metal (Alloy 182 into Alloy 152).

In addition, thermal aging in the primary coolant system of PWRs can cause Cr diffusion along grain boundary of Ni-base weld metal, resulting in the enrichment of Cr in LAS side region near the FB between Ni-base weld metal and LAS. Cr enriched region in the LAS side near FB is very narrow (about 0.4 μm) due to low diffusivity of Cr in α-Fe. Therefore, in the Cr enriched region (is called as FB region in this paper), thermal aging can affect the morphology of Cr rich precipitates, which play an important role in determining material hardness, corrosion resistance, and crack propagation. In that, thermal

aging can degenerate or enhance the resistance of the welds against crack propagation. Since the influence of the thermal aging is a key parameter affecting the crack propagation, the mechanical and microstructural investigations on the influence may improve the understanding of resistance on corrosion and crack propagation at the FB region. Hou et al. [3,14] found that the FB region, which is between Alloy 182 and LAS in an as-welded DMW, has only a few precipitates of $Cr_{23}C_6$ due to the high solubility of C in the LAS side. Nelson et al. [29–31] observed that the FB might be a potential path for crack growth due to the feature: random misorientations were measured between AISI 1080 alloy and 409 stainless steel in a dissimilar metal weld joint through SEM-EBSD.

In these regards, the thermal aging and Cr content of Ni-base weld metal are key parameters affecting the crack propagation, the mechanical investigations on the influence may improve the understanding of resistance on corrosion and crack propagation at the FB region. For these reasons, this study aims to investigate the effects of thermal aging heat treatment on the mechanical properties of (a) the FB region between Alloy 182 and LAS and (b) the FB region between Alloy 152 and LAS through nano-indentation test.

4.2 Experimental

In this study, two different DMW joints were prepared: (1) A508 Gr. 3 / Alloy 182 / Alloy 600 and (2) A533 Gr. B/Alloy 152/ Alloy 690. The bulk mock-up samples of the weld joints were cut with wire-cutting machines and electro-discharging machines to prepare 3 samples for the different heat treatments simulating the thermal aging degradations for 0 y, 15 y and 30 y. The chemical compositions of the used materials are described in Section III. 1. DMW joint of A533 Gr. B/Alloy 152/ Alloy 690 was heat-treated at 400 ºC during the equivalent times to the full power operating times of 0 y, 15 y and 30 y in the primary coolant system of PWRs, preparing the sample treated at 3 conditions. And DMW joint of A508 Gr. 3/ Alloy 182/ Alloy 600 was heat-treated at 400 during the equivalent times to the full power operating times of 0 y, 15 y and 30 y in the primary coolant system of PWRs preparing the sample treated at 3 conditions.

For evaluating mechanical properties, the plate specimens with 15(length, mm) × 15 (width, mm) × 2 (thickness, mm) were prepared through an electrical discharge machining, and then were polished with emery paper up to 9 μm (particle size), diamond paste up to 1 μm, and finally alumina powder of 0.05 μm for creating a flat section with negligible mechanical deformation. After the surface reprocesses, it was done to vibratory polish the specimen for minimizing the residual stress made during the specimen preparation, as well as achieving an even flatter surface. Since the residual stress might affect the evaluation of mechanical properties, it was minimized to obtain precise results [44].

To measure the hardness value of the very narrow region, nanoindentation testing was selected [45–51]. The tester used in this study is Agilent Technologies Nano Indenter G200 equipped with three-sided pyramidal Berkovich tip and a continuous stiffness measurement method, was used at room temperature to determine hardness values. Before the tests, the calibration of the tip geometry was conducted with a fused silica reference material. The test conditions were determined as 0.3 of Poisson's ratio, 1000 nm of total penetration depth, and 0.05 s^{-1} of a strain rate. In the graph indicating of the curve of hardness (y-axis) and penetration depth in metal (x-axis), the raw data for determining hardness values was extracted within the range of the penetration depth into metal (700 nm ~ 1000 nm). Hardness values were determined by Oliver and Pharr analysis [45–51].

To get the reliability on the results, the nanoindentation testing was measured at 15 times along the FB region and the averaged hardness values were selected to explain the effects of long-period thermal aging and type of Ni-base weld metal on the mechanical properties. In each specimen, the hardness measurements were at the FB region 15 times. The values were averaged and used to compare the mechanical properties of the FB regions of Alloy 182 / LAS and Alloy 152 / LAS.

4.3 Results

In an attempt to overcome the limitation of the indenting size, nanoindentation testing was selected to investigate the effects of long-period thermal aging and Cr content of Ni-base weld metal on the mechanical properties of the FB region. The LAS side near the FB region, which consists of Cr-rich precipitates and LAS, is called as 'FB region' in this study, respectively. The nanoindentation testing was conducted along the FB region, as described above.

Figure IV-1 represents the curve of hardness (y-axis) and penetration depth in metal (x-axis) of the FB region of Alloy 182 / LAS in aged weld joints during the equivalent times to the full power operating times of 0 y, 15 y and 30 y. In the graph indicating of the curve of hardness (y-axis) and penetration depth in metal (x-axis), the raw data for determining hardness values was extracted within the range of the penetration depth into metal (700 nm ~ 1000 nm), respectively. Hardness values were determined by Oliver and Pharr analysis [45–51]. As the results, the hardness values of the FB regions are 3.85 ± 0.01 GPa (as-welded, Alloy 182 / LAS), 4.05 ± 0.16 GPa (HT400Y15, Alloy 182 / LAS), and 2.93 ± 0.03 GPa (HT400Y30, Alloy 182 / LAS). The changes of the hardness values were observed with thermal aging heat treatment, the values initially increased after the thermal aging during the operation time 15 y (HT400Y15), and then re-decreased after thermal aging during the operation time 30 y (HT400Y30).

The tendency observed in the FB region of Alloy 182 / LAS was also shown in the FB region of Alloy 152 / LAS. Figure IV-2 represents the curve of hardness (y-axis) and penetration depth in metal

(x-axis) of the FB region of Alloy 152 / LAS of as-welded and aged weld joints at 400 ^{o}C during the equivalent times to the full power operating times of 0 y, 15 y and 30 y. As the results, the hardness values of the FB regions are 4.61 ± 0.01 GPa (as-welded, Alloy 152 / LAS), 4.80 ± 0.02 GPa (HT400Y15, Alloy 152 / LAS), and 3.88 ± 0.02 GPa (HT400Y30, Alloy 152 / LAS). The hardness values measured at the FB region initially had a slight increment after the thermal aging heat treatment corresponding to the operation time of 15 y (HT400Y15), compared to the as-welded weld joint. But it re-decreased by thermal aging heat treatment corresponding to the operation time 30 y (HT400Y30). It is similar with the results measured in the FB region of Alloy 182 / LAS, respectively.

Commonly, in both the FB regions of (a) Alloy 182 / LAS and (b) Alloy 152 / LAS, thermal aging triggered the changes of the hardness values affected by the precipitate morphology, indicating the material hardening in HT400Y15 and the re-softening in HT400Y30 among results at three heat treatment conditions. In the other words, between as-welded state and HT400Y30, the peak of hardness may exist between equivalent times to 0 y (as-welded state) and 30 y (HT400Y30) of the operation time in the primary coolant system of PWRs.

In comparison with the FB regions of (a) Alloy 182 / LAS and (b) Alloy 152 / LAS, totally, the FB region of Alloy 152 / LAS has relatively high hardness values compared to the FB region of Alloy 182 / LAS. Generally, Alloy 152 has relatively low hardness compared to Alloy 182, representing different tendency from the one in the FB region. In that, mechanical properties of Alloy 152 and Alloy 182 affects the one of the FB region slightly. Instead, as described in section IV, the FB region of Alloy 152 / LAS has relatively large and many precipitates compared to the FB region of Alloy 182 / LAS because Alloy 152 contains 29.0 wt. % of Cr and the concentration of Cr is higher than one of Alloy 182 (14.9 wt. % of Cr). It seems that the gap of hardness values was caused by the difference of the precipitate's morphology, respectively.

4.4 Discussion

To study the effects of long-period thermal aging and Cr content of Ni-base weld metal on the integrity of the weld joints, once mechanical evaluations were conducted with the weld joints of Alloy 182 / LAS and Alloy 152 / LAS through nanoindentation testing. In this section, the thermal aging effects (Section 4.4.1) on the microstructures of the FB region will be discussed. The common features and disparities, between Alloy 182 / LAS and Alloy 152 / LAS, will be covered in Section 4.4.2.

4.4.1. Effects of thermal aging on the FB region

The hardness values are dependent on the penetration depth, as shown in Figs. V-1 and V-2. Hardness values were determined by Oliver and Pharr analysis [45–51]. In both the FB regions of (a) Alloy 182 / LAS and (b) Alloy 152 / LAS, thermal aging caused the changes of the mechanical properties by the change of the precipitate morphology, indicating the material hardening in HT400Y15 and the re-softening in HT400Y30 among results at three heat treatment conditions. In the other words, between as-welded state and HT400Y30, the peak of hardness may exist between equivalent times to 0 y (as-welded state) and 30 y (HT400Y30) of the operation time in the primary coolant system of PWRs.

In general, it is known that the hardness of the FB region of Ni-base weld metal and LAS is susceptible to the thermal aging heat treatment because it can discharge the residual stress formed during manufacturing process. The thermal aging heat treatment influences the precipitate's morphology with the nucleation and coarsening. Once, the residual stress is acknowledged to cause the material hardening, but, in case of the FB region, post-weld heat treatment is performed to reduce the stress. In this reason, when the change of the mechanical properties occurs in the FB region after heat treatment, it cannot be explained with the release of the residual stress. Next, in terms on the precipitates, several previous studies [19,22,25] observed the precipitates can affect the hardness of the materials by playing as a barrier to the dislocation movement. Therefore, it seems quite plausible that the predominant factor may mechanical changes during the thermal aging, which would explain the changes observed from the nanoindentation results.

The increased number of the precipitates by the nucleation causes the increment of the hardness [20,52], which might be supported by the results of microstructural evaluations. The Cr enrichment by the thermal aging leaded to the nucleation of the precipitates, meaning the increased number of precipitates at the initial step of thermal aging (HT400Y15). Precipitates are known to act the important role in hardening materials because these are hard particles [53–55]. In this regard, it can increase the hardness values of the materials by providing barriers to dislocation movement.

The thermal aging during the equivalent times to the full power operating times of 30 y (HT400Y30), caused the re-softening of the FB region with the reduced hardness value. This seems similar with thermal aging effects on interface microstructures of Alloy 152 and LAS. Based on the previous study, it seems to can be explained. There are two type mechanisms of (1) material hardening [6,56,57] and (2) material softening [55,58–61] are explained with precipitate morphology. The precipitates disturb the movement of dislocation in the material and cut dislocations, resulting in hardening of the material. After the coarsening of the precipitates, dislocations cannot be cut by sufficiently grown precipitates. Instead, they pass through the precipitate and leave loops around it. The effect of strengthening was weaker than before, and it seems that the re-softening resulted from the reduced number of precipitates by the coarsening, respectively.

In that, the hardening of the FB region was observed due to the nucleation the Cr-rich precipitates at initial thermal aging during the equivalent times to the full power operating times of 15 y

(HT400Y15). Beyond the 15 y, the number of the precipitates was re-decreased with the coarsening of the precipitates although the size of the precipitates was relatively larger. In this regard, the re-softening of the FB region was observed in HT400Y30

The changes of the hardness values by the thermal aging can have an effect on the corrosion rate and crack growth rate of the FB region. First, the reciprocal relation of fracture toughness with hardness is generally observed in many engineering materials and is related to the energy dissipation from the enhance plasticity [62]. It is because that the enhanced plasticity by the increased hardness can keep the crack tip sharp and increase the stress intensity. When the material is under tensile residual stress and the hardness of the material is high, the applied stress will be higher due to the enhanced plasticity. Then, it can cause or accelerate the galvanic corrosion, resulting in the degenerated resistance of corrosion. In this regard, the material hardening reduces the fracture toughness by increasing the stress intensity. In addition, it can affect crack propagation rate by degenerating the fracture toughness [63]. The effects on the corrosion resistance and crack growth rate will be described in the next section "VI. Evaluation of Corrosion Resistance" and "VII. Crack Growth Rate Measurement"

4.4.2. Effects of Ni-base weldment on the FB region

To investigate about the effects on the FB region, two types of the weld joints of Alloy182 / LAS and Alloy152 / LAS were prepared and heat-treated at 400 °C during the equivalent times to the full power operating times of 0 y, 15 y and 30 y in the primary coolant system of PWRs. In comparison with the FB regions of Alloy 182 / LAS and Alloy 152 / LAS, the common features were observed that there is the peak of the hardness values between two heat treatment conditions of the equivalent times to 0 y (as-welded) and 30 y of operation time.

However, it is difficult to determine when dose the peak or the valley occur due to the limited result data. As the disparities of two weld joints it seems that the hardness values in the FB region of Alloy 182 / LAS are low compared to the one of Alloy 152 / LAS, totally. It seems to be because the FB region of Alloy 152 and LAS has relatively many precipitates compared to the FB region of Alloy 182 and LAS, resulting in the hardening in the FB region. As mentioned before, the precipitates (hard particles) disturb the dislocation movement and cut dislocations, leading to the material hardening.

Based on the results, the FB region of Alloy 182 / LAS might have good resistances on corrosion and crack propagation compared to the FB region of Alloy 152 / LAS. First, the reciprocal relation of fracture toughness with hardness is generally observed in many engineering materials and is related to the energy dissipation from the enhance plasticity [62]. It can cause or accelerate the galvanic corrosion, resulting in the degenerated resistance of corrosion, respectively. In addition, it can affect crack

propagation rate by degenerating the fracture toughness [63]. The effects on the corrosion resistance and crack growth rate will be described in the next section "V. Evaluation of Corrosion Resistance" and "VI. Crack Growth Rate Measurement"

4.5 Conclusion

To investigate the effects of long-period thermal aging and Cr content of Ni-base weld metal on the integrity of the weld joints, nanoindentation testing in the FB regions of Alloy 182 / LAS and Alloy 152 / LAS, were performed. The following conclusions can be drawn from the study.

- The area, where the Cr rich precipitates were additionally formed and grown in LAS side near the FB, is called as "FB region". Thermal aging causes the Cr diffusion in interface such as grain boundary and FB, resulting in formation and growth of Cr rich precipitates in the FB region.
- In FB region, with thermal aging, the hardness was increased at the initial step (heat treatment during the equivalent time to the full power operating time of 15 y in the primary coolant system of PWRs) because the number of the Cr rich precipitates, which play a role as a barrier to dislocation's movement, was increased. At the later step (heat treatment during the equivalent time to the full power operating time of 30 y in the primary coolant system of PWRs), the hardness was reduced since the number of the Cr rich precipitates was decreased by the coarsening of the precipitates.
- As the disparity between the FB regions of Alloy 182 / LAS and Alloy 152 / LAS, the FB regions of Alloy 152 / LAS have totally high hardness values compared to the FB regions of Alloy 182 / LAS. It might be because the FB regions of Alloy 152 / LAS have more Cr rich precipitates than the FB of Alloy 182 / LAS.

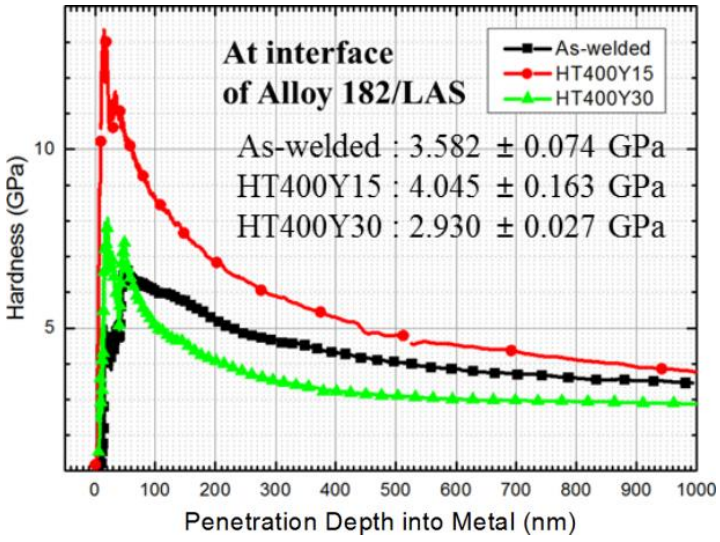

(a) Total sequence

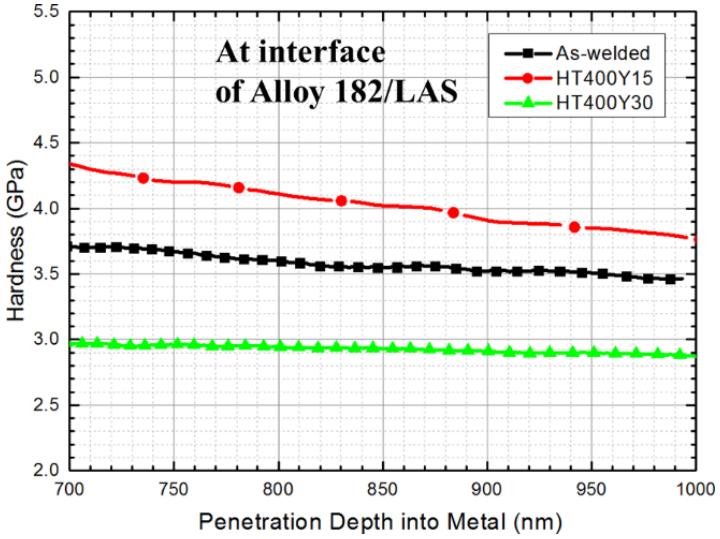

(b) Magnified sequence

Figure IV-1 Curves of hardness-penetration depth of the FB region of Alloy 182 / LAS of aged weld joints at 400 ºC during the equivalent times to the full power operating times of 0 y, 15 y and 30 y in the primary coolant system of PWRs, respectively.

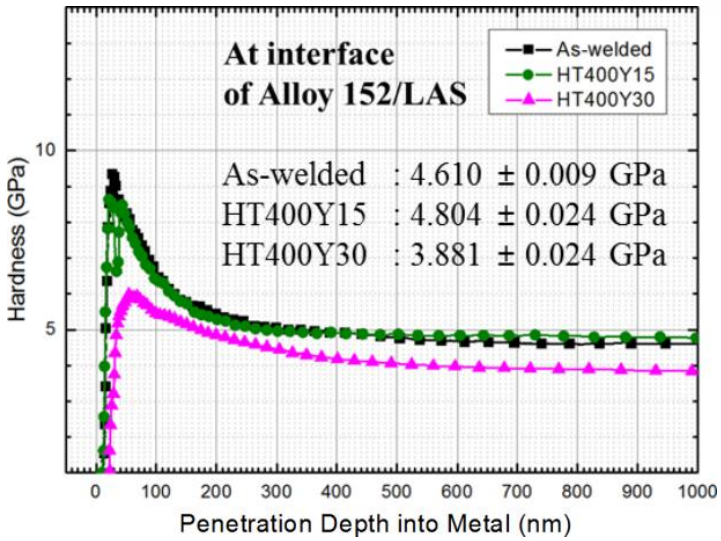

(a) Total sequence

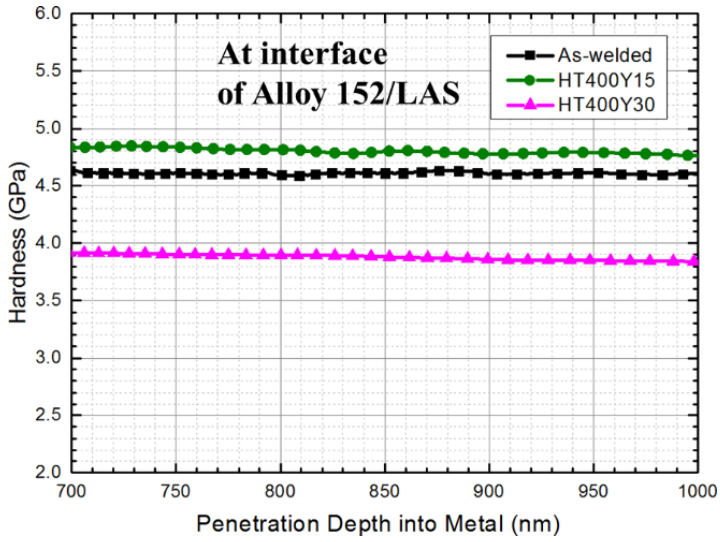

(b) Magnified sequence

Figure IV-2 Curves of hardness-penetration depth of the FB region between Alloy 182 weld metal and LAS of aged weld joints at 400 °C during the equivalent times to the full power operating times of 0 y, 15 y and 30 y in the primary coolant system of PWRs, respectively.

V. EVALUATION OF CORROSION RESISTANCE

5.1 Introduction

There is a concern that the fusion boundary (FB) region (consisting of low-alloy steel (LAS) and Cr-rich precipitates near FB) might be more susceptible to cracking than Ni-base weld metal which experienced frequently cracking issues in the primary coolant system of PWRs. However, the sufficient research was not conducted to evaluated the integrity of the FB region due to some reasons: (i) LAS has good resistance on the cracking compared to Ni-base weld metal and it can seem that the FB region is also resistive to the cracking, and (ii) it is difficult to investigate the resistance on the cracking in the FB region due to the narrow and un-uniform region. In addition, the FB region can additionally be degenerated by the effect of the long-period thermal aging and the replacement of Ni-base weld metal (Alloy 182 into Alloy 152) as described in Section of 'I. INTRODUCTION'. For these reasons, crack growth rate measurements were conducted varying two options: (a) the thermal aging heat treatment condition and (b) Ni-base weld metal (Alloy 182 and Alloy 152). Therefore, this study investigated the effects of long-period thermal aging and type of Ni-base weld metal on microstructures, material properties, corrosion rates and crack propagations in the FB region located between LAS and Ni-base weld metal in dissimilar metal weldments at as-welded and aged states. The weld metals were varied with Alloy 182 and Alloy 152, respectively. In this chapter, the investigation on corrosion resistances was conducted and covered to improve the understanding of these effects on resistance on crack propagation in the FB region.

In case of Ni-base weld metals of Alloy 182 and Alloy 152 (which has 2 times compared to Alloy 182). As the previous study, T. Moss et al. [20,21] observed that Cr oxide of Alloy 690/Alloy 152, which includes higher Cr concentration than Alloy 600/Alloy 182, is thick and has relatively high Cr concentration due to relatively fast diffusion of Cr. It can reduce the Cr depleted zone and intergranular oxidation along grain boundaries, resulting in the improved resistances on corrosion and cracking. Although Alloy 152 was verified through many previous study for the integrity evaluation of the weld metal, resistances on corrosion and crack propagation in the FB region can be more degenerated than before the replacement of Ni-base weld metal (Alloy 182 into Alloy 152).

In addition, thermal aging in the primary coolant system of PWRs can cause Cr diffusion along grain boundary of Ni-base weld metal, resulting in the enrichment of Cr in LAS side region near the FB between Ni-base weld metal and LAS. Cr enriched region in the LAS side near FB is very narrow (about 0.4 μm) due to low diffusivity of Cr in α-Fe. Therefore, in the Cr enriched region (is called as FB region in this paper), thermal aging can affect the morphology of Cr rich precipitates, which play an important role in determining material hardness, corrosion resistance, and crack propagation. In that, thermal

aging can degenerate or enhance the resistance of the welds against crack propagation. Since the influence of the thermal aging is a key parameter affecting the crack propagation, the mechanical and microstructural investigations on the influence may improve the understanding of resistance on corrosion and crack propagation at the FB region. Hou et al. [3,14] found that the FB region, which is between Alloy 182 and LAS in an as-welded DMW, has only a few precipitates of $Cr_{23}C_6$ due to the high solubility of C in the LAS side. Nelson et al. [29–31] observed that the FB might be a potential path for crack growth due to the feature: random misorientations were measured between AISI 1080 alloy and 409 stainless steel in a dissimilar metal weld joint through SEM-EBSD.

In these regards, the thermal aging and Cr content of Ni-base weld metal are key parameters affecting the resistances on corrosion and crack propagation, the evaluation of corrosion resistance may improve the understanding of resistance on crack propagation at the FB region. For these reasons, this study aims to investigate the effects of thermal aging heat treatment on the corrosion resistance of (a) the FB region between Alloy 182 and LAS and (b) the FB region between Alloy 152 and LAS through potentiodynamic electropolarization using a potentiostat.

5.2 Experimental

In this study, two different DMW joints were prepared: (1) A508 Gr. 3 / Alloy 182 / Alloy 600 and (2) A533 Gr. B/Alloy 152/ Alloy 690. The bulk mock-up samples of the weld joints were cut with wire-cutting machines and electro-discharging machines to prepare 3 samples for the different heat treatments simulating the thermal aging degradations for 0 y, 15 y and 30 y. The chemical compositions of the used materials are described in Section III. 1. DMW joint of A533 Gr. B/Alloy 152/ Alloy 690 was heat-treated at 400 ºC during the equivalent times to the full power operating times of 0 y, 15 y and 30 y in the primary coolant system of PWRs, preparing the sample treated at 3 conditions. And DMW joint of A508 Gr. 3/ Alloy 182/ Alloy 600 was heat-treated at 400 during the equivalent times to the full power operating times of 0 y, 15 y and 30 y in the primary coolant system of PWRs preparing the sample treated at 3 conditions.

For evaluating corrosion resistance, the plate specimens with 15 (length, mm) × 15 (width, mm) × 2 (thickness, mm) were prepared through an electrical discharge machining, and then were polished with emery paper up to 9 μm (particle size), diamond paste up to 1 μm, and finally alumina powder of 0.05 μm for creating a flat section with negligible mechanical deformation. After the surface reprocesses, it was done to vibratory polish the specimen for minimizing the residual stress made during the specimen preparation, as well as achieving an even flatter surface.

To investigate the corrosion behaviors in FB regions of Alloy 182/LAS and Alloy 152/LAS, several types of corrosion tests, such as polarization test, exposure test were conducted.

Firstly, to investigate the effect of Ni-base alloy on galvanic corrosion in the FB regions, COMSOL Multiphysics was used to simulate galvanic corrosion of the FB region. Since the simulation requires the Tafel fitting results of Alloy 182, Alloy 152 and LAS and water chemistry of primary water section in nuclear power plants, the corrosion characteristics of Alloy 182, Alloy 152 and LAS in room-temperature water were investigated by potentiodynamic polarization using a PAR 273A potentiostat (Princeton Applied Research, US) and a Solartron 1260A impedance analyzer (Solartron Analytical, US). For room-temperature water tests, the solution, containing 2 ppm (mg/kg) Li, 1200 ppm (mg/kg) B, was prepared as an electrolyte. The electrolyte was purged with a high-purity Ar gas to suppress the effects of dissolved oxygen (DO). In this test system, reference and counter electrodes are a saturated calomel electrode and Pt mesh, respectively. Figure V-1 shows the corrosion cell, where a three-electrode system was installed with a 0.1 M KCl filled external Ag/AgCl electrode (Corr Instruments, US) and a Pt mesh, which are the reference and counter electrodes, respectively. Contact area of working electrodes was 1 cm^2.

Next, polarization tests were performed in room-temperature water and high-temperature water with 2 ppm (mg/kg) Li, 1200 ppm (mg/kg) B to evaluate the corrosion features of the FB regions of Alloy 182/LAS and Alloy 152/LAS. The corrosion characteristics of the FB region were evaluated in an autoclave system specially fabricated for this study, as shown schematically in Figure V-2(a). And, it was performed by potentiodynamic polarization using a PAR 273A potentiostat (Princeton Applied Research, US) and a Solartron 1260A impedance analyzer (Solartron Analytical, US), respectively. To to simulate primary water environment, recirculation loop system was entirely instrumented to measure and control electrical conductivity, pH, dissolved oxygen, and dissolved hydrogen for both the inlet and outlet water and is shown in Figure V-2 (a), which help the experimental environment to be maintained at conditions of 25 cm^3/kg of dissolved hydrogen concentrations, < 5 ppb of dissolved oxygen, 2 ppm (mg/kg) Li, 1200 ppm (mg/kg) B, 320 °C, and 17.5 MPa. Suitable amount of lithium hydroxide monohydrate (LiOH) and boric acid (H_3BO_3) were inserted in dilated water to prepare the primary coolant in the primary coolant system of PWRs and electrical conductivity of this solution was maintained within 21 ~ 22 μS/cm. Figure V-2 (b) shows the corrosion cell, where a two-electrode system was installed with a Pt mesh, which is the reference and counter electrodes. Contact area of working electrodes was 4 cm^2.

Lastly, exposure experiments were performed by measuring the weight change of as-welded and aged specimens, containing the FB region of Alloy 182/LAS and Alloy 152/LAS, after the exposure to primary water environment for 750 h, which condition was maintained with loop control system (shown in VI-2(a)) as described above.

5.3 Results

In this section, the results of corrosion test, which were conducted to investigate the effects of long-period thermal aging and Cr content of Ni-base weld metal on corrosion resistances of the FB regions, are described below.

To begin with, the corrosion characteristic evaluation of each material, such as Alloy 182, Alloy 152 and LAS, were performed to investigate the type of Ni-base weld metal on galvanic corrosion in the FB region. If two dissimilar materials are immersed in a corrosive solution, each material will a develop an electrochemical potential. When the electrochemical potentials of the two materials are significantly different, the more active material will act as the anode and the more noble material will act as the cathode. In case of the weld joint used in this study, LAS is more active metal and plays a role of the anode and Ni-base alloy steel is more noble metal and plays a role of the cathode. Also, dissimilar metals in close physical proximity typically suffer bigger galvanic effects than those which are father apart. It is called as "distance effect" and is dominant when the conductivity of the solution is low since the path of current flow is a main consideration [43,42]. In primary water section of the primary coolant system of PWRs, the conductivity is about 21 μS/cm, which is very low value. In this regard, the FB region can be susceptible to the galvanic corrosion when the region is exposed to corrosive environment.

Therefore, the corrosion characteristic evaluation of each material was performed through potentiodynamic polarization test and used to COMSOL Multiphysics for simulating the galvanic corrosion in the FB region. Figure V-3 represents potentiodynamic electro-polarization curves for the samples of Alloy 182, Alloy 152 and LAS in room temperature water with 1200 ppm of B and 2 ppm of Li. Alloy 152 was the most nobble compared to Alloy 182 and LAS. And LAS is the most active compared to Alloy 182 and Alloy 152. It means that the potential gap between Alloy 182 and LAS is smaller than the one between Alloy 152 and LAS. Tafel fitting results of the electropolarization curves arranged in Table VI-1 and the primary water chemistries were to simulate galvanic corrosion with COMSOL Multiphysics, respectively. As the results shown in Figure V-4, it simulated the galvanic corrosions of weld joints at as-welded state exposed to primary water environment of nuclear power plants for 1,000h, resulting in that the FB region of Alloy 152 and LAS suffers greater galvanic effects that the one of Alloy 182 and LAS since the potential gap between Alloy 182 and LAS is smaller than the one between Alloy 152 and LAS.

However, it is a difficulty about evaluating the corrosion characteristic of the FB region with only COMSOL Multiphysics. So, additional potentiodynamic electro-polarization tests were performed with the specimens of 7mm (width) × 30 mm (length) × 3 mm (thickness), which have 1:1 of Ni-base weld metal and LAS surface area for minimizing variable factors. Figure V-5 Potentiodynamic electro-polarization curves for the FB regions of Alloy 182/LAS and Alloy 152/LAS in room temperature water with 1200 ppm of B and 2 ppm of Li. Tafel fitting results of the electropolarization curves arranged in Table VI-2. Once, in the result of FB region of LAS and Alloy 182, the corrosion resistance (R_P)

decreased, but corrosion rate (I_0) increased with thermal aging heat treatment, representing that the corrosion rate increased after heat treatment time equivalent to 15 y, but re-decrease after one to 30 y. Also, in the result of FB region of LAS and Alloy 152, the corrosion resistance (R_P) decreased, but corrosion rate (I_0) increased with thermal aging heat treatment, representing that the corrosion rate increased after heat treatment time equivalent to 15 y, but re-decrease after one to 30 y. the Tafel fitting results are converted to corrosion rate by Faraday's law. The equation for calculating corrosion rate (anode metal dissolution rate) is (atomic weight of the metal) × (corrosion current: i_{corr}) × (the charge number of which indicate the number of electron exchanged in the dissolution reaction)$^{-1}$ × (Faraday constant)$^{-1}$ × (density of the metal)$^{-1}$. Based on this equation, the corrosion rates are dependent on corrosion current value and arranged in Figure V-6.

Commonly, thermal aging affected corrosion rates by changing the precipitate morphology, indicating the degenerated corrosion resistance in HT400Y15 and the re-covered corrosion resistance in HT400Y30 among results at three heat treatment conditions. In the other words, the peak of corrosion rates may exist between equivalent times to 0 y (as-welded state) and 30 y (HT400Y30) of the operation time in the primary coolant system of PWRs. It seems that the corrosion resistance was affected from the changes of the Cr rich precipitate's morphology.

In comparison with the FB regions of (a) Alloy 182/LAS and (b) Alloy 152/LAS, totally, the FB region of Alloy 152/LAS has relatively high corrosion rate compared to the FB region of Alloy 182/LAS. Generally, Alloy 152 has relatively low corrosion rate compared to Alloy 182, representing different tendency from the one in the FB region. In that, corrosion characteristic of Alloy 152 and Alloy 182 affects the one of the FB region slightly. In that, the FB region of Alloy 152 and LAS suffers greater galvanic effects that the one of Alloy 182 and LAS since the potential gap between Alloy 182 and LAS is smaller than the one between Alloy 152 and LAS, respectively.

Although the results obtained in room temperature test show the similar corrosion behavior, there may be the gap between room temperature water test and high temperature water test. In this reason, potentiodynamic electro-polarization tests in high temperature water were performed for verification of the test in room temperature water. Figure V-7 represents potentiodynamic electro-polarization curves for the FB regions of Alloy 182/LAS and Alloy 152/LAS in primary water chemistry of nuclear power plants. The Tafel fitting results of the electropolarization curves arranged in Table VI-3. The results are also converted to corrosion rates, which are similar with the results in room temperature water, indicating, the peak of corrosion rates may exist between equivalent times to 0 y (as-welded state) and 30 y (HT400Y30) of the operation time in the primary coolant system of PWRs. Totally, the FB region of Alloy 152/LAS has relatively high corrosion rate compared to the FB region of Alloy 182/LAS.

The effects of thermal aging on corrosion behavior of the FB region show same trend that there are the peak of harness and the peak number of Cr rich precipitates between as-welded state and HT400Y30 (thermally aged at 320 °C for 30 y). In this regard, the changes of the precipitate morphology

may affect the corrosion behavior by playing a role of the additional cathode. Cr rich precipitates is the more nobble metal than LAS and Ni-based weld metal. The additional precipitation can mean the increased number of the cathode metal. During the heat treatment, the additional precipitation in HT400Y15 increased the number of the precipitates, but the coarsening of the precipitates in HT400Y30 reduced the number of the precipitates but the size of the precipitates was increased. The area of the precipitates was increased at the initial step (HT400Y15), but was maintained at later step (HT400Y30). It means that the cathode area (the area of the precipitates) increased at the initial step, and it was maintained at the later step.

In this reason, the simple test was performed to evaluate the effects of the cathode area and contact area of anode and cathode by using 13 discs with 20 mm of diameter and 1 mm thickness, consist of stainless steel 316L (cathode) and A508 Gr. 3 LAS (anode). Figure V-10 shows Schematics of specimens for galvanic corrosion test evaluating the effects of the cathode surface and contact surface. As shown in the figure, three specimens were prepared and exposed to HNO_3 for 148 h. Figure V-11 represent Picture of specimens, which shown in Figure V-10, after the exposure in HNO_3 for 148 h and weight loss is dependent on the cathode surface and contact surface on galvanic corrosion. In Figure V-10 (a), the relatively bright region is stainless steel or cathode and dark region represent LAS, which was mainly dissolved during the exposure. To confirm which one suffered the most severe galvanic corrosion, weight loss per unit anode area was measured by comparing the weights before and after the exposure. As the results, the specimen with 6/7 of cathode/anode surface ratio show large amount of dissolution compared to the one with 2/11 of cathode/anode surface ratio. In that, the increase cathode area accelerates the galvanic corrosion. And, when the contact surface between anode and cathode was decreased but the cathode area was not changed, the weight loss was reduced. It means that the contact surface can affect the galvanic corrosion by distance effect although the area of precipitates was maintained.

5.4 Discussion

To investigate the effects of long-period thermal aging and Cr content of Ni-base weld metal on the integrity of the weld joints, several techniques, including potentiodynamic electro-polarization at room temperature water and high temperature water, COMSOL Multiphasic, Huey test, and exposure test, were used in this study. In this section, the effects of thermal aging (Section 5.4.1) on the corrosion resistances of the FB region will be discussed. The common features and disparities, between Alloy 182/LAS and Alloy 152/LAS, will be covered in Section 5.4.2.

5.4.1. Effects of thermal aging on the FB region

Since the FB region (active metal) is located next to Ni-base weld metal (noble metal) and includes the Cr rich precipitates (noble metal), selective corrosion in the FB region occur by the effect of the galvanic corrosion. The corrosion testes, performed with the specimen of the dissimilar metal weld joint, represents the carrion rate of the FB region. Based on the results of potentiodynamic electro-polarization at room temperature water and high temperature water, and exposure test, thermal aging affected corrosion rates and it seems to be affected by the precipitate morphology, indicating the degenerated corrosion resistance in HT400Y15 and the re-covered corrosion resistance in HT400Y30 among results at three heat treatment conditions. In the other words, the peak of corrosion rates may exist between equivalent times to 0 y (as-welded state) and 30 y (HT400Y30) of the operation time in the primary coolant system of PWRs. It indicates the same tendency with the one of microstructural changes (the precipitate morphology).

In detail, when the number of Cr-rich precipitates in the FB region was increased after the heat treatment during the full power operating time of 15 y in the primary coolant system of PWRs, the corrosion rate of the FB region was accelerated with the increased number of the precipitates. The precipitates formed in the FB region is more noble metal than the FB region matrix including the chemical composition similar with LAS. It is thought for the precipitates to cause galvanic corrosion by playing as a role of cathode in galvanic cell. The increase of the cathode area may accelerate the galvanic corrosion, resulting in the degenerated corrosion resistance of the FB region in HT400Y15. For example, when a small LAS (anode, active material) is buttered with a large weld metal (cathode, noble material), it will result in a high current density or a high rate of corrosion on the anode. The corrosion is concentrated by the area difference. In that, the additional precipitation during the heat treatment can increase the corrosion rates as shown in Figs. V-5, V-7 and V-9 by widening the cathode area. In addition, the increased number of the precipitates or the cathodes by the additional precipitation in the FB also extends the contact surfaces between LAS and the cathodes (Cr rich precipitates), leading to the accelerated corrosion rates. There are the related previous studies to support it. Dissimilar metals in close physical proximity usually suffer greater galvanic effects than those which are father apart. It is called as “distance effect” and is dominant when the conductivity of the solution is low since the path of current flow is a main consideration [43,42]. The increased number of the precipitates increase the cathode area and the contact surface of the anode (LAS) and the cathode (Ni-base alloy), resulting in the accelerated corrosion rate of the FB region. In the other words, since the additional precipitation in the FB region after the heat treatment during the full power operating time of 15 y in the primary coolant system of PWRs widens the cathode area and the contact surface of the cathode and the anode, the corrosion rate of HT400Y15 seems to be fast compared to as-welded weld joint (0 y). The results of the simple Huey test also show the effects of the contact surface as shown Figure V-11 and IV-12

representing the more weight loss was shown in specimen with 6 of contact surface between anode and cathode (Figure V-11(b)) compared to the specimen with 4 of the contact surface (Figure V-11(c))

Then, when the number of Cr-rich precipitates in the FB region was re-decreased after the heat treatment during the full power operating time of 30 y in the primary coolant system of PWRs, the corrosion rate of the FB region of HT400Y30 was reduced with the decreased number of the precipitates, compared to HT400Y15. It may be explained with the number of the Cr rich precipitates, which was reduced after the heat treatment during the full power operating time of 30 y. But, the reduced number of the precipitates does not mean the enlarged cathode area. Although the number was reduced in HT400Y30, it was caused by the coarsening of the precipitates and HT400Y15 and HT400Y30 have the similar area of the precipitates in the FB regions. So, in this case, the cathode area cannot explain the recovered corrosion resistance. Instead, the reduced number of the precipitates can reduce the contact surface of the cathode and the anode, and it can cause the gap between the corrosion resistances of HT400Y15 and HT400Y30. As described above, dissimilar metals in close physical proximity usually suffer greater galvanic effects than those which are father apart. It is called as “distance effect” and is dominant when the conductivity of the solution is low since the path of current flow is a main consideration [43,42]. The increase of the contact surface means the increased area where dissimilar metals in close physical proximity. In this regard, between HT400Y15 and HT400Y30, the contact surface was reduced by the coarsening of the precipitates and the corrosion resistance was removed. The results of the simple Huey test also show the effects of the cathode area as shown Figure V-10 and IV-11 representing the more weight loss was shown in specimen with 2/11 of cathode/anode surface ratio (Figure V-11(c)) compared to the specimen with 6/7 of cathode/anode surface ratio (Figure V-11(b)).

The changes of the corrosion resistance by the thermal aging can affect the crack growth rate of the FB region. The crack propagation in the primary coolant environment of the primary coolant system of PWRs include the fracture of the metal and dissolution of the metal. In that, when the corrosion resistance become severely low, the crack growth rate can be accelerated by the fast dissolution rate of the metal. The detailed effects on the crack growth rates will be described in the next section “VI. Crack Growth Rate Measurements”

5.4.2. Effects of Ni-base weldment on the FB region

To investigate about the effects on the FB region, two types of the weld joints of Alloy182/LAS and Alloy152/LAS were prepared and heat-treated at 400 °C during the equivalent times to 0 y, 15 y, and 30 y of operation time. In comparison with the FB regions of Alloy 182/LAS and Alloy 152/LAS,

the common features were observed that there is the peak of the crack growth rates between two heat treatment conditions of the equivalent times to 0 y(as-welded) and 30 y of operation time. However, it is difficult to determine when dose the peak or the valley occur due to the limited result data.

As the disparities of two weld joints, it seems that the corrosion rates in the FB region of Alloy 182/LAS are lower compared to the one of Alloy 152/LAS, totally. It seems to be because the FB region of Alloy 152 and LAS has relatively many precipitates compared to the FB region of Alloy 182. And LAS and Alloy 152 is more noble metal than Alloy 182, resulting in the more susceptible to corrosion in the FB region. In the other words, there two factors affecting the corrosion resistance of the FB regions of Alloy 182/LAS and Alloy 152/LAS: the deferent precipitate morphology in the FB region and the deferent galvanic potential of Ni-base alloys (Alloy 182 and Alloy 152).

Firstly, in terms of the precipitate morphology, it is thought for the precipitates to cause galvanic corrosion by playing as a role of cathode in galvanic cell. The increase of the cathode area and the contact surface of the anode (LAS) and the cathode (Ni-base alloy) may accelerate the galvanic corrosion, resulting in the degenerated corrosion resistance of the FB region. Totally, the FB region of Alloy 152/LAS has slightly more precipitates than the FB region and it can affect the gap of corrosion resistances in the FB regions of Alloy 182/LAS and Alloy 152/LAS

Based on the results, the FB region of Alloy 182/LAS might have good corrosion resistance compared to the FB region of Alloy 152/LAS. The crack propagation in the primary coolant environment of the primary coolant system of PWRs include the fracture of the metal and dissolution of the metal, respectively. In that, when the corrosion resistance become severely low, the crack growth rate can be accelerated by the fast dissolution rate of the metal. The detailed effects on the crack growth rates will be described in the next section “VII. Crack Growth Rate Measurements”

5.5 Conclusion

To investigate the effects of long-period thermal aging and Cr content of Ni-base weld metal on the integrity of the weld joints, corrosion tests in the FB regions, between Alloy 182/LAS and Alloy 152 / LAS, were performed. The following conclusions can be drawn from the results.

- The area, where the Cr rich precipitates was additionally formed and grown in LAS side near the FB, is called as “FB region”. Thermal aging causes the Cr diffusion in interface such as grain boundary and FB, resulting in formation and growth of Cr rich precipitates in the FB region.
- In FB region, with thermal aging, the corrosion rate was increased at the initial step (heat treatment during the full power operating time of 15 y because the number of the Cr rich precipitates, which play a role as a cathode, was increased. The cathode area and the

contact surface of LAS (anode) and Cr rich precipitates (cathode) were increased, leading to the increase of the corrosion rate. At the later step (heat treatment during the full power operating time of 30 y), the corrosion rate was reduced since the number of the Cr rich precipitates was decreased by the coarsening of the precipitates.

- As the disparity between the FB regions of Alloy 182/LAS and Alloy 152/LAS, the FB regions of Alloy 152/LAS have totally high corrosion rates compared to the FB regions of Alloy 182/LAS. It might be because the FB regions of Alloy 152/LAS have more Cr rich precipitates than the FB of Alloy 182/LAS.

Table V-1 Tafel fitting results of the electropolarization curves (shown in Fig. V-1) for the samples of Alloy 182, Alloy 152 and LAS in room temperature water with 1200 ppm of B and 2 ppm of Li

Material	Ba (mV)	Bc (mV)	Io (A/cm2)	Eo (V)
Allloy 182	574.75	198.39	7.18E-06	-0.308
Alloy 152	823.71	242.72	5.25E-06	-0.296
LAS	263.62	238.54	1.26E-05	-0.458

Table V-2 Tafel fitting results of the electropolarization curves (shown in Figure V-5) for the FB regions of Alloy 182/LAS and Alloy 152/LAS in room temperature water with 1200 ppm of B and 2 ppm of Li

	Material	Heat Treatment	Tafel Fitting			
			Ba	Bc	Io (A/cm^2)	Eo (V)
Interface	Alloy182/LAS	As-welded	506.0	457.34	3.09E-06	-0.689
		HT400Y15	872.5	496.24	1.02E-05	-0.665
		HT400Y30	211.9	311.23	5.67E-06	-0.683
	Alloy152/LAS	As-welded	742.5	486.83	7.16E-06	-0.653
		HT400Y15	859.9	693.01	1.20E-05	-0.630
		HT400Y30	511.8	566.4	9.15E-06	-0.658

Table V-3 Tafel fitting results of the electropolarization curves (shown in Figure V-5) for the FB regions of Alloy 182/LAS and Alloy 152/LAS in primary water chemistry of nuclear power plants.

	Material	Heat Treatment	Tafel Fitting			
			Ba (mV)	Bc (mV)	Io (A/cm^2)	Eo (V)
Interface	Alloy182/LAS	As-welded	59.1	63.286	3.05E-06	-0.464
		HT400Y15	95.7	100.87	6.76E-06	-0.461
		HT400Y30	62.6	75.147	4.79E-06	-0.450
	Alloy152/LAS	As-welded	85.1	121.62	4.13E-06	-0.462
		HT400Y15	102.1	131.56	1.14E-05	-0.457
		HT400Y30	95.1	67.49	9.02E-06	-0.458

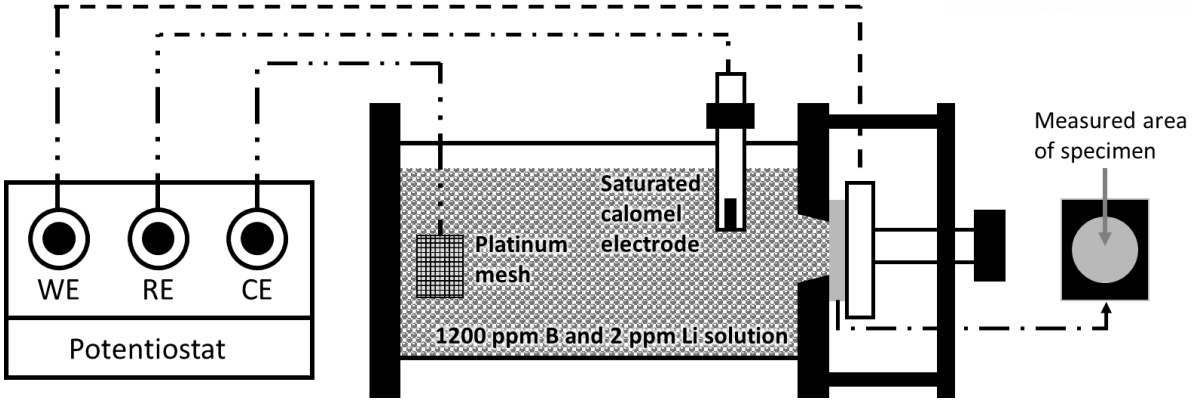

Figure V-1 Experimental setup for potentiodynamic polarization test at room temperature. External Ag/AgCl reference electrode and Pt mesh of counter electrode are installed in the cell.

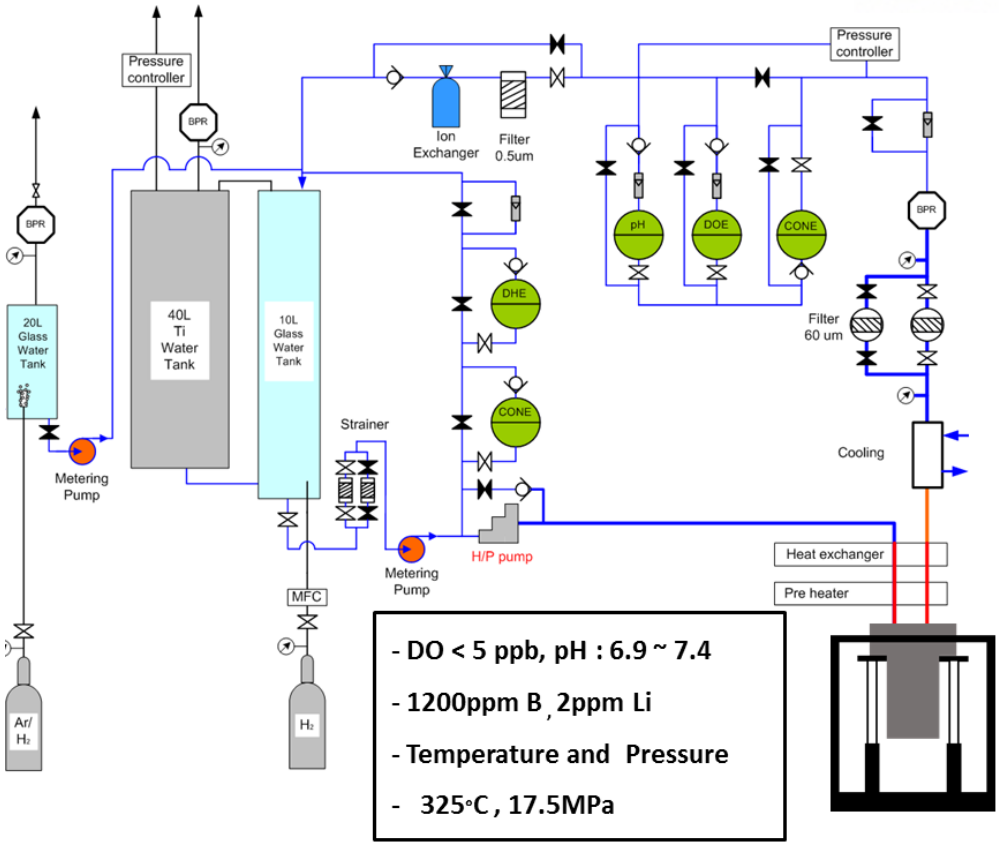

(a) Recirculation loop system simulating primary water chemistry of nuclear power plants

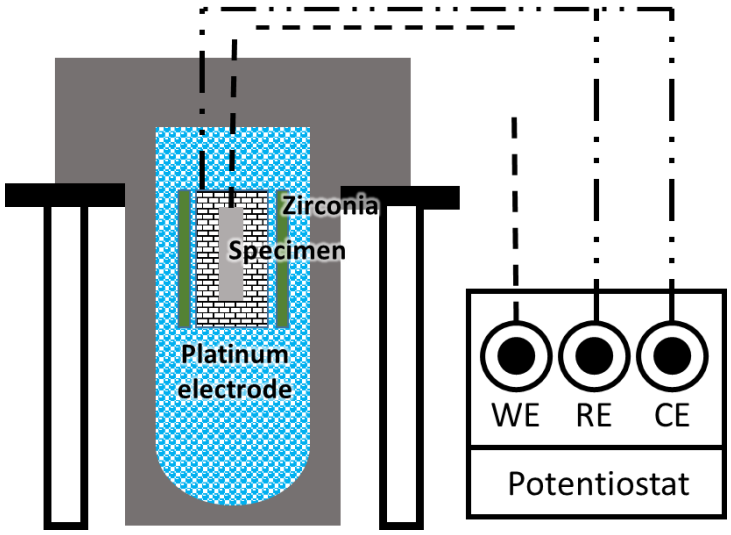

(b) High temperature corrosion cell

Figure V-2 Schematics of (a) recirculation loop system simulating primary water chemistry of nuclear power plants and (b) High temperature corrosion cell for weld joints. Pt electrode was used as both reference electrode and counter electrode.

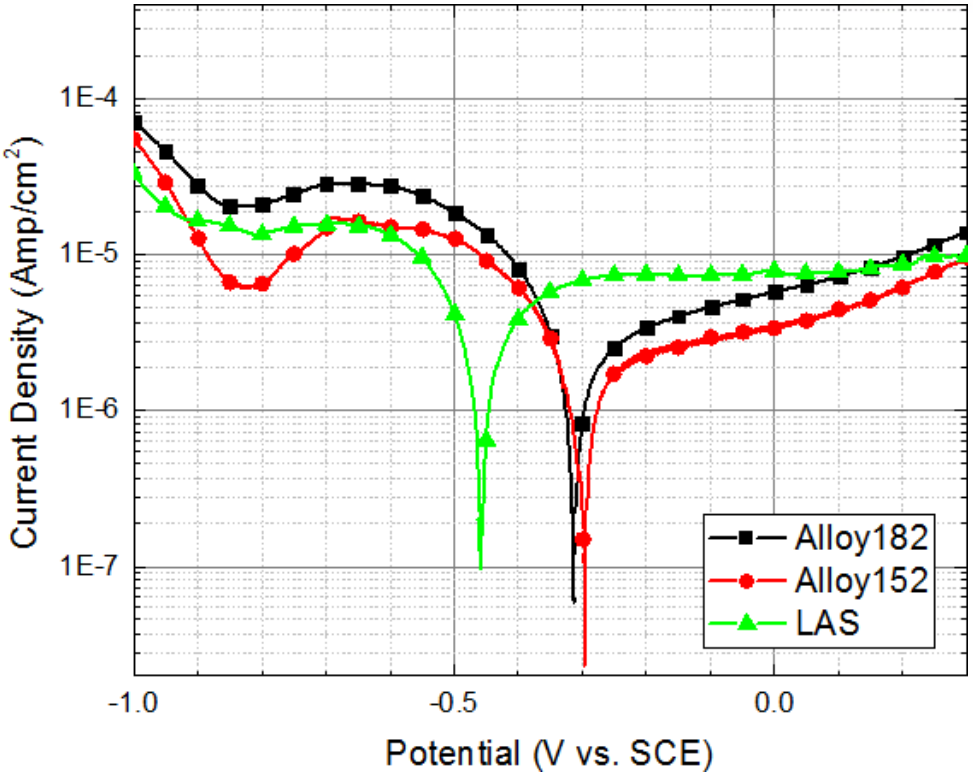

Figure V-3 Potentiodynamic electro-polarization curves for the samples of Alloy 182, Alloy 152 and LAS in room temperature water with 1200 ppm of B and 2 ppm of Li.

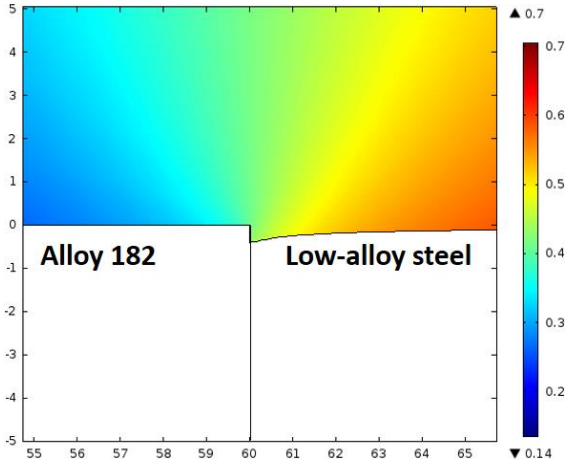

(a) As-welded DMW including Alloy 182 and LAS

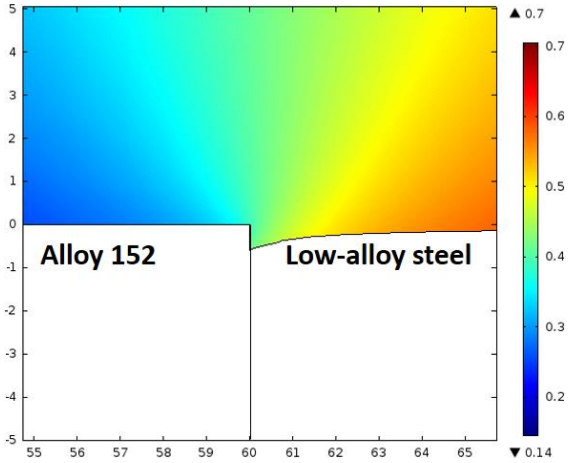

(b) As-welded DMW including Alloy 152 and LAS

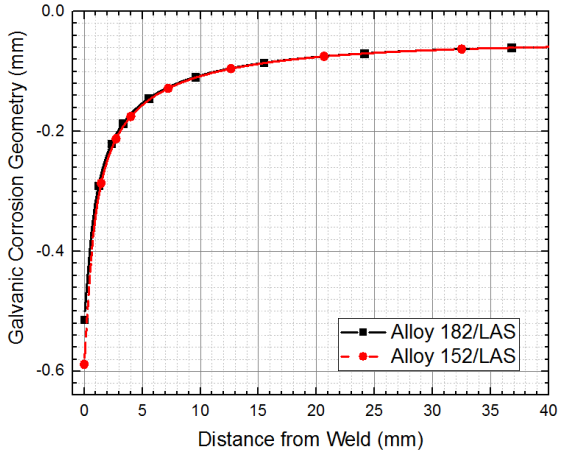

(c) Depth of galvanic corrosion in LAS side near Alloy 182 and Alloy 152

Figure V-4 Depths of galvanic corrosion estimated with COMSOL Multiphysics and the Tafel fitting results shown in Table V-2. It simulated the galvanic corrosions of weld joints at as-welded state exposed to primary water environment of nuclear power plants for 1,000h.

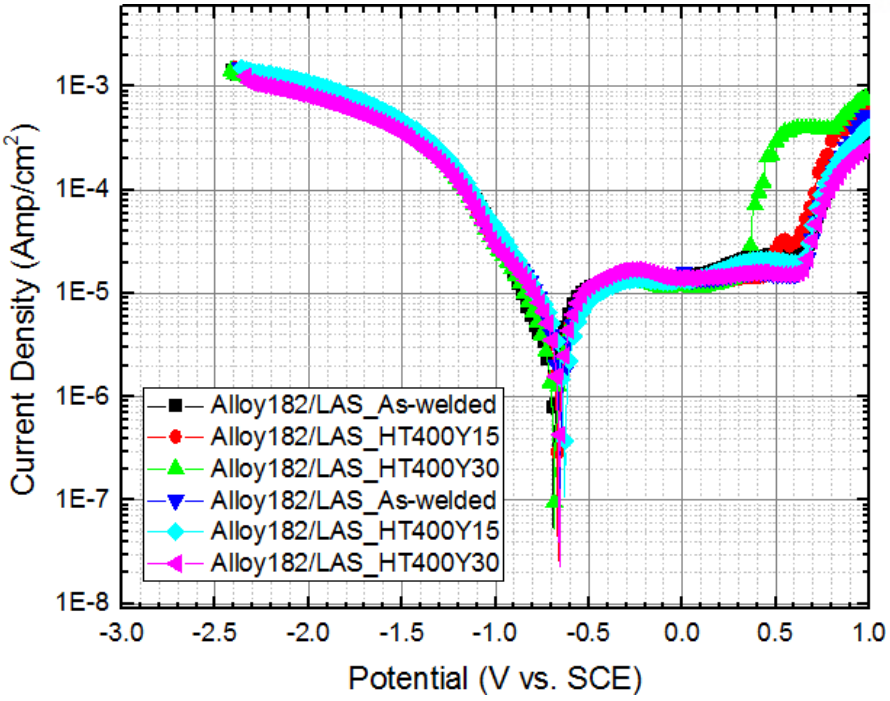

Figure V-5 Potentiodynamic electro-polarization curves for the FB regions of Alloy 182/LAS and Alloy 152/LAS in room temperature water with 1200 ppm of B and 2 ppm of Li.

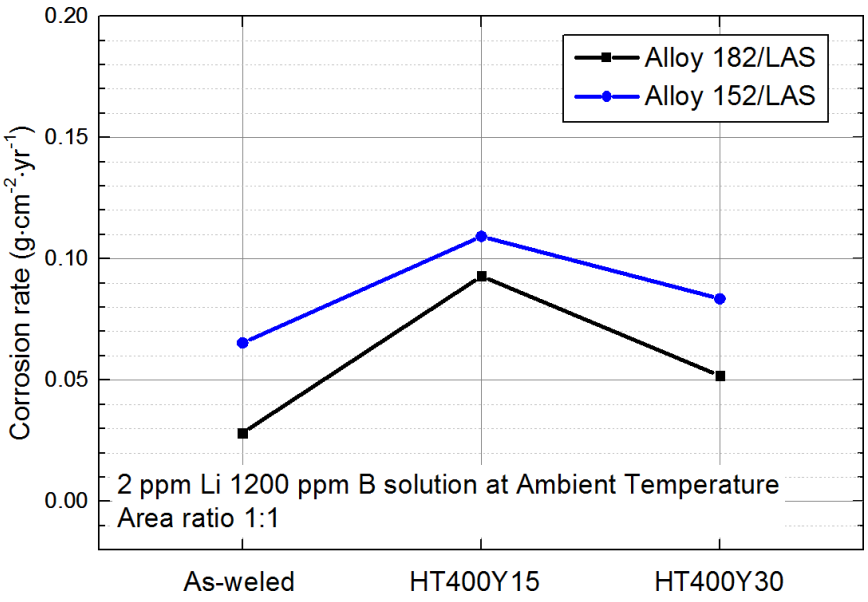

Figure V-6 Corrosion rates, which were estimated with Tafel fitting results shown in Table VI-2, represent the corrosion resistance of the FB regions of Alloy 182/LAS and Alloy 152/LAS.

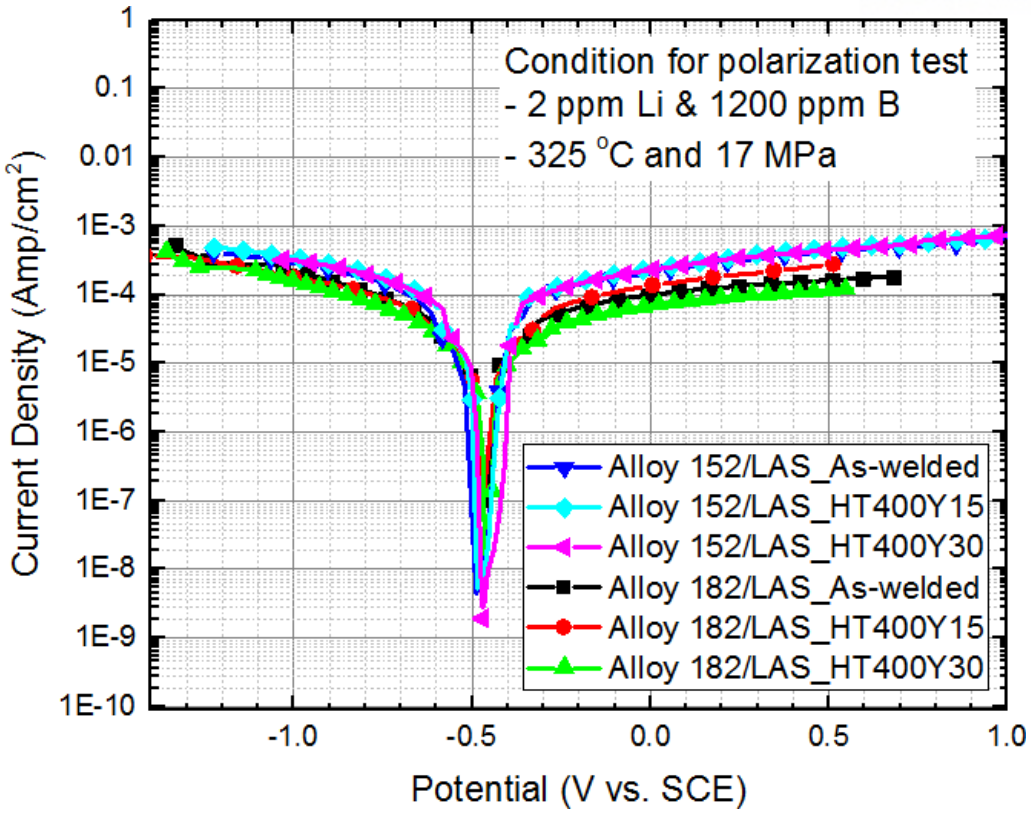

Figure V-7 Potentiodynamic electro-polarization curves for the FB regions of Alloy 182/LAS and Alloy 152/LAS in primary water chemistry of nuclear power plants.

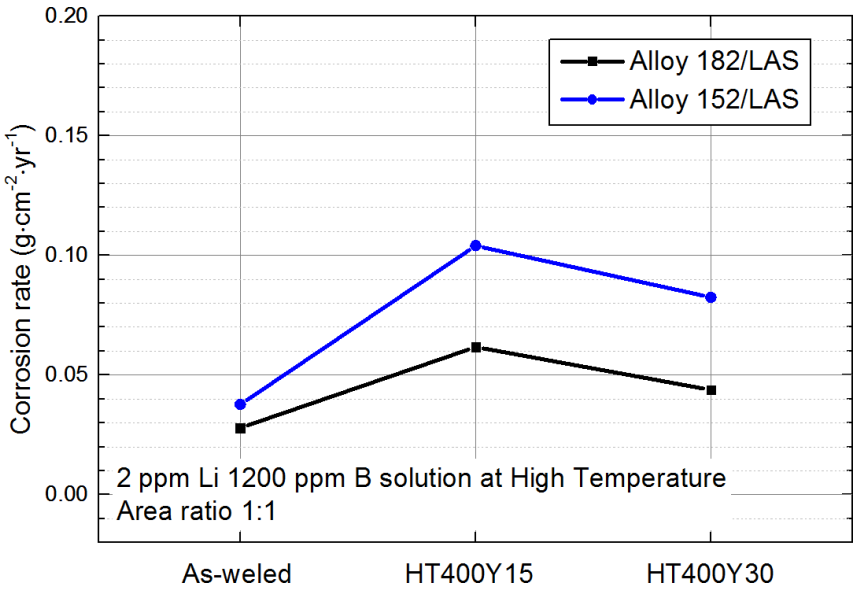

Figure V-8 Corrosion rates, which were estimated with Tafel fitting results shown in Table V-3, represent the corrosion resistance of the FB regions of Alloy 182/LAS and Alloy 152/LAS.

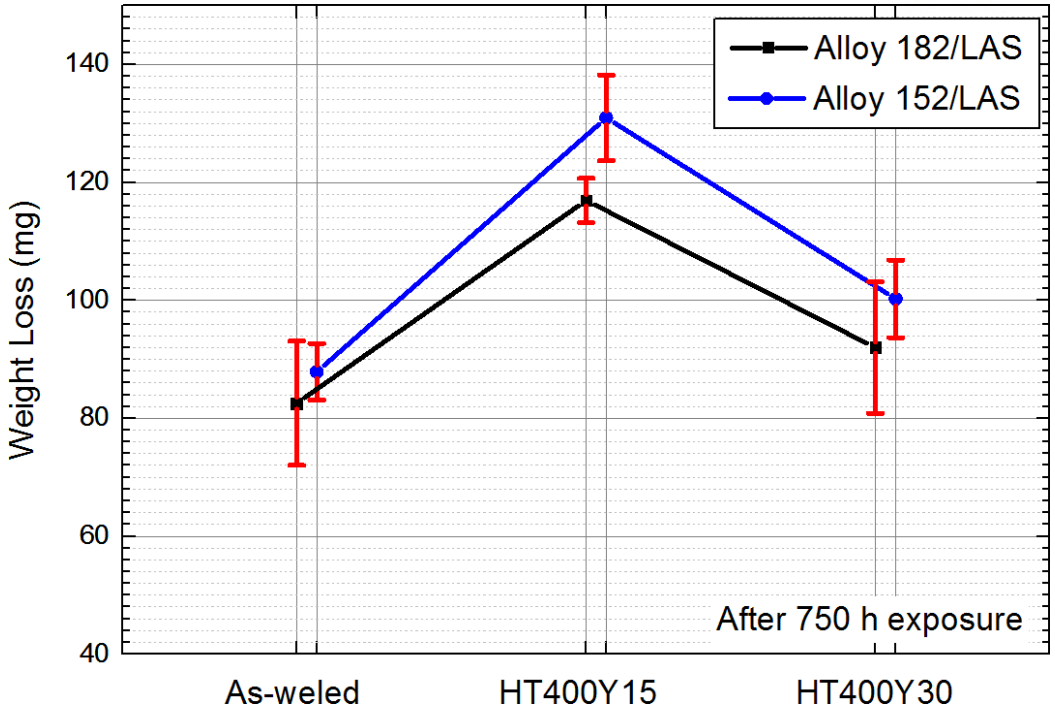

Figure V-9 Weight loss, which is the weight gap between before and after the exposure to primary water environment of nuclear power plant for 750 h, represents the corrosion resistance of the FB regions of Alloy 182/LAS and Alloy 152/LAS.

(a) 2/11 of cathode/anode surface ratio & 2 of contact surface between anode and cathode

(b) 6/7 of cathode/anode surface ratio & 6 of contact surface between anode and cathode

(c) 6/7 of cathode/anode surface ratio & 4 of contact surface between anode and cathode

Figure V-10 Schematics of specimens which consist of 13 of discs with 20 mm of diameter and 1 mm thickness, for galvanic corrosion for evaluating the effects of the cathode surface and contact surface on galvanic corrosion. Grey disc is LAS (anode) and black disc is stainless steel 316L (cathode).

(a) specimens exposed in HNO_3 for 148 h

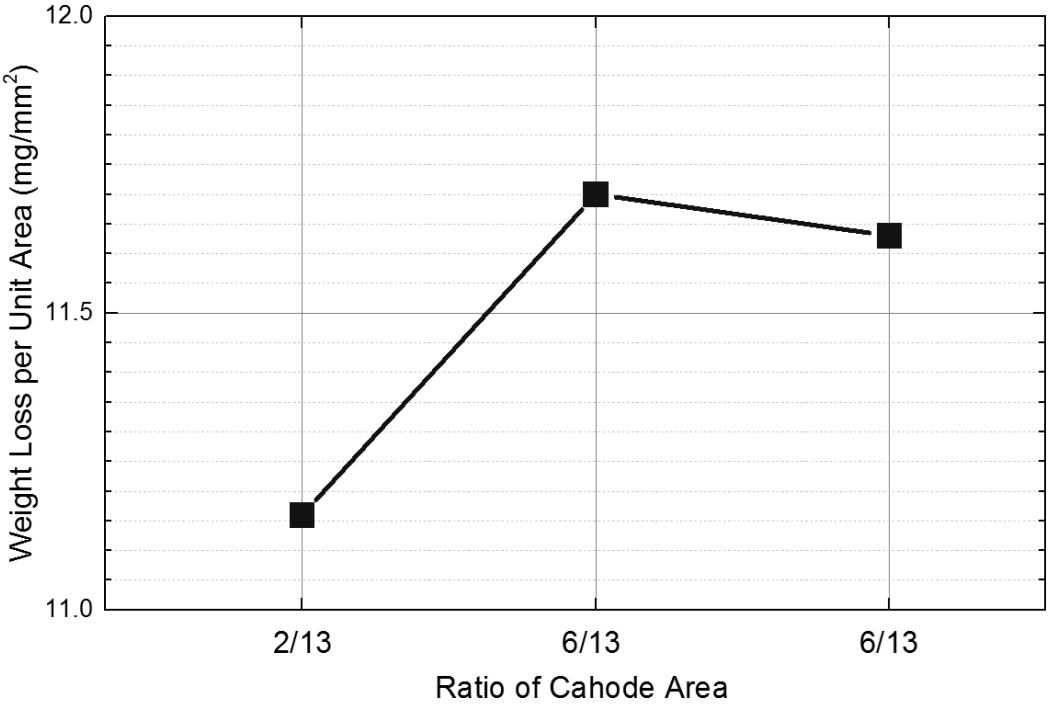

(b) Weight loss per unit area of specimen which consist of LAS (anode) and stainless steel 316L (cathode)

Figure V-11 (a) Picture of specimens, which shown in Fig. V-10, after the exposure in HNO_3 for 148 h and weight loss is dependent on the cathode surface and contact surface on galvanic corrosion.

VI. CRACK GROWTH RATE MEASUREMENTS

6.1 Introduction

There is a concern that the fusion boundary (FB) region (consisting of low-alloy steel (LAS) and Cr-rich precipitates near FB) might be more susceptible to cracking than Ni-base weld metal which experienced frequently cracking issues in the primary coolant system of PWRs. However, the sufficient research was not conducted to evaluated the integrity of the FB region due to some reasons: (i) LAS has good resistance on the cracking compared to Ni-base weld metal and it can seem that the FB region is also resistive to the cracking, and (ii) it is difficult to investigate the resistance on the cracking in the FB region due to the narrow and un-uniform region.

To begin with, LAS is not susceptible to the cracking under constant loading compared to Ni-base weld metal [64–67]. Some researchers investigated the crack growth rate measurement under constant loading in high temperature water environment, observing that the crack growth rate of LAS was less than 1×10^{-10} mm/s at 60 MPa$\sqrt{m}$ of stress intensity. Data points at 1×10^{-10} mm/s were reported as "no growth". In case of Ni-base weld metal, Alloy 82/182 has data points above 1×10^{-10} mm/s, and reported to be susceptible to cracking. To prevent the problems, Alloy 182 was replaced with Alloy 152, which has 2 times of Cr content compared to Alloy 182. And then, the cracking problem has not been reported in Alloy 52/152 because the material has good resistance to the crack growth (less than 1×10^{-10} mm/s) [16]. As the previous study, T. Moss et al. [20,21] observed that Cr oxide of Alloy 690 / Alloy 152, which includes higher Cr concentration than Alloy 600 / Alloy 182, is thick and has relatively many Cr concentration due to relatively fast diffusion of Cr. It can reduce the Cr depleted zone and intergranular oxidation along grain boundaries, resulting in the improved resistances on corrosion and cracking. In summary, the Ni-base weld metal (Alloy 52/152) and LAS might be considered as 'immune region' to cracking. In this regard, the FB region might seem to be resistive to crack growth, but it had not been investigated through sufficient studies. Most of all, the FB region contains the Cr-rich precipitates (more nobble metal) and are located next to Ni-base weld metal (more nobble metal) although the FB region is also low-alloy steel. It means that the FB region may be affected by galvanic corrosion or localized penetration into the FB region or act as the active path for cracking. For the reason, the FB region might be more susceptible to cracking.

Next, for the crack growth rate measurements, constant loading test was selected to verify that the FB region is more susceptible to cracking than Ni-base weld metals when crack approach the FB region. There are several methods to evaluated the resistance to cracking in high temperature water: static loading test at steady-state power operation, slow strain rate tension test (considering start-up or shut-down and thermal stratification) and low/high cycle testing (considering thermal fatigue and thermal

stratification). Because of its relevance for practical applications, constant loading test was usually preferred to evaluates the susceptibility to the cracking and there are many data obtained through the test method. In addition, constant loading is available without the active loading system using spring loading system (as shown in Fig. VI-1). Because of these advantages, the constant loading test was selected to measure the crack growth rate of the FB region.

In addition, the FB region can additionally be degenerated by the effect of the long-period thermal aging and the replacement of Ni-base weld metal (Alloy 182 into Alloy 152) as described in Section of 'I. INTRODUCTION'. For these reasons, crack growth rate measurements were conducted varying two options: (a) the thermal aging heat treatment condition and (b) Ni-base weld metal (Alloy 182 and Alloy 152).

6.2 Experimental

In this study, two different DMW joints were prepared: (1) A508 Gr. 3 / Alloy 182 / Alloy 600 and (2) A533 Gr. B/Alloy 152/ Alloy 690. The bulk mock-up samples of the weld joints were cut with wire-cutting machines and electro-discharging machines to prepare 3 samples for the different heat treatments simulating the thermal aging degradations for 0 y, 15 y and 30 y. The chemical compositions of the used materials are described in Section III. 1. DMW joint of A533 Gr. B/Alloy 152/ Alloy 690 was heat-treated at 400 ^{o}C during the equivalent times to the full power operating times of 0 y, 15 y and 30 y in the primary coolant system of PWRs, preparing the sample treated at 3 conditions. And DMW joint of A508 Gr. 3/ Alloy 182/ Alloy 600 was heat-treated at 400 during the equivalent times to the full power operating times of 0 y, 15 y and 30 y in the primary coolant system of PWRs preparing the sample treated at 3 conditions.

As shown in Fig. VI-1(a), the single edge bend specimens for evaluating corrosion resistance were prepared using an electrical discharge machine, and a polishing machine. The specimens with 30 (length, mm) × 6.9 (width, mm) × 4 (thickness, mm) and notch bottom radius curvature of 0.25 mm, which were cut from as-welded and heat-treated mock-up samples through an electrical discharge machining, and then were polished with emery paper up to 9 μm (particle size), diamond paste up to 6 μm for creating a flat section with negligible mechanical deformation.

Once, to make machine-notched crack sharpened and approach the FB region, the specimens are fatigue-cracked at sine wave (10 Hz, Load ratio: 0.1, Max. Load: 1500 N) following ASTM E399 and E2769 using a 100 kN servo-hydraulic dynamic testing machine (INSRTON 8801). It was conducted in air at room temperature. The crack growth rate was determined with grown crack length under constant strain and experiment time. And then, in the primary coolant environment (high temperature, and high pressure water) of PWRs, the crack growth rate measurements were performed under constant

loading (applying approximately 10 MPa√m of stress intensity) using springs and grips. Once, the constant strain was applied to the specimen using spring and grips (as shown in Fig. VI-1(b)). The stress intensity factor was calculated following ASTM E2769.

And, to simulate primary water environment, recirculation loop system was entirely instrumented to measure and control electrical conductivity, pH, dissolved oxygen, and dissolved hydrogen for both the inlet and outlet water and is shown in Fig. VI-2 (a), which help the experimental environment to be maintained at conditions of 25 cm^3/kg of dissolved hydrogen concentrations, < 5 ppb of dissolved oxygen, 2 ppm (mg/kg) Li, 1200 ppm (mg/kg) B, 320 °C, and 16.5 MPa. Suitable amount of lithium hydroxide monohydrate (LiOH) and boric acid (H_3BO_3) were inserted in dilated water to prepare the primary coolant in the primary coolant system of PWRs and electrical conductivity of this solution was maintained within 21 ~ 22 μS/cm.

6.3 Results

In this section, the results of crack growth rate measurements, which were conducted to investigate the effects of (i) long-period thermal aging and (ii) Cr content of Ni-base weld metal on the crack growth rates of the FB region, are described below.

As shown in Fig. VI-1, the FB region is located between Ni-base weld metal (yellow area) and LAS (grey area), respectively. Crack growth rate measurements were evaluated along the FB region under the constant strain of about 3 %, as described above. Figure VI-3 represents Fractographies of crack propagation specimens showing cracking was propagated along the FB region of Alloy 182 and LAS. In the figures, there are four regions which consist of (1) machine notch, (2) fatigue crack for crack sharpening, (3) crack propagated under constant strain, and (4) post-crack. Post-test fractography was conducted to normalize the process and to establish more accurate crack length values. And, Figure VI-4 represents Fractographies of crack propagation specimens showing cracking was propagated along the FB region of Alloy 152 and LAS. Post-test fractography was conducted to normalize the process and to establish more accurate crack length values, respectively. The crack lengths were measured following ASTM E399 and used to determine crack growth rate under constant loading (applying approximately 10 MPa√m of stress intensity). The results are indicated in Fig. VI-6, representing Distribution of crack growth rate of the FB regions of Alloy 182 / LAS measured through constant strain crack propagation experiments. Based on the results of crack growth rate measurements in the FB regions of Alloy 182 / LAS, the crack growth rates of as-welded, HT400-Y15, HT400-Y30 samples were $5.11 \times 10^{-9} \pm 2.31 \times 10^{-9}$ mm/s, $1.11 \times 10^{-8} \pm 0.21 \times 10^{-8}$ mm/s, and $3.31 \times 10^{-9} \pm 1.18 \times 10^{-9}$ mm/s. The crack growth rate of the FB region was found to change with thermal aging heat treatment. The

crack growth rates were initially increased with thermal aging equivalent to 15 y (HT400Y15) compared to the as-welded weld joint but decreased with thermal aging equivalent to 30 y (HT400Y30).

In addition, this tendency was observed in the FB region of Alloy 152 / LAS. VI-7, representing Distribution of crack growth rate of the FB regions of Alloy 152 / LAS measured through constant strain crack propagation experiments. Based on the results of crack growth rate measurements in the FB regions of Alloy 152 / LAS, the crack growth rates of as-welded, HT400-Y15, HT400-Y30 samples were $7.20 \times 10^{-9} \pm 3.07 \times 10^{-9}$ mm/s, $1.63 \times 10^{-8} \pm 0.46 \times 10^{-8}$ mm/s, and $7.33 \times 10^{-9} \pm 2.00 \times 10^{-9}$ mm/s. The crack growth rate of the FB region was found to change with thermal aging heat treatment. The crack growth rates were initially increased with thermal aging equivalent to 15 y (HT400Y15) compared to the as-welded weld joint but decreased with thermal aging equivalent to 30 y (HT400Y30).

Commonly, in both the FB regions of (a) Alloy 182 / LAS and (b) Alloy 152 / LAS, thermal aging triggered the changes of the changes of the crack growth rates by the change of the precipitate morphology, mechanical properties and corrosion resistance, indicating the degradation in HT400Y15 and the recovery in HT400Y30 among results at three heat treatment conditions. In the other words, between as-welded state and HT400Y30, the peak of crack growth rates may exist between equivalent times to 0 y (as-welded state) and 30 y (HT400Y30) of the operation time in the primary coolant system of PWRs.

In comparison with the FB regions of (a) Alloy 182 / LAS and (b) Alloy 152 / LAS, totally, the FB region of Alloy 152 / LAS has relatively high crack growth rates compared to the FB region of Alloy 182 / LAS. Generally, Alloy 152 has relatively low crack growth rates compared to Alloy 182, representing different tendency from the one in the FB region. Instead, as described in section IV, the FB region of Alloy 152 / LAS has relatively large and many precipitates compared to the FB region of Alloy 182 / LAS because Alloy 152 contains 29.0 wt. % of Cr and the concentration of Cr is higher than one of Alloy 182 (14.9 wt. % of Cr). It seems that the gap of crack growth rates values was caused by the difference of the precipitate's morphology, mechanical properties and corrosion resistance, respectively. The detailed explanation was described in the next section.

6.4 Discussion

As described above, the data points of the FB regions were measured through the crack growth rate measurements and are distributed between 3.13×10^{-9} mm/s and 1.63×10^{-8} mm/s (at the stress intensity of about 10 MPa$\sqrt{m}$). The crack growth rates of the FB region were demonstrated to be higher compared to LAS (no crack growth at the stress intensity) and Alloy 152 Ni-base weld metal (no crack growth at the stress intensity). When the material does not have the pre-existing (selective) path, it has relatively good resistance to cracking under constant loading compared to the materials with the pre-

existing path (such as, sensitized grain boundary, slip band, etc.). In this regard, although the FB region consists of LAS, the FB region, which is located next to Ni-base weld metal (noble metal) and include Cr-rich precipitates (noble metal), can affected by the galvanic corrosion, meaning that the FB region might be the pre-existing path (relatively susceptible to cracking). The selective dissolution of the FB region by the galvanic corrosion was observed and discussed in the section "V. Evaluation of Corrosion Resistance", representing that it might be contributed to the results. Some data points of the crack growth rates were similar with that of Alloy 182 ($1 \times 10^{-9} \sim 1 \times 10^{-8}$ mm/s at the stress intensity) and some of the points are higher than that of Alloy 182. It means that the FB region is highly susceptible to cracking compared to Alloy 182 and can be the weakest point than other materials.

In addition, the FB region can additionally be degenerated by the effect of the long-period thermal aging and the replacement of Ni-base weld metal (Alloy 182 into Alloy 152) as described in Section of 'I. INTRODUCTION', respectively. In this section, the effects of thermal aging (Section 6.4.1) on the crack propagations of the FB region will be discussed. The common features and disparities, between Alloy 182 / LAS and Alloy 152 / LAS, will be covered in Section 6.4.2.

6.4.1. Effects of thermal aging on the FB region

Based on the results of crack growth rate measurements in the primary water environment of the primary coolant system of PWRs, thermal aging affected crack growth rates and it seems to be affected by the precipitate morphology, mechanical properties and corrosion resistances, indicating the accelerated crack growth rate in HT400Y15 and the reduced crack growth rate in HT400Y30 among results at three heat treatment conditions. In the other words, the peak of corrosion rates may exist between equivalent times to 0 y (as-welded state) and 30 y (HT400Y30) of the operation time in the primary coolant system of PWRs. It indicates the same tendency with the one of microstructural changes (the precipitate morphology), the changes of microstructures (Cr rich precipitate's morphology), mechanical properties and corrosion rates.

In detail, when the number of Cr-rich precipitates in the FB region was increased after the heat treatment during the full power operating time of 15 y in the primary coolant system of PWRs, the corrosion rate of the FB region was accelerated with the increased number of the precipitates and the hardness of the FB region was increased with the increased number as described the previous section. Once the accelerated corrosion resistance by the addition precipitation in the FB region. Because the crack propagation in the primary coolant environment of the primary coolant system of PWRs include the fracture of the metal and dissolution of the metal, the accelerated corrosion rate can cause the accelerated crack growth rate. In addition, the increased hardness can accelerate the crack propagation.

The reciprocal relation of fracture toughness with hardness is generally observed in many engineering materials and is related to the energy dissipation from the enhance plasticity. The increase of the hardness decreased the energy dissipation and enhance the plasticity, resulting in the increased stress intensity. The increased stress intensity can accelerate the crack propagation by degenerating the fracture toughness. In this regard, the initial thermal aging during the full power operating time of 15 y made the crack propagation rate along the FB accelerated by the material hardening and the degenerated corrosion resistance with the addition precipitation of $Cr_{23}C_6$ in the FB region. The crack propagation of HT400Y15 seems to be fast compared to as-welded weld joint (0 y).

Then, when the number of Cr-rich precipitates in the FB region was re-decreased after the heat treatment during the full power operating time of 30 y in the primary coolant system of PWRs, the crack growth rate of the FB region of HT400Y30 was reduced with the decreased number of the precipitates compared to HT400Y15. It may be explained with the hardness and corrosion rate of the FB region, which was reduced after the heat treatment during the full power operating time of 30 y. Once the hardness was decreased with the reduced number of the precipitates, leading to the suppressed crack propagation rate. As described above, the reciprocal relation of fracture toughness with hardness is generally observed in many engineering materials and is related to the energy dissipation from the enhance plasticity. The re-softening of the material has the more energy dissipation than the harder material, making the crack tip blunt easily. In that, the re-softening reduces the stress intensity and enhances the fracture toughness. In this regard, the reduction of the hardness may be contributed to the decreased crack growth rate in the FB region of HT400Y30. Next, the recovered corrosion resistance also decreases the crack growth rate in the FB region. Since the crack can be propagated by not only the fracture of the metal but also the dissolution of the metal, it seems that the recovered corrosion resistance reduced the crack growth rate in the FB region. The crack propagation of HT400Y15 seems to be fast compared to HT400Y30.

6.4.2. Effects of Ni-base weldment on the FB region

To investigate about the effects on the FB region, two types of the weld joints of Alloy182 / LAS and Alloy152 / LAS were prepared and heat-treated at 400 °C during the full power operating times of 0 y, 15 y and 30 y. In comparison with the FB regions of Alloy 182 / LAS and Alloy 152 / LAS, the common features were observed that there is the peak of the crack growth rates between two heat treatment conditions of the equivalent times to 0 y(as-welded) and 30 y of operation time. However, it is difficult to determine when dose the peak or the valley occur due to the limited result data.

As the disparities of two weld joints, it seems that the crack propagation rates in the FB region of Alloy 182 / LAS are lower compared to the one of Alloy 152 / LAS, totally. It seems to be because the FB region of Alloy 152 and LAS has relatively fast corrosion rates compared to the FB region of Alloy 182 and LAS. The FB region of Alloy 152 and LAS has relatively high hardness values compared to the FB region of Alloy 182 and LAS.

Firstly, in terms of the corrosion rate, the corrosion resistance can affect the crack growth rate in the FB region since the crack can be propagated by not only the fracture of the metal but also the dissolution of the metal. Totally, the FB region of Alloy 152 / LAS has slightly higher corrosion rate than the FB region of Alloy 182 / LAS and it can affect the gap of corrosion propagation rates in the FB regions of Alloy 182 / LAS and Alloy 152 / LAS. Next, in terms of the hardness values, the hardness can affect the crack growth rate in the FB region since the reciprocal relation of fracture toughness with hardness is generally observed in many engineering materials and is related to the energy dissipation from the enhance plasticity. Totally, the FB region of Alloy 152 / LAS has slightly higher hardness values than the FB region of Alloy 182 / LAS and it can affect the gap of corrosion propagation rates in the FB regions of Alloy 182 / LAS and Alloy 152 / LAS.

In sum, the FB region of Alloy 182 / LAS might have good resistance on the crack propagation compared to the FB region of Alloy 152 / LAS. The crack propagation in the primary coolant environment of the primary coolant system of PWRs include the fracture of the metal and dissolution of the metal, respectively. In that, when the corrosion rates and the hardness values become severely high, the crack growth rate can be accelerated by the fast dissolution rate of the metal and the weak fracture toughness.

6.5 Conclusion

To investigate the effects of long-period thermal aging and Cr content of Ni-base weld metal on the integrity of the weld joints, crack growth rate measurements of the FB regions of Alloy 182 / LAS and Alloy 152 / LAS, were performed. The following conclusions can be drawn from the study.

- The FB regions, which consist of LAS and Cr-rich precipitates and are located next to FB, are susceptible to cracking in the primary coolant environment of PWRs compared to LAS, Alloy 152 and Alloy 182 by indicating the relatively fast crack growth rates compared to the other materials.
- The resistance on the cracking of the FB region was degenerated with thermal aging heat treatment, representing that the crack growth rate was increased at the initial step (heat treatment during the full power operating time of 15 y) because the corrosion rate was accelerated and the increased hardness caused the increased stress intensity and the

weakened fracture toughness. At the later step (heat treatment during the full power operating time of 30 y), the crack growth rate was reduced since the corrosion rate was lowered and the decreased hardness caused the decreased stress intensity and the enhanced fracture toughness.

- As the disparity between the FB regions of Alloy 182 / LAS and Alloy 152 / LAS, the FB regions of Alloy 152 / LAS have totally fast crack growth rates compared to the FB regions of Alloy 182 / LAS. It might be because the FB regions of Alloy 152 / LAS have the weaker corrosion rate and the high hardness than the FB of Alloy 182 / LAS.

Table VI-1 Distribution of crack growth rate of the FB regions of Alloy 182 / LAS and Alloy 152 / LAS measured through constant strain crack propagation experiments.

Material		Crack Growth Rate (mm/s)	
		Average	Standard Deviation
Alloy182/LAS	As-welded	5.10E-09	2.31E-09
	HT400Y15	1.11E-08	2.10E-09
	HT450Y30	3.13E-09	1.18E-09
Alloy152/LAS	As-welded	7.20E-09	3.07E-09
	HT400Y15	1.63E-08	4.63E-09
	HT450Y30	7.33E-09	2.00E-09

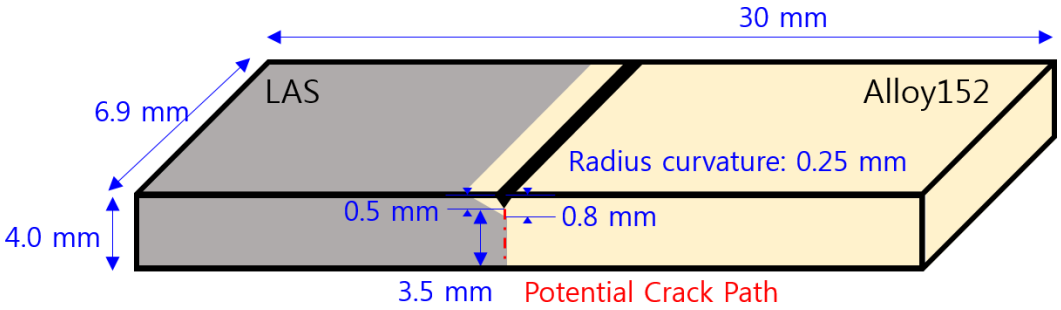

(a) Specimen for crack propagation rate measurement

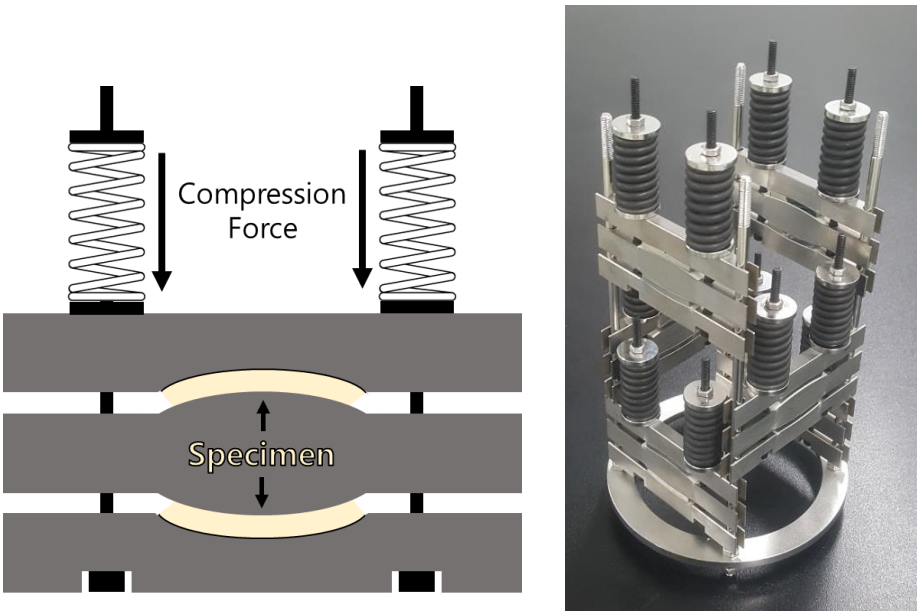

(b) Experimental set-up of crack propagation rate measurement (R= 100 m)

Figure VI-1 Schematics of (a) specimen and (b) experimental set-up for crack propagation rate measurement. The radius of the grips is about 100 mm for applying constant strain.

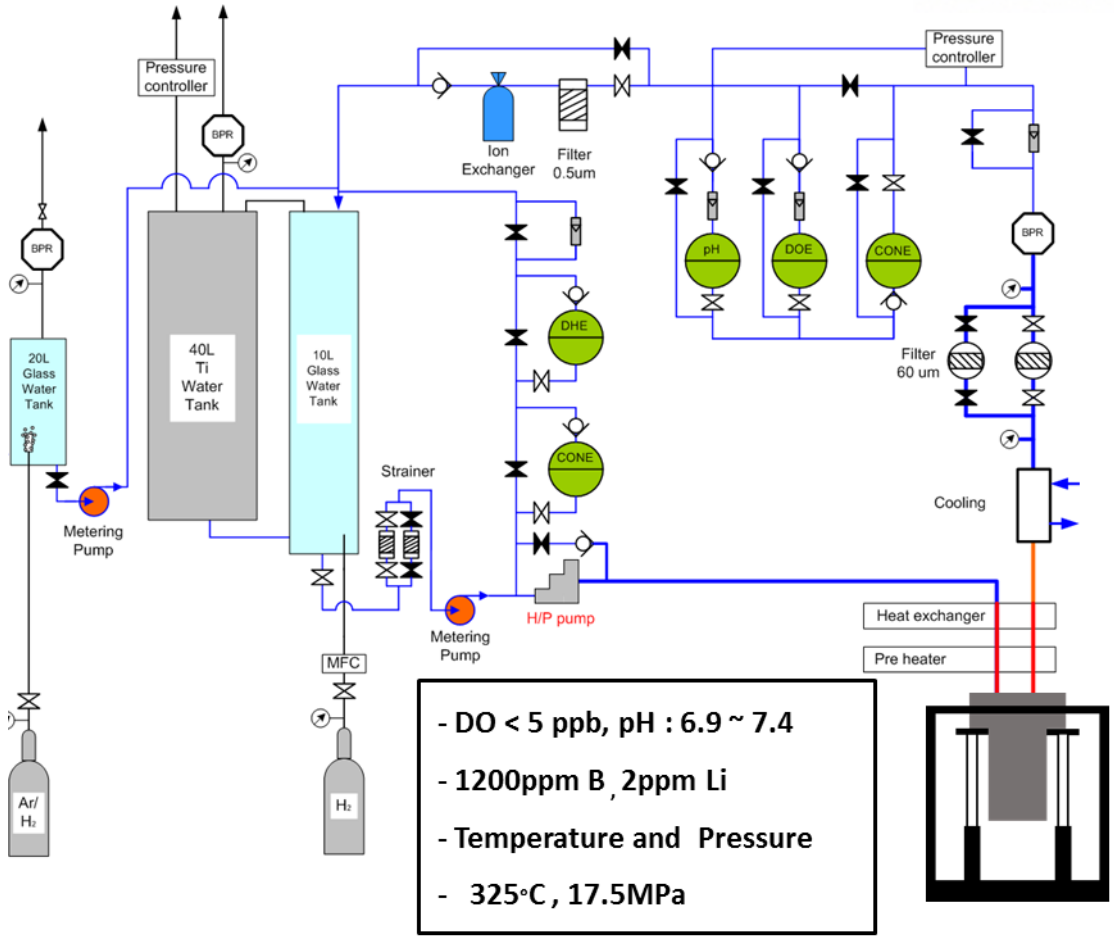

Figure VI-2 Schematics of recirculation loop system simulating primary water chemistry of nuclear power plants.

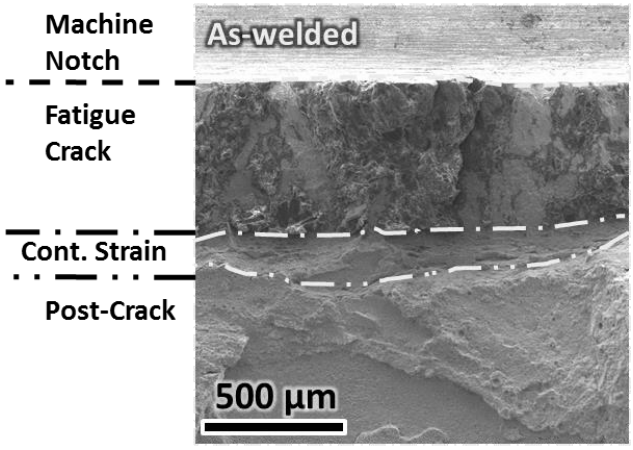

(a) As-welded DMW

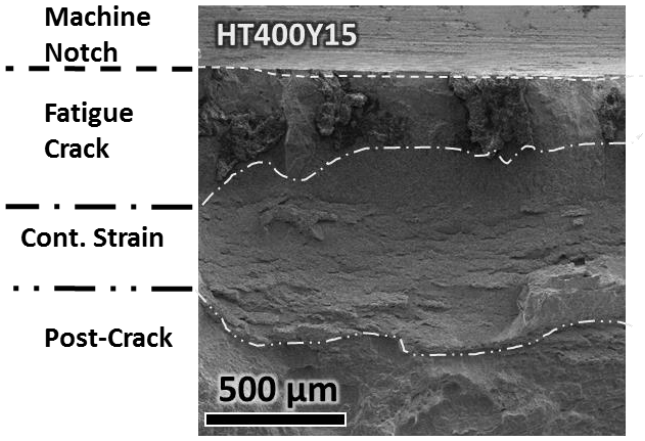

(b) HT400-Y15

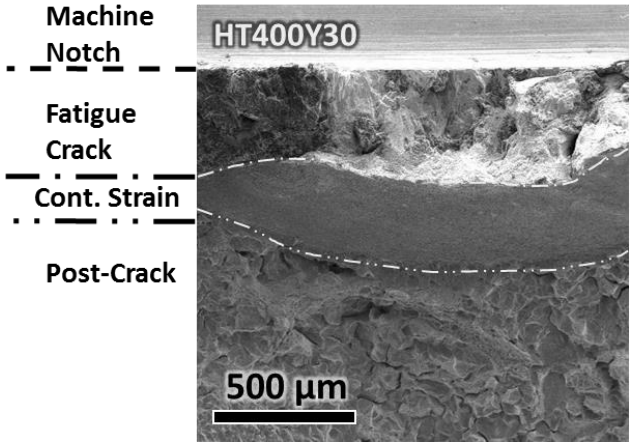

(c) HT400-Y30

Figure VI-3 Fractographies of crack propagation specimens showing cracking was propagated along the FB region of Alloy 182 and LAS.

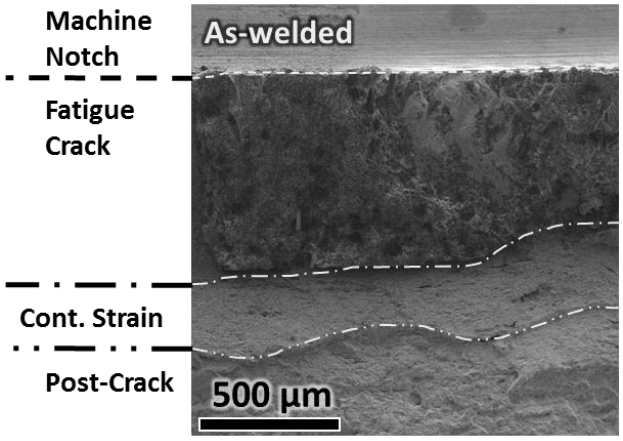

(a) As-welded DMW

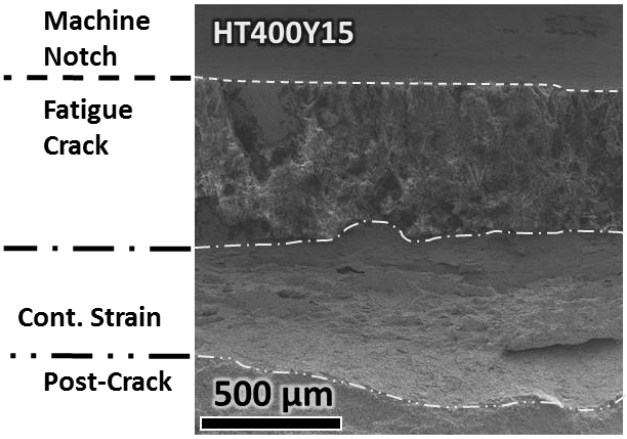

(b) HT400-Y15

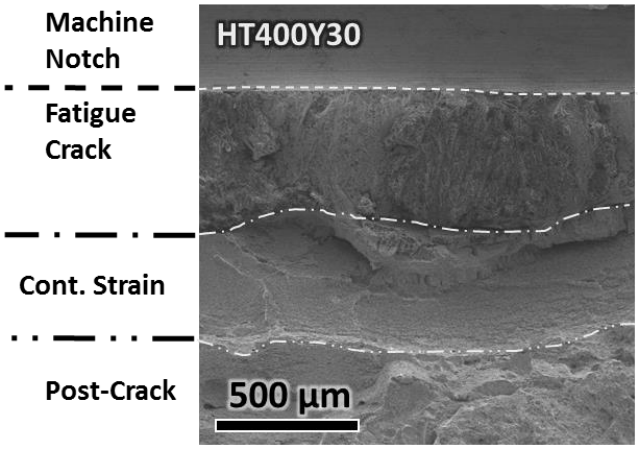

(c) HT400-Y30

Figure VI-4 Fractographies of crack propagation specimens showing cracking was propagated along the FB region of Alloy 152 and LAS.

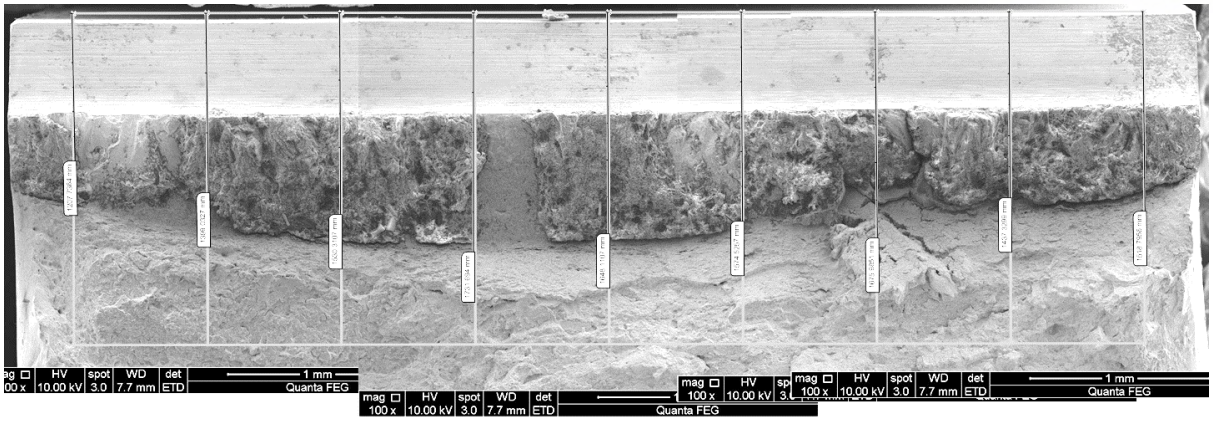

Figure VI-5 Crack length, which was formed under constant strain, was measured by drawing 9 of lines parallel to the crack growth direction. The average crack length was used as the representative value (as suggested in ASTM E399).

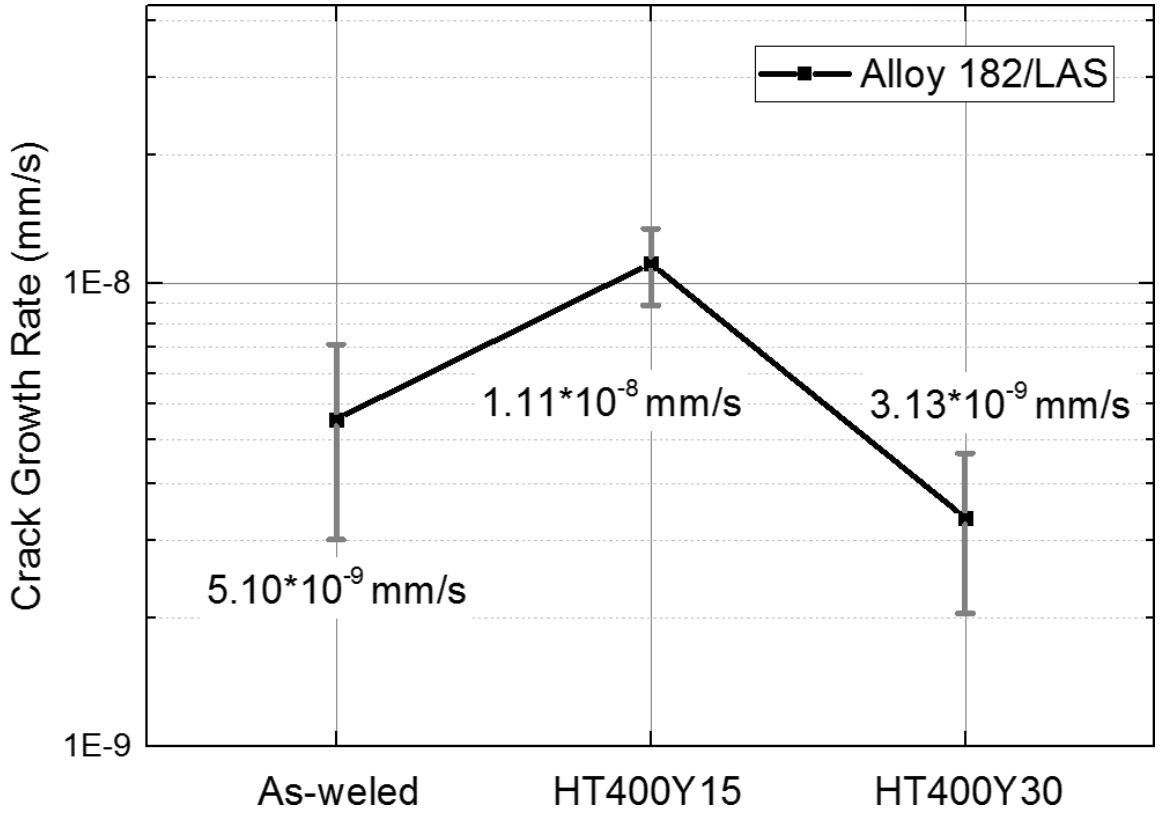

Figure VI-6 Distribution of crack growth rate of the FB regions of Alloy 182 / LAS and Alloy 152 / LAS measured through constant strain crack propagation experiments.

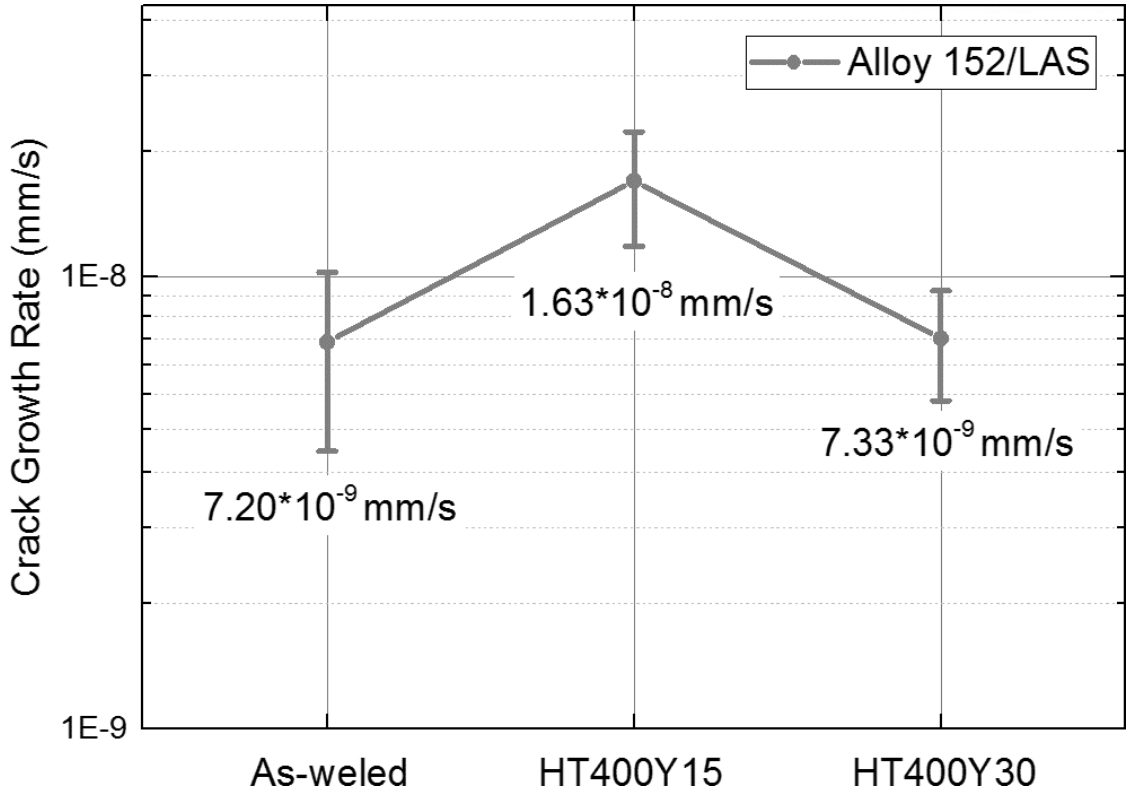

Figure VI-7 Distribution of crack growth rate of the FB regions of Alloy 182 / LAS and Alloy 152 / LAS measured through constant strain crack propagation experiments.

VII. SUMMARY AND RECOMMENDATIONS

7. 1 Summary

The leakage issues have frequently been reported to occur from Ni-base weld metal (Alloy 82/182) in the primary coolant environment of PWRs. For the reasons, many researches on cracking of Ni-base weld metal was actively conducted and is in progress. There is not sufficient studies and interest on fusion boundary (FB) region (consisting of low-alloy steel (LAS) and Cr-rich precipitates near FB) despite of the concern that the FB region might be more susceptible to cracking than Ni-base weld metal which experienced frequently cracking issues in the primary coolant system of PWRs.

Based on the results of crack growth rate measurements, the data points of the FB regions were measured through the crack growth rate measurements and are distributed between 3.13×10^{-9} mm/s and 1.63×10^{-8} mm/s (at the stress intensity of about 10 MPa√m). The crack growth rates of the FB region were demonstrated to be higher compared to LAS (no crack growth at the stress intensity) and Alloy 152 Ni-base weld metal (no crack growth at the stress intensity). In additional, some data points of the crack growth rates were similar with that of Alloy 182 ($1 \times 10^{-9} \sim 1 \times 10^{-8}$ mm/s at the stress intensity) and some of the points are higher than that of Alloy 182. It means that the FB region is highly susceptible to cracking compared to Alloy 182 and can be the weakest point than other materials.

In addition, the FB region can additionally be degenerated by the effect of the long-period thermal aging and the replacement of Ni-base weld metal (Alloy 182 into Alloy 152) as described in Section of 'I. INTRODUCTION'. For these reasons, crack growth rate measurements were conducted varying two options: (a) the thermal aging heat treatment condition and (b) Ni-base weld metal (Alloy 182 and Alloy 152). In this study, two different DMW joints were prepared: (1) A508 Gr. 3 / Alloy 182 / Alloy 600 and (2) A533 Gr. B/Alloy 152/ Alloy 690. The bulk mock-up samples of the weld joints were cut with wire-cutting machines and electro-discharging machines to prepare 3 samples for the different heat treatments simulating the thermal aging degradations for 0 y, 15 y and 30 y. Detailed instrumental analyses of the FB regions, between Alloy 182 / LAS and Alloy 152 / LAS, were performed to investigate the effects of thermal aging and type of Ni-base alloy on microstructures, mechanical properties, corrosion rates and crack propagation in the FB region. The following conclusions can be drawn from the study

About the effects of (a) long-period thermal aging, the Cr rich precipitates were additionally formed at the initial step (heat treatment at 400 ^{o}C during the equivalent times to the full power operating times of 15 y in the primary coolant system of PWRs) and the number density was increased. The additional precipitation causes that the hardness was increased at the initial step because the number of the Cr rich precipitates, which play a role as a barrier to dislocation's movement, was increased. The

additional precipitation causes that the corrosion rate was increased at the initial step because the Cr rich precipitates play a role as a cathode. The cathode area and the contact surface of LAS (anode) and Cr rich precipitates (cathode) were increased, leading to the increase of the corrosion rate. The crack growth rate was increased at the initial step because the corrosion rate was accelerated and the increased hardness caused the increased stress intensity and the weakened fracture toughness. At the later step (heat treatment at 400 ºC during the equivalent times to the full power operating times of 30 y in the primary coolant system of PWRs), the Cr rich precipitates were coarsened and the number density was decreased. The hardness was reduced since the number of the Cr rich precipitates was decreased by the coarsening of the precipitates. The corrosion rate was reduced since the number of the Cr rich precipitates was decreased by the coarsening of the precipitates. The crack growth rate was reduced since the corrosion rate was lowered and the decreased hardness caused the decreased stress intensity and the enhanced fracture toughness.

Next, on the effect of (b) Cr content of Ni-base weld metal, the FB regions of Alloy 152 / LAS have totally large and many Cr rich precipitates compared to the FB regions of Alloy 182 / LAS because Alloy 152 have more Cr concentration than Alloy 182. The microstructural gap leads to the differences of hardness and corrosion rates. The Cr rich precipitate is acknowledged to play a role as a barrier to dislocation's movement and play a role as a cathode in a galvanic cell. The cathode area and the contact surface of LAS (anode) and Cr rich precipitates (cathode) were increased, leading to the increase of the corrosion rate. In these reasons, The FB regions of Alloy 152 / LAS have high harnesses and fast corrosion rates compared to the FB regions of Alloy 182 / LAS. As the results, the FB regions of Alloy 152/LAS have totally fast crack growth rates compared to the FB regions of Alloy 182/LAS. It might be because the FB regions of Alloy 152 / LAS have the weaker corrosion rate and the high hardness than the FB of Alloy 182 / LAS.

In summary, the FB regions are susceptible to cracking in the primary coolant environment of PWRs compared to LAS, Alloy 152 and Alloy 182 by indicating the relatively fast crack growth rates compared to the other materials. The resistance on the cracking of the FB region was degenerated with thermal aging heat treatment, representing that the crack growth rate was increased at the initial step (heat treatment during the full power operating time of 15 y) because the corrosion rate was accelerated and the increased hardness caused the increased stress intensity and the weakened fracture toughness. The weakest point is thought to be observed between the full power operating times of 0 y and 30 y. In the other words, the integrity of the weld joint may be threatened by the FB region susceptible to cracking.

7. 2 Recommendations

The FB regions are susceptible to cracking in the primary coolant environment of PWRs compared to LAS, Alloy 152 and Alloy 182. Although the fusion boundary between Alloy 152 and low-alloy steel is not exposed to the reactor coolant directly, however, coolant can permeate when the crack approaches the fusion boundary and then it can cause more severe cracking issue based on the result of this study. The barrier (buttering layer of Ni-base weld metal) between the primary coolant and the FB region is thin thickness of 6 mm. To improve the integrity of the dissimilar metal weld joints, it is thought that the thickness of the barrier should be increased by conducting the overlay welding.

Thermal aging affects mechanical properties, corrosion rates, and crack propagations in the FB region by changing the Cr rich precipitate's morphology. The number of the precipitates increases at the initial heat treatment step (15 y) and decreased at the later step (30 y). When the number of the precipitates is maximum, the FB region might be the weakest in terms of corrosion rate and crack propagation. In this regard, when the heat treatment is additionally performed to make the saturation of the precipitation before the operation, the thermal degradation with the operation might be avoided. Such data can do the important role to assess long-term thermal aging and the effect of Cr content on the corrosion at the fusion boundary which is susceptible to corrosion.

However, this study investigated 3 samples for the different heat treatments simulating the thermal aging degradations for 0 y, 15 y and 30 y. The thermal aging heat treatment conditions are not enough to determine when the FB region is the most susceptible to cracking. Therefore, this region should be focused when the further corrosion studies are conducted, and the life prediction model should consider this region and thermal aging effect on that point to more precisely estimate the critical period of structural material to corrosion issues when the plant operates in full power. Therefore, the non-destructive examinations are required to prevent the crack propagation into the FB region and the period of the examinations should become shorter than ever. ㄴ

VIII. REFERENCE

[1] M. Sireesha, V. Shankar, S.K. Albert, S. Sundaresan, Microstructural features of dissimilar welds between 316LN austenitic stainless steel and alloy 800, Mater. Sci. Eng. A. 292 (2000) 74–82. doi:10.1016/S0921-5093(00)00969-2.

[2] S.C. Yoo, K.J. Choi, C.B. Bahn, S.H. Kim, J.Y. Kim, J.H. Kim, Effects of thermal aging on the microstructure of Type-II boundaries in dissimilar metal weld joints, J. Nucl. Mater. 459 (2015) 2–12. doi:10.1016/j.jnucmat.2015.01.009.

[3] J. Hou, Q. Peng, Y. Takeda, J. Kuniya, T. Shoji, Microstructure and stress corrosion cracking of the fusion boundary region in an alloy 182-A533B low alloy steel dissimilar weld joint, Corros. Sci. 53 (2011) 4309–4317. doi:10.1016/j.corsci.2011.08.046.

[4] A. International, Basic Understanding of Weld Corrosion, 2006 ASM Int. (2006) 1–13. doi:10.1361/corw2006p001.

[5] S. Hirano, K. Hamasaki, K. Okimuara, Maintenance Activities for Alloy 600 in PWR Plants - Part 1, E-Journal Adv. Maint. 2 (2009). http://www.jsm.or.jp/ejam/Vol.2.No.2/GA/13/article.html (accessed May 25, 2017).

[6] F. Delabrouille, B. Viguier, L. Legras, E. Andrieu, Effect of the chromium content on the corrosion of nickel based alloys in primary water of pressurised nuclear reactors, Mater. High Temp. 22 (2005) 287–292. doi:10.3184/096034005782744182.

[7] M. Kanzaki, Y. Masaki, T. Kudo, Effect of Cr and Ni on Stress Corrosion Cracking Susceptibility in Ni-Cr-Fe Alloys Under Simulated Pressurized Water Reactor Primary Conditions, Corrosion. 71 (2015) 1027–1035. doi:10.5006/1696.

[8] T. TERACHI, T. YAMADA, T. MIYAMOTO, K. ARIOKA, K. FUKUYA, Corrosion Behavior of Stainless Steels in Simulated PWR Primary Water—Effect of Chromium Content in Alloys and Dissolved Hydrogen—, J. Nucl. Sci. Technol. 45 (2012) 975–984.

[9] T. Yonezawa, N. Sasaguri, K. Onimura, Effects of metallurgical factors on stress corrosion cracking of Ni-base alloys in high temperature water, in: Proc. 1988 JAIF Int. Conf. Water Chem. Nucl. Power Plants, 1988: p. 490.

[10] K. Arioka, T. Yamada, T. Miyamoto, M. Aoki, Intergranular Stress Corrosion Cracking Growth Behavior of Ni-Cr-Fe Alloys in Pressurized Water Reactor Primary Water, Corrosion. 70 (2014) 695. doi:10.5006/1205.

[11] F. Delabrouille, L. Legras, F. Vaillant, P. Scott, B. Viguier, E. Andrieu, Effect of the chromium content and strain on the corrosion of nickel based alloys in primary water of pressurized water reactors, in: 12th Int. Conf. Environ. Degrad. Mater. Nucl. Power Syst. React., 2005: pp. 903–911.

[12] K.R. Rao, S. Hunt, P. Riccardella, Companion guide to the ASME boiler & pressure vessel code : criteria and commentary on select aspects of the boiler & pressure vessel and piping codes., ASME Press, 2006.

[13] J. Hou, Q.J. Peng, T. Shoji, J.Q. Wang, E.H. Han, W. Ke, Effects of cold working path on strain concentration, grain boundary microstructure and stress corrosion cracking in Alloy 600, Corros. Sci. 53 (2011) 2956–2962. doi:10.1016/j.corsci.2011.05.037.

[14] J. Hou, Q.J. Peng, Y. Takeda, J. Kuniya, T. Shoji, J.Q. Wang, E.H. Han, W. Ke, Microstructure and mechanical property of the fusion boundary region in an Alloy 182-low alloy steel dissimilar weld joint, J. Mater. Sci. 45 (2010) 5332–5338. doi:10.1007/s10853-010-4581-6.

[15] I.S. Hwang, S.U. Kwon, J.H. Kim, S.G. Lee, An intraspecimen method for the statistical characterization of stress corrosion crack initiation behavior, Corrosion. 57 (2001) 787–793. doi:10.5006/1.3280613.

[16] J. Gorman, S. Hunt, P. Riccardella, PWR Reactor Vessel Alloy 600 Issues, in: Companion Guid. to ASME Boil. Press. Vessel Code, Vol. 3, Second Ed., ASME, Three Park Avenue New York, NY 10016-5990, n.d.: pp. 63–84. doi:10.1115/1.802205.ch44.

[17] J.H. Kim, Y.J. Kim, S.H. Lee, H.Y. Bae, C.Y. Oh, J.S. Kim, N.Y. Hur, H.B. Park, S.G. Lee, J.S. Kim, Effects of Geometry of Reactor Pressure Vessel Upper Head Control Rod Drive Mechanism Penetration Nozzles on J-Groove Weld Residual Stress, Trans. of the KSME-A. 35 (2011) 1337–1345.

[18] ATLAS STEELS, (2010). http://www.atlassteels.com.au/documents/TN7-Galvanic_Corrosion_rev_Aug_2010.pdf (accessed May 25, 2017).

[19] K.J. Choi, T. Kim, S.C. Yoo, S. Kim, J.H. Lee, J.H. Kim, Fusion boundary precipitation in thermally aged dissimilar metal welds studied by atom probe tomography and nanoindentation, J. Nucl. Mater. 471 (2016) 8–16. doi:10.1016/j.jnucmat.2015.12.047.

[20] T. Moss, G.S. Was, Accelerated Stress Corrosion Crack Initiation of Alloys 600 and 690 in Hydrogenated Supercritical Water, Metall. Mater. Trans. A Phys. Metall. Mater. Sci. 48 (2017). doi:10.1007/s11661-016-3898-4.

[21] T. Moss, G. Cao, G.S. Was, Oxidation of Alloy 600 and Alloy 690: Experimentally Accelerated Study in Hydrogenated Supercritical Water, Metall. Mater. Trans. A Phys. Metall. Mater. Sci. 48 (2017). doi:10.1007/s11661-016-3897-5.

[22] K.J. Choi, S.C. Yoo, T. Kim, C.B. Bahn, J.H. Kim, Effects of aging temperature on microstructural evolution at dissimilar metal weld interfaces, J. Nucl. Mater. 462 (2015) 54–63. doi:10.1016/j.jnucmat.2015.03.044.

[23] J.J. Kim, S.H. Shin, J.A. Jung, K.J. Choi, J.H. Kim, First-principles study of interstitial diffusion of oxygen in nickel chromium binary alloy, Appl. Phys. Lett. 100 (2012) 131904. doi:10.1063/1.3696079.

[24] H.O. Nam, I.S. Hwang, K.H. Lee, J.H. Kim, A first-principles study of the diffusion of atomic oxygen in nickel, Corros. Sci. 75 (2013) 248–255. doi:10.1016/j.corsci.2013.06.006.

[25] K.J. Choi, J.J. Kim, B.H. Lee, C.B. Bahn, J.H. Kim, Effects of thermal aging on microstructures of low alloy steel-Ni base alloy dissimilar metal weld interfaces, J. Nucl. Mater. 441 (2013) 493–502. doi:10.1016/j.jnucmat.2013.07.003.

[26] D.D. Pruithi, M.S. Anand, R.P. Agarwala, Diffusion of Chromium in Inconel 600, J. Nucl. Mater. 64 (1977) 206–210.

[27] S.I. Baik, M.J. Olszta, S.M. Bruemmer, D.N. Seidman, Grain-boundary structure and segregation behavior in a nickel-base stainless alloy, Scr. Mater. 66 (2012) 809–812. doi:10.1016/j.scriptamat.2012.02.014.

[28] A. Andrieu, A. Pineau, P. Joly, F. Roch, On Modeling of Thermal Embrittlement in PWR Steels using the Local Approach to Fracture a) b), (2013) 1–10.

[29] T.W. Nelson, J.C. Lippold, M.J. Mills, Nature and evolution of the fusion boundary in ferritic-austenitic dissimilar weld metals, Part 1 - nucleation and growth, Weld. J. (Miami, Fla). 78 (1999).

[30] T.W. Nelson, J.C. Lippold, M.J. Mills, Nature and evolution of the fusion boundary in ferritic-austenitic dissimilar metal welds - Part 2: on-cooling transformations, Weld. J. (Miami, Fla). 79 (2000).

[31] T.W. Nelson, J.C. Lippold, M.J. Mills, Investigation of boundaries and structures in dissimilar metal welds, Sci. Technol. Weld. Join. 3 (1998).

[32] F.G. Caballero, M.K. Miller, S.S. Babu, C. Garcia-Mateo, Atomic scale observations of bainite transformation in a high carbon high silicon steel, Acta Mater. 55 (2007) 381–390. doi:10.1016/j.actamat.2006.08.033.

[33] K.J. Choi, S.H. Shin, J.J. Kim, J.A. Jung, J.H. Kim, Nano-structural and Nano-chemical analysis of Ni-base alloy/low alloy steel dissimilar metal weld Interfaces, Nucl. Eng. Technol. 44 (2012) 491–500. doi:10.5516/NET.07.2012.009.

[34] J. Kim, S.H. Kim, K.J. Choi, C.B. Bahn, I.S. Hwang, J.H. Kim, In-situ investigation of thermal aging effect on oxide formation in Ni-base alloy/low alloy steel dissimilar metal weld interfaces, Corros. Sci. 86 (2014) 295–303. doi:10.1016/j.corsci.2014.06.006.

[35] D.J. Larson, D.T. Foord, A.K. Petford-Long, T.C. Anthony, I.M. Rozdilsky, A. Cerezo, G.W.D. Smith, Focused ion-beam milling for field-ion specimen preparation:: preliminary investigations, Ultramicroscopy. 75 (1998) 147–159. doi:10.1016/S0304-3991(98)00058-8.

[36] D.J. Larson, D.T. Foord, A.K. Petford-Long, H. Liew, M.G. Blamire, A. Cerezo, G.D.W. Smith, Field-ion specimen preparation using focused ion-beam milling, Ultramicroscopy. 79 (1999) 287–293. doi:10.1016/S0304-3991(99)00055-8.

[37] M.K. Miller, K.F. Russell, Atom probe specimen preparation with a dual beam SEM/FIB miller, Ultramicroscopy. 107 (2007) 761–766. doi:10.1016/j.ultramic.2007.02.023.

[38] K. Oh-ishi, C.L. Mendis, T. Ohkubo, K. Hono, Effect of laser power and specimen temperature on atom probe analyses of magnesium alloys, Ultramicroscopy. 111 (2011) 715–718. doi:10.1016/j.ultramic.2011.01.002.

[39] K.F. Russell, M.K. Miller, R.M. Ulfig, T. Gribb, Performance of local electrodes in the local electrode atom probe, Ultramicroscopy. 107 (2007) 750–755. doi:10.1016/j.ultramic.2007.02.028.

[40] K. Thompson, D. Lawrence, D.J. Larson, J.D. Olson, T.F. Kelly, B. Gorman, In situ site-specific specimen preparation for atom probe tomography, Ultramicroscopy. 107 (2007) 131–139. doi:10.1016/j.ultramic.2006.06.008.

[41] T.-F. Chen, G.P. Tiwari, Y. Iijima, K. Yamauchi, Volume and grain boundary diffusion of chromium in Ni-base Ni-Cr-Fe alloys, Mater. Trans. 44 (2003) 40–46. doi:10.2320/matertrans.44.40.

[42] J.R. (Joseph R.. Davis, Corrosion : understanding the basics, ASM International, 2000. https://books.google.co.kr/books?id=D0nAMorpSIYC&pg=PA129&lpg=PA129&dq=galvanic+corrosion,+distance+effect&source=bl&ots=yfzFn98v6e&sig=Hct2yqz-TIraslwygLyVIIohFZU&hl=ko&sa=X&ved=0ahUKEwjVp4zGqIXUAhWBnJQKHV__DXsQ6AEIYjAH#v=onepage&q=galvanic corrosion%2C distance effect&f=false (accessed May 23, 2017).

[43] X.G. Zhang, Galvanic Corrosion, in: Uhlig's Corros. Handb. Third Ed., 2011: pp. 123–143. doi:10.1002/9780470872864.ch10.

[44] B. Gault, A. La Fontaine, M.P. Moody, S.P. Ringer, E.A. Marquis, Impact of laser pulsing on the reconstruction in an atom probe tomography, Ultramicroscopy. 110 (2010) 1215–1222. doi:10.1016/j.ultramic.2010.04.017.

[45] J. Dean, J.M. Wheeler, T.W. Clyne, Use of quasi-static nanoindentation data to obtain stress–strain characteristics for metallic materials, Acta Mater. 58 (2010) 3613–3623. doi:10.1016/j.actamat.2010.02.031.

[46] J. Dean, G. Aldrich-Smith, T.W. Clyne, Use of nanoindentation to measure residual stresses in surface layers, Acta Mater. 59 (2011) 2749–2761. doi:10.1016/j.actamat.2011.01.014.

[47] Y. Gaillard, C. Tromas, J. Woirgard, Study of the dislocation structure involved in a nanoindentation test by atomic force microscopy and controlled chemical etching, Acta Mater. 51 (2003) 1059–1065. doi:10.1016/S1359-6454(02)00509-8.

[48] S.R. Kalidindi, S. Pathak, Determination of the effective zero-point and the extraction of spherical nanoindentation stress–strain curves, Acta Mater. 56 (2008) 3523–3532. doi:10.1016/j.actamat.2008.03.036.

[49] Z.-H. Xu, X. Li, Sample size effect on nanoindentation of micro-/nanostructures, Acta Mater. 54 (2006) 1699–1703. doi:10.1016/j.actamat.2005.11.043.

[50] D. Casellas, J. Caro, S. Molas, J.M. Prado, I. Valls, Fracture toughness of carbides in tool steels evaluated by nanoindentation, Acta Mater. 55 (2007) 4277–4286. doi:10.1016/j.actamat.2007.03.028.

[51] J. Alkorta, J.M. Martínez-Esnaola, J. Gil Sevillano, Critical examination of strain-rate sensitivity measurement by nanoindentation methods: Application to severely deformed niobium, Acta Mater. 56 (2008) 884–893. doi:10.1016/j.actamat.2007.10.039.

[52] W.C. Oliver, G.M. Pharr, Measurement of hardness and elastic modulus by instrumented indentation: Advances in understanding and refinements to methodology, J. Mater. Res. 19 (2004) 3–20. doi:10.1557/jmr.2004.19.1.3.

[53] B. Alexandreanu, B. Capell, G.S. Was, Combined effect of special grain boundaries and grain boundary carbides on IGSCC of Ni-16Cr-9Fe-xC alloys, Mater. Sci. Eng. A. 300 (2001) 94–104. doi:10.1016/S0921-5093(00)01705-6.

[54] Y. Zhao, I.C. Choi, Y.J. Kim, J. Il Jang, On the nanomechanical characteristics of thermally-treated alloy 690: Grain boundaries versus grain interior, J. Alloys Compd. 582 (2014) 141–145. doi:10.1016/j.jallcom.2013.08.044.

[55] V. Mohles, Simulation of dislocation glide in precipitation hardened materials, Comput. Mater. Sci. 16 (1999) 144–150. doi:10.1016/S0927-0256(99)00056-7.

[56] O.A. Ojo, M.C. Chaturvedi, Liquation microfissuring in the weld heat-affected zone of an overaged precipitation-hardened nickel-base superalloy, Metall. Mater. Trans. A Phys. Metall. Mater. Sci. 38 (2007) 356–369. doi:10.1007/s11661-006-9025-1.

[57] P.M. Scott, An overview of materials degradation by stress corrosion in PWRs, Eurocorr 2004. 51 (2004) 3–11. doi:10.1533/9781845693466.1.3.

[58] G.S. Was, P.L. Andresen, Stress Corrosion Cracking Behavior of Alloys in Aggressive Nuclear Reactor Core Environments, Corrosion. 63 (2007) 19–45. doi:10.5006/1.3278331.

[59] S. Erlach, F. Danoix, H. Leitner, P. Auger, I. Siller, H. Clemens, Precipitation reactions during the early stages of aging in a Ni and Al alloyed martensitic medium carbon steel, Surf. Interface Anal. 38 (2006) 1380–1385. doi:10.1002/sia.

[60] Z. Guo, W. Sha, Quantification of Precipitation Hardening and Evolution of Precipitates, Mater. Trans. 43 (2002) 1273–1282. doi:10.2320/matertrans.43.1273.

[61] A.J. Kulkarni, K. Krishnamurthy, S.P. Deshmukh, R.S. Mishra, Effect of particle size distribution on strength of precipitation-hardened alloys, J. Mater. Res. 19 (2004) 2765–2773. doi:10.1557/JMR.2004.0364.

[62] A.K. Vasudevan, K. Sadananda, Role of slip mode on stress corrosion cracking behavior, Metall. Mater. Trans. A Phys. Metall. Mater. Sci. 42 (2011) 405–414. doi:10.1007/s11661-010-0471-4.

[63] L.Y. Zhao, H. Xue, F.Q. Yang, Y.K. Gui, Analysis on Mechanical Parameters at SCC Tip in Fusion Boundary Region of Dissimilar Weld Joint, Appl. Mech. Mater. 457–458 (2013) 459–462. doi:10.4028/www.scientific.net/AMM.457-458.459.

[64] M.H. Majeed, Modelling of Short Corrosion Crack Growth of Low-Alloy Steel in a Chemical environment, 7 (2015).

[65] H.P. Seifert, Literature Survey on the Stress Corrosion Cracking of Low-Alloy Steels in High-Temperature Water, (2002).

[66] J.H. Kim, Y.J. Oh, I.S. Hwang, D.J. Kim, J.T. Kim, Fracture behavior of heat-affected zone in low alloy steels, J. Nucl. Mater. 299 (2001) 132–139. doi:10.1016/S0022-3115(01)00688-2.

[67] M. Ernestova, M. Zamboch, B. Devrient, A. Roth, U. Ehrnsten, J. Fohl, T. Weissenberg, D. Gomez-Briceno, J. Lapena, S. Ritter, Crack growth behaviour of low-alloy steels for pressure boundary components under transient light water reactor operating conditions-CASTOC, Part 2: VVER conditions, Eur. Fed. Corros. Publ. 51 (2007) 186. doi:10.1533/9781845693466.3.186.

ACKNOWLEDGEMENT

UNIST 대학원에 입학한 지 어느새 6 년이 지났습니다. 아직도 너무나도 많은 부족하기에 지난 날들이 너무나도 아쉽기만 합니다. 제가 난관과 마주하여 힘겨워 할 때 주위의 많은 분들의 도움이 있어 이렇게 이런 감사의 글을 쓸 수 있을까 싶습니다. 이 자리를 빌어 다시 한번 저에게 도움을 주신 모든 분들께 감사드립니다.

우선, 원자력 재료에 대해 잘 모르던 시절, 하나부터 열까지 지도해주시고, 연구자의 자세에 대해 성심 성의껏 지도해주신 김지현 교수님께 가장 큰 감사의 말씀을 전합니다. 어려운 난관에 부딪힐 때마다 그것을 뚫을 수 있는 끈기와 체력을 교수님 지도 아래 기를 수 있었습니다. 감사합니다. 반치범 교수님, 지난 원자력학회에서, 당시 ANL 에 재직하실 때 처음 뵈었습니다. 지난 심사동안 주셨던 교수님 의견들을 제 연구의 거름이 되도록 많은 노력을 하겠습니다. 방인철 교수님, 지난 6 년동안 많은 배움을 얻었습니다. 원자로 시스템 전체 측면에서 봐야한다는 말씀과 함께, 나무만 바라보던 시점에서 숲 전체를 보는 시점을 가지게 되었습니다. 감사합니다. 또한, 바쁘신 중에도 논문심사를 맡아 주신 김지현, 권순용, 반치범, 방인철, 안상준 교수님께 감사합니다. 논문에 대한 유익한 말씀과 충고가 많은 도움이 되었습니다.

연구실에서 많은 시간을 함께 했던 김종진, 신상훈, 박정석, 정주앙 선배님, 그리고 김기동, 김정원, 김승현, 김태호, 송인영, 이정현, 유승창, 함준혁, 김태용, 이윤주 후배의 많은 도움이 있었습니다. 2011 년 초창기 대학원생들이 다같이 모여 생활하였던 102 동 406 호 분들에게 울산에 연고도 없던 저에게 많은 것들을 베풀어 주신 김종진, 신상훈, 박정석, 정주앙 선배님께 감사드립니다. 그리고 연구실 후배들에게도 큰 감사의 말씀을 전합니다. 그리고 원자력공학과 다른 연구실 대학원분들에게도 깊은 감사의 말씀을 드립니다.

마지막으로 제가 하는 것마다 믿어 주시고 격려해주신 사랑하는 부모님과 와이프에게도 깊은 감사의 말씀을 드립니다. 제 미래에 대해서 확신을 가지지 못할 때 격려와 믿음이 없었다면 이 자리는 없었을 것입니다. 깊은 사랑으로 올바른 길을 갈 수 있도록 해 주신 부모님. 감사합니다. 그리고 제 친동생과 친척들께도 감사의 인사 드립니다.

2017 년 7 월

최경준